Protocadherin-gamma (Pcdh-γ) and its role in sensory axons and epidermal reinnervation

by

Honyi Ong

A thesis submitted in partial fulfillment of the requirements for the degree of

Master of Science

Neuroscience

University of Alberta

Abstract

Peripheral nerve injuries (PNI) and peripheral nerve diseases/neuropathy (PND) are common clinical conditions characterized by varying degrees of sensory, autonomic and motor dysfunctions. Despite significant advancement in microsurgical techniques to repair the injured nerves, functional recovery from PNI and PND is often suboptimal. Disabilities ranging from muscle weakness, skin numbness to chronic neuropathic pain often accompany PNI and PND patients, severely affecting their quality of life. A series of molecules and pathways are recognized to participate in axon regeneration, but one unexplored area is how those newly regrowing sensory axons reconnect and reinnervate one of their chief targets: the skin. Building on preliminary work from my former graduate student colleague, Dr. Rebecca Long, my project focuses on protocadherin-gamma (Pcdh-γ), a molecule that has been proposed by researchers to be a strong candidate to serve as cell identity marker in the mammalian nervous system. Pcdh-γ has been shown to play a role in regulating interneuron survival and synaptogenesis during developmental stages in the central nervous system (CNS). In adult mice, conditional knockout of Pcdh-γ in retinal starburst amacrine cells (SACs) and Purkinje neurons is associated with neurite self-avoidance defects and fasciculation of dendrites. In pyramidal neurons, however, conditional knockout of Pcdh-γ led to dendritic simplification and thinning of cortical layers.

Current literature has yet to study Pcdh-γ in the peripheral nervous system (PNS), especially in the context of axon regeneration, given its role of directing dendrite morphology in the CNS. In this project, by using both *in vitro* and *in vivo* experiments, we explored the roles played by Pcdh-γ in sensory axons. Our *in vitro* experiment showed that knockdown of Pcdh-γ in uninjured DRG neurons is associated with greater neurite extension and more branchpoints per neuron. Our *in vivo* experiment revealed to us that footpads of mice that received Pcdh-γ

knockdown through siRNA administration displayed greater epidermal reinnervation: higher intraepidermal nerve fiber density (IENFD). These exciting findings shed light on the potential roles of Pcdh-γ in axon regeneration/growth and skin epidermal reinnervation. In the final experiment, we studied Rac1 as a potential downstream signaling molecule of Pcdh-γ knockdown. We proposed that Rac1 inhibition might attenuate those axon morphological changes we observed from the knockdown of Pcdh-γ. The greater total neurite extension and branchpoints per neuron that resulted from Pcdh-γ knockdown were indeed nullified with Rac1 inhibition. Ultimately, by understanding the molecular mechanisms of Pcdh-γ in skin epidermal reinnervation, a new molecular approach to treat PNI and PND could be discovered.

Preface

The research presented in this thesis is original work completed by Honyi Ong, with edits suggested by the examining committee, under the supervision of Dr. Douglas Zochodne. All animal research in this thesis received research ethics approval from the University of Alberta Animal Research Ethics Board and Animal Care and Use Committee (ACUC), and was carried out in accordance with the University of Alberta Health Sciences Laboratory Animal Services (HSLAS) and the Sciences Animal Support Services (SASS) standards and guidelines. Experiment 2 (section 2.3.2) was done in collaboration with Dr. Long (former PhD student who completed her study in 2020). No part of this thesis has been previously published.

Acknowledgements

First and foremost, I would like to thank my supervisor, Dr. Douglas Zochodne, who welcomed me into the lab during my undergraduate degree in Honors Neuroscience program here at University of Alberta. With his mentorship and guidance, I was able to explore my research interests in the field of neuroscience. From undergraduate research courses: Neuro 498 and Neuro 499, to my current MSc. Neuroscience program, I had thoroughly enjoyed the research experience and gained lots of knowledge about peripheral nerve regeneration. On top of that, I would also like to thank Dr. Matt LaRouche, Dr. Rebecca Long, Mr. Trevor Poitras, Dr. Prashanth Komirishetty, Dr. Aparna Areti for always helping me in my experiments. It was truly an honor to have the opportunity to work in the Zochodne laboratory. I would also like thank NMHI Student Program Administrator, Amber Lapointe for all the help that she had provided me. Thank you for always answering my questions regarding the program requirements, scholarship applications, exam guidelines and others. Finally, to my family, thank you for always supporting me and trusting me. I am very grateful to have met all these amazing souls during my MSc. journey.

Table of Contents

Abstract ii
Preface iv
Acknowledgements v
List of Figures viii
List of Abbreviations x
Chapter 1: Introduction 1
1.1 Cutaneous sensory fibers and their journey to the skin 2
1.2 Peripheral axon regeneration 5
1.3 Limitations of peripheral axon regeneration 8
1.4 Molecular approach to promote axon regeneration 9
Chapter 2: Protocadherin-gamma (Pcdh-γ) 11
2.1 The Chemoaffinity Hypothesis 11
2.2 Clustered protocadherin (Pcdh) 13
2.2 Roles of Pcdh in the CNS 14
2.3 Project rationale 16
2.3.1 Experiment 1 16
2.3.2 Experiment 2 19
2.3.3 Experiment 3 22
Chapter 3: Experimental Procedures and Methods 26
3.1 Animal care 26
3.2 Animal euthanasia 26
3.3 Sciatic nerve crush injury 26
3.4 siRNA *in vivo* knockdown model 27
3.5 Cell culture 27
3.6 *in vitro* Pcdh-γ knockdown experiment by AAV-Cre 28
3.7 In-cell western assay 29
3.8 *in vitro* Rac1 inhibition experiment 30
3.9 Cell culture immunocytochemistry 30
3.10 DRG analyses and quantification 31
3.11 Fluorescence intensity measurement 32

3.12 Footpad immunohistochemistry 33

3.13 Confocal microscopy acquisition 34

3.14 Quantification of footpad epidermal innervation 35

3.15 Statistical analyses 36

Chapter 4: Results 37

4.1 Confirmation of Pcdh-γ knockdown in uninjured adult mouse DRG neuron through in-cell western assays and fluorescence intensity measurement. 37

4.2 Pcdh-γ knockdown in uninjured adult mouse DRG neuron led to greater total neurite extension and more branchpoints per neuron. 41

4.3 Footpads of mice that received Pcdh-γ siRNA knockdown following sciatic nerve crush injury showed higher number of nerve fibers per epidermal length and area. 45

4.4 Footpads of mice that received Pcdh-γ siRNA knockdown following sciatic nerve crush injury shows increased branching of vertical axons and shorter interfiber distances. 49

4.5 Footpads of mice that received Pcdh-γ knockdown contain more DAPI-stained nuclei per epidermal area and greater DAPI-stained cell size 52

4.6 Rac1 inhibition reverts the increased branchpoints observed in Pcdh-γ knockdown DRG neurons. 54

Chapter 5: Discussion 58

5.1 Knockdown of Pcdh-γ through AAV-Cre recombinase system and siRNA 58

5.2 Impacts of Pcdh-γ knockdown on axon growth 59

5.3 Impacts of Pcdh-γ knockdown on branching complexity 61

5.4 Impacts of Pcdh-γ knockdown on keratinocytes 63

5.5 Rac1 as a possible downstream signaling molecule of Pcdh-γ 64

5.6 Limitations 66

5.7 Future directions 68

Chapter 6: Conclusion 70

References 72

Appendix 79

List of Figures

Figure 1: Structure of footpad epidermal innervation. **79**

Figure 2: Organization of the mammalian clustered protocadherin (Pcdh) gene. **79**

Figure 3: A summarized version of the experimental plan for Experiment 1. ..... **80**

Figure 4: A summarized version of the experimental plan for Experiment 2. ..... **80**

Figure 5: A summarized version of the experimental plan for Experiment 3. ..... **81**

Figure 6: In-cell western assays showing the knockdown of Pcdh-γ in DRG neurons that were transfected with AAV-iCre-mCherry. **82**

Figure 7: Fluorescence intensity measurement confirmed the knockdown of Pcdh-γ in uninjured mouse DRG neurons transfected with AAV-iCre-mCherry. **83**

Figure 8: DRG neurons that received Pcdh-γ knockdown showed greater total neurite extension and more branchpoints per neuron. **86**

Figure 9: Epidermal reinnervation of the footpad of sciatic nerve crushed mice. **87**

Figure 10: Dermal reinnervation of the footpad of sciatic nerve crushed mice following Pcdh-γ siRNA knockdown. **88**

Figure 11: Vertical branching of footpad epidermal reinnervation in mice after sciatic nerve crush injury. **89**

Figure 12: Interfiber distance of the intraepidermal nerve fibers of the footpad of sciatic nerve crushed mice following Pcdh-γ siRNA knockdown. **90**

Figure 13: Number of DAPI-stained nuclei per mm2 of epidermis, DAPI-stained cellular size and number of DAPI-stained nuclei in close contact with axon of the footpad of sciatic nerve crushed mice following Pcdh-γ siRNA knockdown. **91**

Figure 14: Rac1 inhibition reverts the increased branchpoints observed in Pcdh-γ knockdown DRG neurons. **93**

Figure 15: Current progress on breeding for Pcdh-γ conditional knockout mice and behavioural tests that are waiting to be conducted on these mice. **94**

List of Abbreviations

AAV	adeno-associated virus
ATF3	activated transcription factor 3
APC	adenomatous polyposis coli
BDNF	brain-derived neurotrophic factor
CMAP	compound motor action potential
CNS	central nervous system
CNTF	ciliary neurotrophic factor
CV	conduction velocity
DRG	dorsal root ganglion
DPN	diabetic polyneuropathy
DSCAM	down syndrome cell adhesion molecule
GAP-43	growth associated protein 43
HSP27	heat shock protein 27
iCre	improved Cre recombinase
IENF	intraepidermal nerve fibers
MAG	myelin-associated glycoproteins
NGF	nerve growth factor
Nogo	neurite outgrowth inhibitor proteins
nNOS	neuronal nitric oxide synthase
NT-3	neurotrophin-3
Pcdh	protocadherin
Pcdh 7	protocadherin 7
Pcdh-α	protocadherin-alpha
Pcdh-β	protocadherin-beta
Pcdh-γ	protocadherin-gamma
PNI	peripheral nerve injuries
PND	peripheral nerve diseases/peripheral neuropathy
PNS	peripheral nervous system

PTEN	phosphatase and tensin homolog deleted on chromosome 10
Rac1	Ras-related C3 botulinum toxin substrate 1
RAG	regeneration-associated gene
Rb	retinoblastoma protein
qRT-PCR	real time quantitative reverse transcription polymerase chain reaction
rSAC	retinal starburst amacrine cell
SC	Schwann cell
siRNA	small-interfering RNA
SNAP	sensory nerve action potential

Chapter 1: Introduction

The peripheral nervous system (PNS) can be divided into 2 divisions: i) the afferent or sensory division that carries sensory information to the central nervous system (CNS), comprised of the spinal cord and brain for higher processing and ii) the efferent or motor division that carries motor information to the effectors/muscles or organs of the body to initiate a movement/response. The efferent or motor division can be further divided into two subdivisions: i) the autonomic nervous system which regulates involuntary physiological processes such as heart rate, blood pressure, respiration, digestion, sexual arousal and others, and ii) the somatic nervous system which regulates the voluntary control of the body movements through the skeletal muscles[1,2]. As suggested by the word 'peripheral', peripheral nerves are located outside of the CNS and when they are injured or damaged by diseases, communication between the CNS and the rest of the body is disrupted. Peripheral nerve injuries (PNI) and peripheral nerve diseases/neuropathy (PND) are common clinical conditions characterized by varying degrees of sensory, autonomic and motor dysfunction. PNI typically involves an external physical insult to the body: overstretching/crushing of muscles, which can directly lead to nerve contusion or axotomy. Common causes of PNI include vehicular motor accidents, penetrating injuries from knives or firearms, sports injuries, falling and others[3]. According to a study by Li et. al using the National Electronic Injury Surveillance System (NEISS), PNI significantly increased between 2009-2018 ($p=0.002$) with an overall incidence rate reaching 36.9 per 1,000,000 persons per year[3]. PND, on the other hand, does not involve an external physical insult to the body, but is due to pathological dysregulation of nerve functioning arising from disorder or disease conditions. Autoimmune diseases such as the Guillain-Barre syndrome, Sjogren's syndrome, lupus, rheumatoid arthritis are commonly associated with peripheral neuropathy. The most common form of acquired PND, however, comes from diabetes

mellitus[4]. Diabetic polyneuropathy (DPN) which targets over 50% of diabetic mellitus patients, is now known to target over 4% of the Canadian population[5]. In DPN, patients first experience skin numbness in the extremities and eventually may fail to recognize limb sensations or injuries, leading to ulceration and amputation of limbs[5]. Despite the ability of the peripheral nervous system (PNS) to regenerate, functional recovery from PNI and PND are often suboptimal. Patients are often left with debilitating disabilities and dysfunctions, ranging from the loss of skin sensation to allodynia and paresthesia, and in severe cases, autonomic dysregulation and muscle weakness[6,7].

1.1 Cutaneous sensory fibers and their journey to the skin

All cutaneous sensory neurons can be classified as either Aα, Aβ, Aδ or C fibers based on their cell body sizes/axon diameters, degree of myelination and axonal conduction velocities. Out of these four classes of fibers, Aα sensory neuron exhibits the greatest cell body size/axon diameter and the highest degree of myelination. It conducts impulses at the highest velocity (80-120m/s). Aα sensory neuron mediates proprioception and receive information from the muscle spindle and golgi tendon organ (also known as proprioceptors). Aβ sensory neuron also possesses large cell body size/axon diameter and is highly myelinated (although not as extensive as Aα sensory neuron). Aβ fiber conducts impulses at 40-80m/s. Aβ sensory neuron mediates mechanosensation and receives inputs from mechanoreceptors such as Meissner's corpuscles, Pacinian corpuscles, Merkel discs and Ruffini endings. Aδ sensory neuron has lightly myelinated axon processes and exhibits intermediate/slow (5-30m/s) axonal conduction velocities. C-type sensory neurons are the smallest and most abundant, with unmyelinated axons and the slowest conduction velocities (0.5-2m/s). Thinly myelinated Aδ and unmyelinated C fibers displayed high mechanical and thermal thresholds and are therefore thought to be nociceptors[8]. These sensory neurons have their cell bodies located within the dorsal root ganglion (DRG), just outside of the spinal cord. They are

typically pseudounipolar, having a single axon that extends from the cell body which bifurcates into a central process that projects into the dorsal horn of the spinal cord and a peripheral process that travels to the extremities to innervate the body including dermal sensory structures or terminate as free nerve endings in the epidermis[8,9]. For the purpose of this research project, the epidermal innervation of skin by these cutaneous sensory fibers, namely Aδ and C fibers, are of particular interest. Specifically, these cutaneous sensory fibers penetrate the dermal-epidermal junction/basement membrane and form the intraepidermal nerve fibers (IENF) (Figure 1). The assessment of IENF density has gained interest in the recent years for the diagnosis of PNI and PND, as those conditions are often associated with a reduced IENF density[1,10].

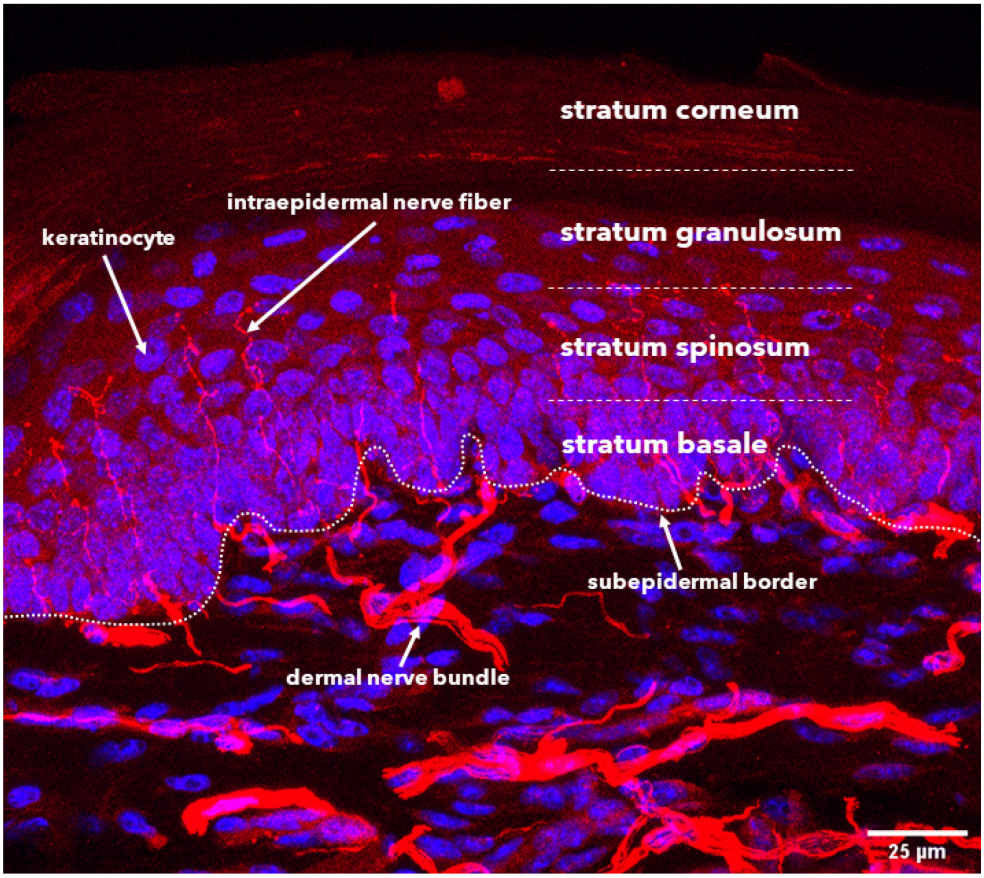

Figure 1: Structure of footpad epidermal innervation. A representative confocal image taken from mouse footpad epidermis section. Intrapidermal nerve fibers (IENF) penetrate the subepidermal border and consist of mainly Aδ and C fibers.

Sensory fibers possess one of the longest axons in the vertebrate animals, reaching a length of about 1m for those axons that innervate the foot of an adult human[11]. As these sensory axons navigate their paths to the extremities, they encounter many different types of tissues and signals. These include other cells in the ganglia from which they originate, the mesenchyme through which they travel through, axons of other neurons with which they fasciculate and the skin cells at their termini[9]. To ensure that these axons reach the correct innervation targets and pattern their receptive fields appropriately, they must be able to integrate those instructive cues that they encounter. Several molecules such as brain-derived neurotrophic factor (BDNF), neurotrophin-3 (NT-3), had been identified by researchers to play a crucial role in guiding the axons to their respective innervation targets[9]. However, the journey does not end at the dermis/epidermis of the skin. Once these cutaneous sensory axons reached their innervation targets, they need to establish their receptive fields and coordinate the partitioning of their dendritic trees with neighbouring terminals. Patterning of the axonal trees is especially important as they ensure optimal coverage of sensory fields so that the organism can accurately detect and localize stimuli along the surface of the body[12]. Molecules such as nerve growth factor (NGF), Plexin A4, Slit/Robo signaling system had been identified by researchers as positive cues that contribute to axon branching and territorial patterning in the skin[9,12]. Alternatively, molecules such as semaphorin had been shown by researchers to provide essential repulsive cues during axon guidance process to prevent misdirected axonal growth[13,14]. Together, these attractive and repulsive components of the microenvironment ensures that axonal growth is favored in the direction of their respective targets.

Often in the case of PNI or PND, axon death/degeneration occurs (see below, 1.2) and this eliminates the repertoire of sensory axons in the epidermis, causing a loss of sensation. For optimal functional recovery, these sensory fibers need to regrow, reinnervate their original/proper targets

and re-establish their axonal territories[9,12]. This process of reinnervation might be an easier task for those axons that innervate discrete structures in the dermis that are already spaced out in an organized manner such as hair follicles, Merkel cells and various corpuscles, but poses a challenge for those cutaneous sensory fibers that penetrate the epidermis and terminate as free endings[9]. Currently, there remains uncertainty over what molecules or signaling pathways regulate the sensory axon pathfinding process in mammals, especially after a PNI where neurons are required to traverse environments rich in growth-inhibitory molecules such as proteoglycans and myelin-associated proteins[15]. Insight on this would be crucial to promote optimal functional recovery in PNI and PND patients.

1.2 Peripheral axon regeneration

Immediately following an acute neuronal injury, a series of well-orchestrated molecular and morphological events are triggered that lead to axon degeneration. 'Wallerian degeneration' is the term that is used to describe the inflammatory responses that are initiated at the distal nerve stump following a nerve transection PNI which lead to distal axon disintegration. 'Wallerian-like degeneration' is a broader term that is used to describe the same series of events and it encompasses all forms of axon injuries[7]. In Wallerian/Wallerian-like degeneration, denervated Schwann cells (SCs) help to remove axon myelin and revert to proliferating state. These formerly myelinating SCs then proliferate within the basal lamina tubes, producing cytokines/trophic factors and phagocytose detached debris[16]. Trophic factors produced by denervated Schwann cells and directly from the injured axons activate resident macrophages and lead to recruitment of hematogenous macrophages. These activated macrophages help to remove axon debris and produce factors that facilitate migrating SCs into forming bands of Büngner[7,11]. At the same time, a 'cell body reaction' first described by Lieberman in 1971, that is characterized by cell soma hypertrophy, displacement

of nucleus to an eccentric position and dissolution of Nissl bodies, starts developing[17].After a lag period, a growth cone emerges from the proximal nerve stump and begins to trail along the bands of Büngner. During axon regeneration, neurotrophic factors such as brain-derived neurotrophic factor (BDNF), nerve growth factor (NGF) and ciliary neurotrophic factor (CNTF) are secreted by those myelinating SCs forming bands of Büngner to guide extending axons towards the appropriate targets[7,16,17].

However, these myelinating SCs/bands of Büngner only accompany regenerating axons as far as the dermal-epidermal junction and for many years, these cutaneous sensory fibers were thought to enter the epidermis as bare axon nerve terminals[7]. It is only until recently that SCs had been shown to exist at the subepidermal border of the skin, extending their processes into the epidermis and forming glia-neural complexes with those cutaneous sensory fibers. Similar to myelinating SCs, Remak SCs associated with unmyelinated axons can also dedifferentiate back to an immature state following PNI to aid in axon regeneration[18]. Surprisingly, these terminal SCs in addition to providing metabolic support for the cutaneous sensory axons, also function as a sensory receptor, intimately associated with the unmyelinated nociceptive nerves and convey noxious thermal and mechanical information to them. Abdo et al. showed that these terminal SCs act like chemical synapses and optogenetic stimulation of these SCs were able to elicit firing activities in the cutaneous sensory neurons, initiating pain sensation and resulting in nocifensive behaviours in mice[19]. A series of intrinsic alterations involving downregulation of constitutively expressed neuronal molecules such as neurofilament subunits, neuropeptides, and upregulation of regeneration-associated genes (RAGs) also developed within the perikarya following PNI to aid in regeneration[20,21]. Examples of upregulated RAGs include β-tubulin which has been shown to be crucial for growth cone advancement, growth-associated protein 43 (GAP-43) which has been

shown to aid in neuronal pathfinding and branching during regeneration, activated transcription factor 3 (ATF3) that promotes the intrinsic growth state of injured axons, etc[7,22–24]. Other RAGs such as neuronal nitric oxide synthase (nNOS), galanin peptide, heat shock protein 27 (HSP27) have also been implicated in peripheral nerve regeneration[7]. The full list of RAGs is still being explored using RNA sequencing and how exactly RAGs exert their influence on regeneration at both the level of the perikaryon and distal nerve branches are not well understood. For instance, calcitonin gene-related peptide (CGRP) is downregulated at the perikarya of sensory neurons following an injury, yet distal regrowing branches showed a rise in CGRP mRNA expression through local axon synthesis[25]. In contrast, GAP43 is upregulated at both the perikarya and outgrowing axons following an injury[26]. All these events are thought to establish a conducive microenvironment for axon regeneration so that optimal functional recovery following PNI or in PND could be achieved.

Besides the events that happen within and around the injured axon, collateral sprouting of adjacent intact nerves has also been shown to be one of the mechanisms contributing to functional recovery/reinnervation after PNI[27,28]. Following rapid Wallerian-like degeneration, a growth-permissive environment free of growth inhibitory proteins such as myelin-associated glycoproteins (MAG) and neurite outgrowth inhibitors (Nogo), and rich in neurotrophic factors (mainly mediated by the dedifferentiation of mature SCs) is produced around the injured axon region. Local undamaged neurons can then respond to this injury-induced environment by extending their axon sprouts to functionally synapse with the denervated targets[29]. Nevertheless, how those locally undamaged neurons overcome the inhibitory barrier of their own SCs and myelin proteins, which normally are restricting axonal growth to maintain axonal function is not well understood[30].

Whether this process of collateral sprouting activates a transcription program similar to those of the newly developing neurons has yet to be explored.

1.3 Limitations of peripheral axon regeneration

Over the past century, two dogmas have dominated the field of nerve regeneration in mammals: i) CNS neurons lack the ability to regenerate and ii) PNS neuron can regenerate easily and completely[15]. The first of these dogmas had already been disproved by Albert Aguayo and colleagues in a series of elegant experiments showing that CNS neurons when placed in a PNS environment, can regenerate in adult rats after experiencing a focal injury[31,32]. The second dogma, however, has been more difficult to challenge. Despite the remarkable ability of PNS neurons to regenerate, this does not always translate into successful functional recovery in patients. The major underlying factors for these suboptimal outcomes could be attributed to the failure of SCs in maintaining a growth permissive environment, the slow rate of axon growth (1-4mm per day) and the inability of axons to sustain RAG upregulation for the course of regeneration[7,15,20,21]. Furthermore, research studies on PNI often employed rodent models where the distance over which injured nerves are required to regenerate is small compared with human nerve injuries[15]. Oftentimes, these models may not fully recapitulate the PNI and PND in humans, rendering challenges in identifying useful therapeutic advances for clinical trials. SCs, being a major player in axon regeneration, after losing axonal contact for a prolonged period of time (chronically denervated), undergo atrophy and the bands of Büngner eventually disintegrate, leaving regrowing axons with no extrinsic support. Gordon and colleagues have shown that this decline of regenerative capacity in chronically denervated nerves starts at 8 weeks after injury and 6 months into chronic denervation, there is almost no regeneration from axons[33]. In recent years, there have been significant advancements in human nerve repair, however, most of these developments are

limited to the optimization of surgical techniques and there remains a lack of therapeutic approaches directed at the molecular mechanisms of nerve regeneration[15].

1.4 Molecular approach to promote axon regeneration

Due to the aforementioned challenges (refer to 1.3), successful axon regeneration that results in optimal functional recovery in patient is rarely achieved. To overcome those challenges, the options are to identify how to accelerate the intrinsic growth rate of axon regeneration or to sustain the growth-permissive environment provided by Schwann cells and upregulation of RAGs[15]. Molecular targets which play a role in cell growth are of particular interest since amplifying their signals may allow us to augment the process of axon regeneration. Several tumour suppressor proteins such as phosphatase and tensin homolog deleted on chromosome 10 (PTEN), adenomatous polyposis coli (APC) and retinoblastoma protein 1 (Rb1), have been identified and studied by the Zochodne laboratory to provide valuable insight in developing novel molecular approaches for treating PNI and PND. Inhibition of the aforementioned tumour suppressor proteins' signaling through administration of small-interfering RNA (siRNA) or pharmacological inhibitors is associated with improved axon regeneration[34–36].

Besides enhancing neurite outgrowth, insights on how newly regrowing axons reconnect with their original targets such as the skin, and what molecules influence this process of reinnervation are of particular importance if optimal functional recovery from PNI and PND is to be achieved. This thesis project will focus on protocadherin-gamma (Pcdh-γ), a molecule that has recently come under the research spotlight as a candidate to act as cell identity marker in the mammalian nervous system (refer to section 2). Through studying this molecule and its role in the

mammalian PNS, we hope to better understand one promising molecular mechanism that underlies sensory axon pathfinding and patterning during epidermal reinnervation.

Chapter 2: Protocadherin-gamma (Pcdh-γ)

2.1 The Chemoaffinity Hypothesis

In the establishment of neurocircuitry, neurons and their axons have to reach the correct innervation targets in an orderly and timely fashion, and pattern their processes in an appropriate manner such that information could be relayed to other neurons or CNS. Two elegant studies had sparked an idea among researchers on how neurons form these complex patterns of synaptic connections that underlie our sensations and behaviours. The first experiment done by Langley in 1895 analyzed regeneration in the autonomic nervous system of a cat[37]. Langley observed that axons from multiple levels of the spinal cord (C1-C4 cervical nerves) entered the superior cervical ganglion but eventually went on and innervated distinct peripheral organs. When these sympathetic nerves were cut and allowed to regenerate, surprisingly, the fibers of each spinal nerve only become connected with those targets with which they were previously connected to despite the new axons entering the same ganglion and having encountered intermixed targets[37,38]. The second series of experiments done by Roger Sperry assessed the return of visual function following the transection of optic nerves in amphibia: newts, toads and frogs (central axons regenerate poorly in mammals but well in lower vertebrates). The most ground-breaking finding from the work is that with rotation of the eye, orderly but inverted vision was restored, meaning that the animal behaved as if it saw the world in an upside-down fashion. The implication was that the retinal axons had regenerated and reconnected with their original synaptic targets but not the targets that would now make functional sense (since the eyeballs were rotated, the retinal axons should reconnect with new synaptic targets but not their original targets which were in inverted alignment, if upright vision was to be restored)[38–41]. Both of the studies drew similar conclusions that there must be "some special chemical relation between each class of nerve fibers such that they are induced to

grow towards a cell of its own class and form its terminal branches"[37–41]. Furthermore, both researchers proposed that this kind of cell recognition was likely to involve interactions along the path that axons traverse as they grow towards their targets as well as at the target itself, processes now called axon guidance and target selection, respectively[37,38,40]. The chemoaffinity hypothesis states that neurons make synaptic connections with their targets based on interactions with specific molecular markers and these markers aid not only with synaptogenesis, but also act as guidance cues for their respective axons[38,40,42].

During development or regeneration, the proper establishment of neurocircuitry requires neurons to be able to demonstrate self-avoidance: a phenomenon whereby neurites arising from the same cell body/neuronal subtype able to recognize and repel each other (self/non-self recognition). By doing so, innervation redundancy is avoided and optimal coverage of a receptive field by different types of neurons is enabled[38,43]. Given the wide variety of neuronal subtypes that exists within the nervous system, the molecules that can serve as cell identity markers must fulfill the following roles: i) offer a huge diversity of isoforms, ii) each isoform must possess distinct binding specificities and iii) differential expression among neurons to stamp each neuron with a distinct identity[38]. Not surprisingly, this molecule/protein typically arises from a multigene family. In Drosophila melanogaster, it has been confirmed that down syndrome cell adhesion molecule (DSCAM) 1 from the larger DSCAM family is responsible for stamping neuronal identity[44–46]. In mammals, evidence suggests that clustered protocadherin (Pcdh), particularly protocadherin-gamma (Pcdh-γ), one of the three subfamilies of Pcdh, as being a strong candidate to serve as cell identity marker.

2.2 Clustered protocadherin (Pcdh)

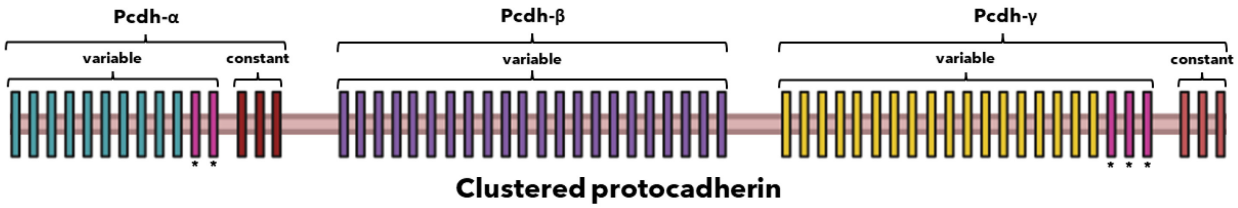

Figure 2: Organization of the mammalian clustered protocadherin (Pcdh) gene. Pcdh gene is organized into three subclusters: Pcdh-α (cyan), Pcdh-β (purple) and Pcdh-γ (yellow). Pcdh-α and Pcdh-γ contain variable exons and constant exons while Pcdh-β contains only variable exons. Variable exons marked with * are more closely related to each other than with those within their subclusters. During splicing, a unique promoter is chosen stochastically to encode a single variable exon and then spliced onto the 3 constant exons downstream which encode for the intracellular domain. Pcdh-β does not contain constant exons and each of its 22 variable exons encode the entire transmembrane protein with unique intracellular domain.

Clustered protocadherin (Pcdh) is the largest subgroup in the cadherin superfamily of homophilic cell adhesion proteins. Pcdh genes are primarily expressed within the mammalian nervous system and their protein products are concentrated at, but not restricted to synaptic sites[47,48]. Pcdh genes are organized into three subfamilies, namely Pcdh-α, Pcdh-β and Pcdh-γ, each containing 14, 22 and 22 variable exons respectively (Figure 2). During transcription, a unique promoter is stochastically chosen which encodes a single variable exon out of these three gene subclusters. For Pcdh-α and Pcdh-γ, each variable exon encodes the extracellular and transmembrane domains of the protein, which is then spliced with constant exon encoding a common intracellular domain. Pcdh-β does not contain constant exons and each of its 22 variable exons encode the entire transmembrane protein with unique intracellular domain[38]. Products of Pcdh interact through homophilic binding in an isoform-dependent manner with products of all three subclusters to form homo-/hetero-multimers. Specifically, Schreiner and Weiner have shown that Pcdh-γ forms cis-tetramers on the same cell surface and engages in homophilic binding with tetramers on other cell surfaces. Given the fact that Pcdh-γ contains 22 variable exons, unrestricted

tetramerization in a cis manner (interactions with other isoforms on the same cell surface), coupled with strictly homophilic binding interactions in trans fashion (interactions with other tetramers on other cell surfaces) allow 234256 distinct adhesive interfaces to be formed[49,50]. Taking into account of Pcdh-α and Pcdh-β in multimer formation, this combinatorial expression could greatly expand the repertoire of specificities, allowing Pcdh to stamp each neuron with distinct identity. To date, Pcdh is believed to be the best candidate to act as a cell identity marker in the mammalian nervous system.

2.2 Roles of Pcdh in the CNS

Out of the three subclusters of Pcdh, Pcdh-γ is the most extensively studied, followed by Pcdh-α, while Pcdh-β is the least studied. Mice lacking Pcdh-α were viable and fertile but displayed a decrease in dendrite arborization and spine loss in hippocampal neurons, both *in vitro* and *in vivo*[51]. Furthermore, Pcdh-α mutant mice showed abnormal sorting of olfactory sensory neurons into glomeruli, a defect that parallels those observed in the olfactory system of fly DSCAM1 mutants, indicating that Pcdh-α play a role in axon guidance and targeting[52,53]. Loss of Pcdh-γ, in contrast, is associated with devastating neurological defects and neonatal lethality. Mice with Pcdh-γ global knockout experienced massive apoptosis of spinal interneurons but neurons in retinal, cerebral cortex, cerebellum and hippocampus appeared to be spared, showing that Pcdh-γ is dispensable in certain neuronal subtypes[54].

Similar to Pcdh-α, Pcdh-γ conditional knockout/knockdown is associated with reduced dendritic arborization in cortical layer V pyramidal neurons (apical and basal dendrites), hippocampal neurons, subventricular zone progenitor cells and olfactory bulb granule cells[51,55,56]. This redundancy of functions between Pcdh-α and Pcdh-γ might just be the consequence of

combinatorial expression of Pcdh isoforms. The most captivating finding, however, is that Pcdh-γ seems to be the molecule that mediates neurite self-avoidance in the CNS. One of our collaborators on this project, the Lefebvre laboratory from the University of Toronto, has shown that Pcdh-γ knockout in retinal starburst amacrine cells (SACs) and cerebellar Purkinje cells led to aberrant self-crossing of sister/isoneuronal dendrites[57]. However, the researchers also showed that introduction of a single Pcdh-γ isoform expression rescues this self-avoidance defect, as long as other neuronal subtypes in the surrounding express the wild type Pcdh-γ gene. Surprisingly, introduction of only a single Pcdh-γ isoform into the system decreased the interactions among dendrites of neighbouring SACs (reduced heteroneuronal interactions)[57]. These findings suggest that homophilic Pcdh-γ interactions generate a repulsive signal that leads to neurite self-avoidance. Furthermore, this process of neurite self-avoidance appears to rely solely on the differences between the isoforms expressed on neurons rather than the particulars of their identity. In other words, no single Pcdh-γ isoform seems to be necessary and any isoform is sufficient for neurite self-avoidance. To date, most of the research done on Pcdh are limited to the CNS and the role of Pcdh in the PNS, especially in the context axon regeneration is not known.

Dr. Long (previously a graduate student in the Zochodne laboratory who completed her PhD in 2020) showed that Pcdh-γ siRNA knockdown *in vitro* led to greater neurite outgrowth. Uninjured DRG neurons that received Pcdh-γ siRNA knockdown exhibited longer total neurite extension, more branches and branchpoints per neurons, a result that was not expected given the findings in the CNS[58]. Furthermore, staining of Pcdh-γ showed that this protein is expressed throughout the mammalian PNS, not limited to neuron only (axon and soma), but also in skin (keratinocytes)[58]. Given the research foundations of Pcdh-γ roles in the CNS, these intriguing findings by Dr. Long prompted us to study the roles of Pcdh-γ in the mammalian PNS, especially

in the context of epidermal reinnervation where axons are required to arrive at the right locations and establish their repertoire (proper patterning) with the right targets, a process analogous to the establishment of neurocircuitry during development.

2.3 Project rationale

This thesis project aims to address the gap in research about the roles of Pcdh-γ in the mammalian PNS by employing both *in vitro* and *in vivo* model. This thesis project is in collaboration with Dr. Long (Zochodne laboratory) and with help from the Lefebvre laboratory (University of Toronto).

Overall hypothesis: Inhibition of Pcdh-γ expression in sensory axons and skin increases neurite outgrowth and promotes skin epidermal reinnervation.

2.3.1 Experiment 1

Objective: To re-evaluate the *in vitro* impact of Pcdh-γ knockdown on neurite outgrowth, using adeno-associated virus (AAV) expressing Cre recombinase on mouse DRG neurons with floxed Pcdh-γ gene ($Pcdh^{flox/flox}$).

Hypothesis: DRG neurons from the adult Pcdh-γ double-floxed ($Pcdh\text{-}\gamma^{flox/flox}$) mice which are transfected with Cre expressing AAV will display greater peripheral neuron growth (DRG neuron growth) compared to those that received control AAV (without Cre).

Rationale: Validation for this work and approach is available in previous work from our laboratory[58]**.** Previously, the Zochodne laboratory reported that knockdown of retinoblastoma protein 1 (Rb1) through administration of siRNA led to greater DRG neurite outgrowth *in vitro*. Furthermore, mice that underwent sciatic nerve transection injury in the setting of Rb1 knockdown

using adenovirus expressing Cre recombinase (Ad-CMV-Cre) showed improved axon regeneration (both axon profile and behaviour)[36]. Dr. Long adopted a similar protocol in her *in vitro* Pcdh-γ studies and examined the impact of siRNA knockdown of Pcdh-γ in uninjured adult DRG neurons. She found that DRG neurons which received Pcdh-γ siRNA knockdown exhibited longer total neurite extension, more branches and branchpoints per neuron compared to those that received scrambled siRNA (control)[58]. To confirm these results, in this thesis project, AAV expressing Cre recombinase was employed to knockdown Pcdh-γ *in vitro* in uninjured DRG adult neurons with double floxed Pcdh-γ gene (Pcdh-$\gamma^{flox/flox}$). In the CNS, knockdown of Pcdh-γ in the retinal starburst amacrine cells (SACs) and Purkinje neurons was associated with neurite self-avoidance defects such as fasciculation of dendrites and extensive overlapping of sister dendrites (refer to 2.2)[57]. Therefore, to expand on Dr Long's finding, sister neurite and neighbouring neurite crossings of cultured DRG neurons (isoneuronal and heteroneuronal neurite interactions) were also examined in this experiment.

Experimental Plan: The Lefebvre laboratory from the University of Toronto had kindly donated 2 female adult Pcdh-γ double-floxed mice (Pcdh-$\gamma^{flox/flox}$) and a breeding colony was set up to maintain this line of mice. Uninjured DRGs from both male and female adult Pcdh-γ double-floxed mice were harvested and cultured in media containing either AAV-iCre-mCherry (Pcdh-γ knockdown group) or AAV-mCherry (control group) (refer to 3.5, 3.6). After 24 hours, cell cultures were fixed and stained for analyses (refer to 3.9). Using WIS Neuromath software, I examined the total neurite extension per neuron, proportion of neurons sprouted, average neurite projection length per neuron, number of branches and branchpoints per neuron. Using manual counting method, I also evaluated the total number of crossings/interactions between isoneuronal neurites and heteroneuronal neurites (refer to 3.10). For isoneuronal neurite interactions/neurite

self-crossings, 300 DRG neurons were randomly chosen for evaluation (50 DRG neurons per culture from a total of 6 cultures). For heteroneuronal neurite interactions/neighbouring neurite crossings, 41 pairs of DRG neurons from Pcdh-γ knockdown group and 36 pair of DRG neurons from control group were chosen for evaluation. To confirm the knockdown of Pcdh-γ in the DRG neurons, in-cell western assays were performed (refer to 3.7). Fluorescence intensity measurement was also performed to provide additional result/further confirmation for Pcdh-γ knockdown in DRG neurons (refer to 3.11). A summarized figure version of this experimental plan can be found in Figure 3.

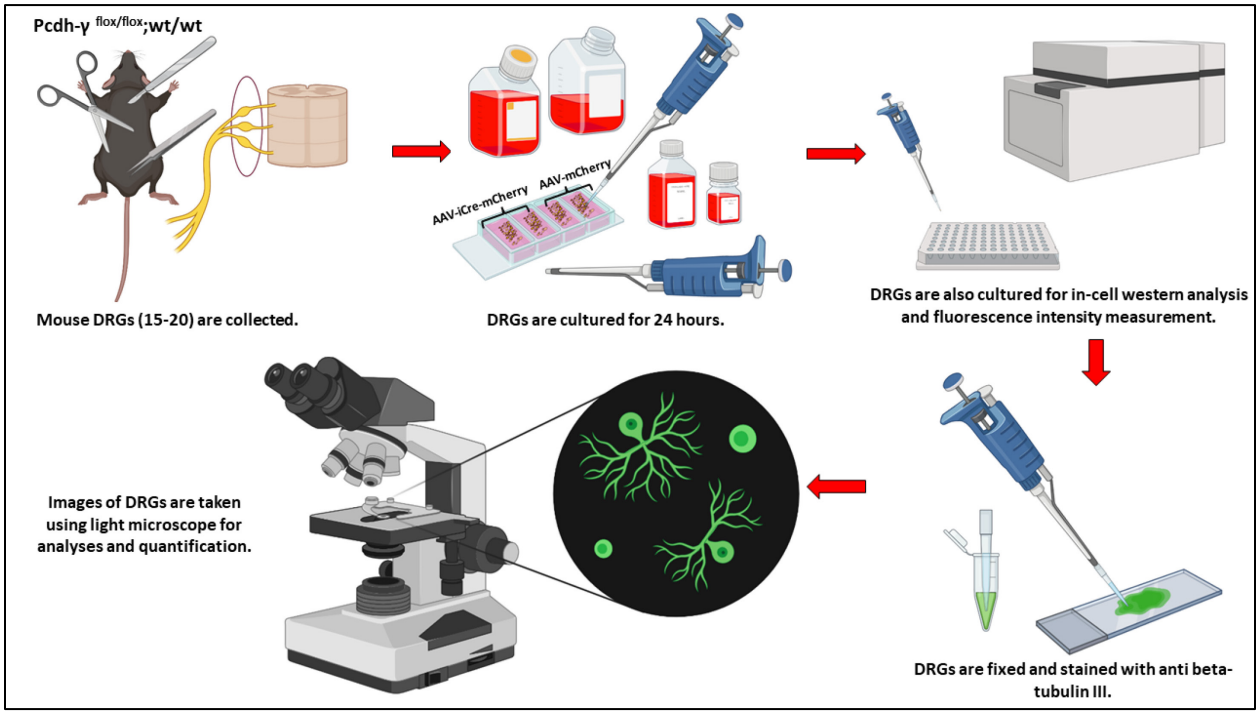

Figure 3: Figure shows a summarized version of the experimental plan for Experiment 1. Objective: To re-evaluate the *in vitro* impact of Pcdh-γ knockdown on neurite outgrowth, using adeno-associated virus (AAV) expressing Cre recombinase on mouse DRG neurons with floxed Pcdh-γ gene ($Pcdh^{flox/flox}$).

2.3.2 Experiment 2

Objective: To determine the *in vivo* effect of Pcdh-γ knockdown on peripheral axon regeneration following an injury using a mouse model.

Hypothesis: Footpads of mice that received Pcdh-γ siRNA knockdown following sciatic nerve crush injury will display greater epidermal reinnervation compared to those that received scrambled siRNA.

Rationale: As mentioned previously (refer to 2.2), in Dr. Long's PhD work, it was noted that *in vitro* siRNA knockdown of Pcdh-γ in uninjured adult DRG neurons led to greater neurite outgrowth[58]. This finding is certainly unexpected because CNS studies revealed that global knockout of Pcdh-γ in mice were associated with massive spinal interneuron apoptosis and conditional knockdown of Pcdh-γ was associated with thinner cortical layer V due to a decrease in dendritic arborizations, both of which are signs of axon loss[51,54,55]. These CNS studies, however, emphasized the role played by Pcdh-γ during the developmental stage of the mouse and we wonder if Pcdh-γ would continue to play the same roles during axon regeneration following PNI where neurons need to regrow and arrive at the correct targets for reinnervation (a process analogous to the establishment of neurocircuitry during development). Furthermore, Dr. Long showed that Pcdh-γ was expressed in both the sensory neurons and keratinocytes, suggesting that there might be an important interaction between them as sensory axons are required to reinnervate the skin (keratinocytes) after PNI if proper functional recovery is to occur[58]. Our hypothesis is based on the possibility that loss of Pcdh-γ might reduce repulsive interactions between the axons and keratinocytes as both express Pcdh-γ.

Experimental plan: The first part of the experiment: inflicting sciatic nerve crush injury to the mice and administering siRNA (either Pcdh-γ siRNA or scrambled siRNA) was completed by Dr. Long in 2019 (refer to 3.3, 3.4). Four different groups were set up for this experiment: i) PCDH siRNA ipsi group: right footpad of mice that underwent sciatic nerve crush injury at its right hindlimb and received Pcdh-γ siRNA knockdown, ii) PCDH siRNA contra group: left footpad of mice of PCDH siRNA ipsi group that received no sciatic nerve crush injury and no injection, iii) SCR siRNA ipsi group: right footpad of mice that underwent sciatic nerve crush injury at its right hindlimb and received scrambled siRNA knockdown and iv) left footpad of mice of SCR siRNA ipsi group that received no sciatic nerve crush injury and no injection (refer to 3.4). PCDH siRNA ipsi and SCR siRNA ipsi are the treatment groups while PCDH siRNA contra and SCR siRNA contra groups are the controls for their respective groups. After the *in vivo* siRNA knockdown procedures, footpads of those mice were harvested and transferred to me for fixation and cryoprotection. The rest of the experiment (further processing and analyses) was all completed by myself. Footpad tissues were sectioned and stained (refer to 3.12). Confocal images of the epidermal innervation pattern of these footpads were taken and analyzed (refer to 3.13, 3.14). Instead of confining the analysis to axon counts, a measure known as intraepidermal nerve fiber density (IENFD) as suggested by the European Federation of Neurological Societies (EFNS) in human work, we expanded our analysis of skin epidermal reinnervation (refer to 3.14). To study the interactions of keratinocytes with axons, we evaluated the number of DAPI-stained keratinocytes per epidermal area, size of DAPI-stained keratinocyte and the number of DAPI-stained keratinocytes in close contact with axons. Since Pcdh-γ knockdown has been associated with dendrite fasciculation and branching defect in the CNS, we also decided to look at the number of branching neurites from the axons and their interfiber distances. Lastly, the number of dermal

axons was also included to check if the effect of Pcdh-γ knockdown starts manifesting before those cutaneous sensory neurons penetrate the subepidermal border/basement membrane. To summarize, the twelve analyses of skin epidermal innervation are: i) number of axons per mm^2 (per epidermal area), ii) number of axons per mm (per epidermal length), iii) number of vertical axons per mm, iv) number of horizontal axons per mm, iv) number of branching neurites from vertical axons, v) interfiber distances (10-30µm/ short; 30-50µm/ medium; >50µm/ long), vi) number of dermal axons, vii) number of vertical dermal axons, viii) number of horizontal dermal axons, ix) number of DAPI-stained nuclei per mm^2 (per epidermal area), x) number of DAPI-stained nuclei touching or in close contact (<10µm) with axons, xi) number of DAPI-stained nuclei in close contact per mm of axons and xii) DAPI-stained cell size (refer to 3.14). There were 4 samples for each group and for each sample, 15 images were randomly taken across the footpad sections of that particular sample using a confocal microscope. A total of 240 footpad images (60 for each group) were analyzed for each of the 12 aspects of skin epidermal innervation that were previously mentioned. A summarized version of this experimental plan can be found in Figure 4.

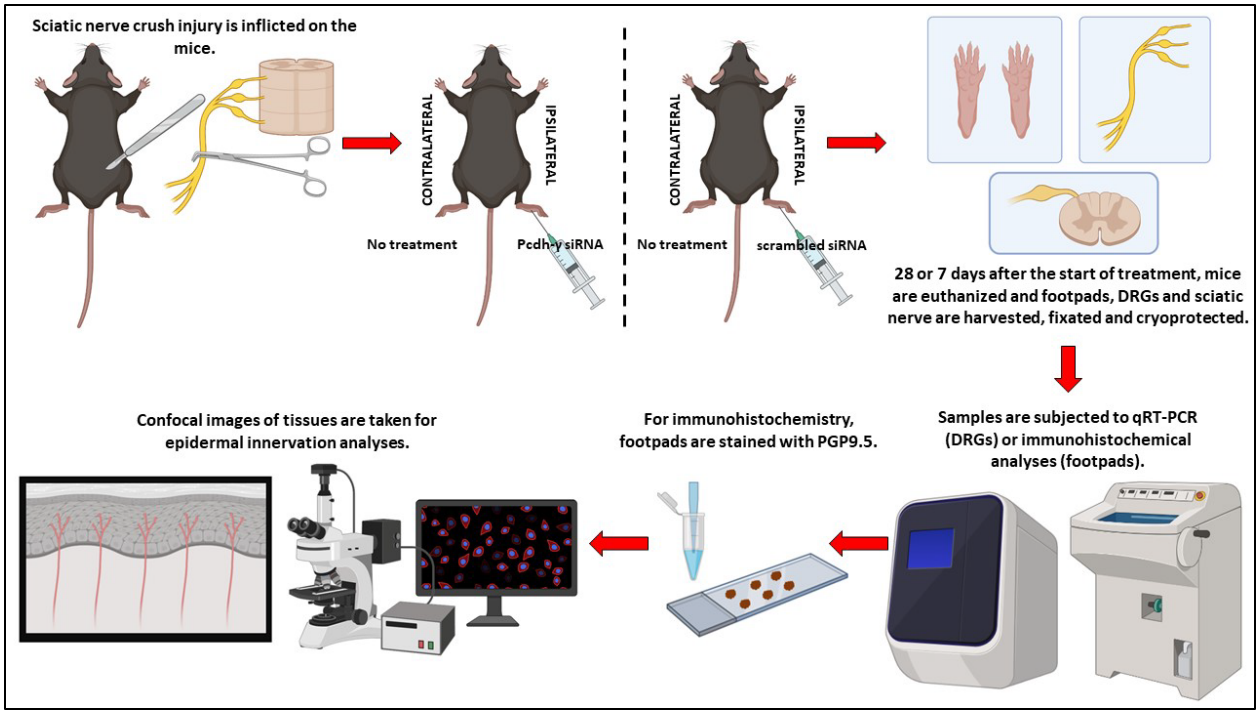

Figure 4: A summarized version of the experimental plan for Experiment 2. Objective: To determine the *in vivo* effect of Pcdh-γ knockdown on peripheral axon regeneration following an injury using mouse model.

2.3.3 Experiment 3

Objective: To determine the impact of Rac1 inhibition on DRG neurite outgrowth as one of the possible downstream signaling cascade for Pcdh-γ knockdown.

Hypothesis: Rac1 inhibition attenuates the increased total neurite extension and branchpoints per neuron observed from Pcdh-γ knockdown.

Rationale: Rac1 (Ras-related C3 botulinum toxin substrate 1) is a member of the Rho GTPases family. Rho GTPases act as molecular toggle switches, cycling between the active GTP-bound state and inactive GDP-bound state to regulate cytoskeletal dynamics. Specifically, Rac1 has been shown to act as one of the central regulators of actin reorganization and in the nervous system,

Rac1 has been implicated in cellular processes such as cell proliferation, neuronal migration and axon development[59,60]. Suo et al. showed that in CNS, hippocampal neuron dendritic branching defects caused by Pcdh clusters knockdown (Pcdh-α and Pcdh-γ) could be rescued by transfecting the cells with Rac1V12 (a constitutively active form of Rac1). It was also revealed that proline-rich tyrosine kinase 2 (Pyk2) inhibits Rac1 as overexpression of Pyk2 caused a decrease in activation of Rac1 and hence the subsequent dendritic (and spine) defects in hippocampal neurons. Furthermore, inhibition of Rac1 alone was sufficient to recapitulate the dendritic simplification defects observed from Pcdh clusters knockdown. These findings led the researchers to propose a model that Pcdh regulate the dendritic complexity by activating Rac1 through inhibition of Pyk2[51]. However, one thing to be noted is that Rac1V12 failed to rescue the spine loss (loss of typical mushroom-/stub-shaped dendritic spines) observed in hippocampal neurons of Pcdh clusters knockdown mice, indicating that Pcdh might regulate spine morphogenesis through a different downstream signaling molecule[51]. Studies looking at protocadherin 7 (Pcdh7), a member of the non-clustered Pcdh subgroup of the cadherin superfamily also reported that osteoclast differentiation defects observed in Pcdh7 knockout mice could be rescued with retroviral transduction of the constitutively active form of Rac1, further supporting the role of Rac1 as a downstream signaling molecule of Pcdh[61]. Based on these findings, we wondered if Pcdh-γ exerts its impact on neurite outgrowth in the PNS using a similar downstream signaling cascade. If Rac1 activation is required to rescue branching simplification defects observed from Pcdh clusters knockdown hippocampal neurons, we would expect that Rac1 inhibition in the DRG neurons would exacerbate branching defects, perhaps severely reducing the number of branches and branchpoints per neuron. Hence, *in vitro* experiments using uninjured adult mouse DRG neurons were set up to compare the difference in neurite outgrowth between those that received only Pcdh-

γ knockdown and those that received both Pcdh-γ knockdown and Rac1 inhibition. In our work, we questioned whether enhanced neurite outgrowth and branching that follows Pcdh-γ knockdown might rely on Rac1 action within growth cones or other parts of the neuron.

Experimental plan: For this experiment, DRGs from both male and female adult Pcdh-γ double-floxed (Pcdh-$\gamma^{flox/flox}$) mice were harvested and cultured in media in a 4-well chamber slide (refer to 3.5, 3.6). These harvested DRGs were split evenly into four groups: i) Pcdh-γ knockdown group: those that received AAV-iCre-mCherry, ii) Pcdh-γ knockdown + Rac1 inhibitor group: those that received AAV-iCre-mCherry + Rac1 inhibitor, iii) control group: those that received AAV-mCherry and iv) control + Rac1 inhibitor group: those that received AAV-mCherry + Rac1 inhibitor (refer to 3.8) to determine the impact of Rac1 inhibition on neurite outgrowth. After 24 hours, cell cultures were fixed and stained for analyses (refer to 3.9, 3.10). A summarized figure version of this experimental plan can be found in Figure 5.

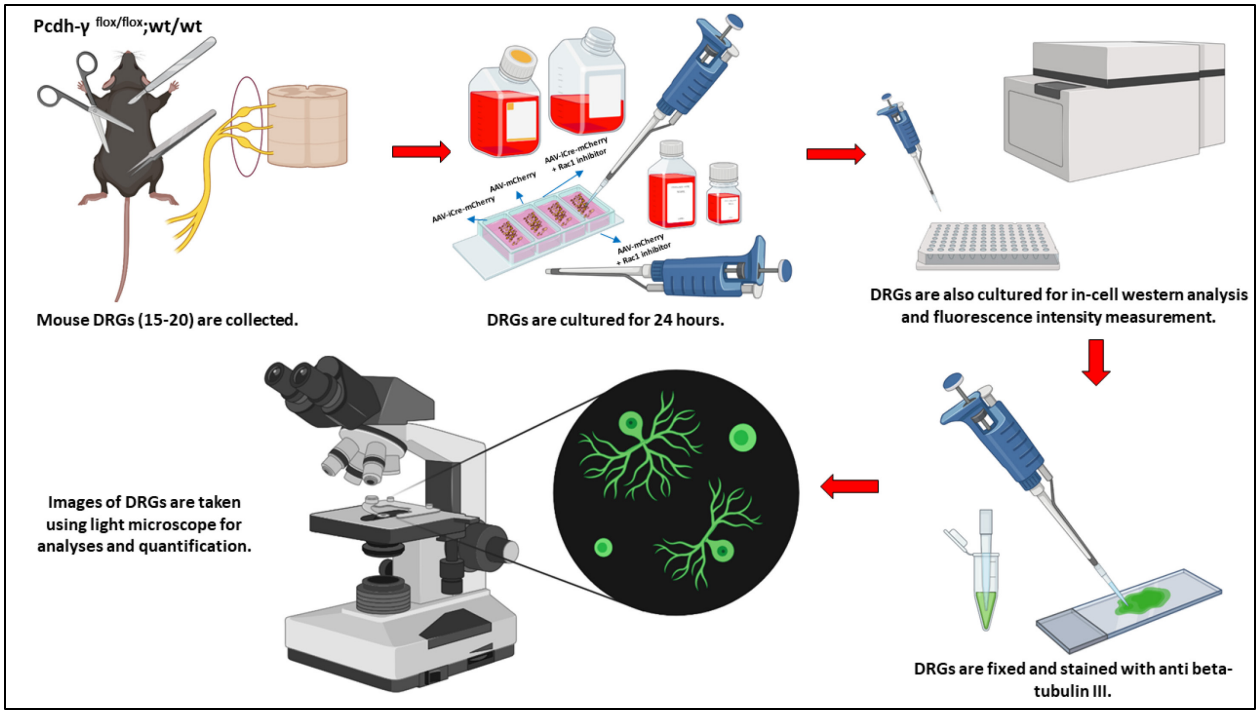

Figure 5: A summarized version of the experimental plan for Experiment 3. Objective: To determine the impact of Rac1 inhibition on DRG neurite outgrowth as one of the possible downstream signaling cascade for Pcdh-γ knockdown.

Chapter 3: Experimental Procedures and Methods

3.1 Animal care

C57BL/6 mice of both sexes were used for all experiments. All mice used were of 6 to 20 weeks old (adult). All experiments were carried out according to the approved standards of operating procedures and complied with the University of Alberta Animal Care and Use Committee, following guidelines from the Canadian Council on Animal Care.

3.2 Animal euthanasia

Mice were euthanized through cardiac exsanguination after reaching a surgical anesthetic plane following inhalation of isoflurane. Anesthetized mice were then placed in supine position and an incision was made on the skin region overlying the sternum. The diaphragm of the mouse was cut using surgical scissors to expose the heart. The left ventricle of the heart was then snipped to allow for exsanguination. All mice were then subjected to a secondary euthanasia procedure: cervical dislocation, to ensure death.

3.3 Sciatic nerve crush injury

Mice were anesthetized using inhaled 2% isoflurane. After the mouse had reached surgical plane, the right hind leg of each mouse was shaved and disinfected. While keeping the mouse at surgical plane, the mouse was placed in prone position and the femur was located before a small incision below that bone was made to expose the sciatic nerve. The entire sciatic nerve trunk was then crushed using forceps (holding the forceps for 15 seconds) in two orthogonal orientations (ie. 90°), rendering the crushed sciatic nerve trunk ‘translucent’. The wound was then sutured and checked twice a day post-surgery to ensure that there was no infection or inflammation. All mice

that had undergone the sciatic nerve crush injury was also administered buprenorphine (analgesia) through subcutaneous injection twice a day during daily checking for three days post-surgery[58].

3.4 siRNA *in vivo* knockdown model

Prior to injections into the mouse, Pcdh-γ siRNA or scrambled siRNA (negative control) was first mixed with HiPerfect Transfection Reagent (Qiagen) and left to sit for 15 minutes at room temperature. Saline was also added to the mixture to increase the volume of bolus injected into the animal. 50µL of the siRNA solution (5µL/0.1nmol of siRNA + 15µL of HiPerfect Transfection Reagent + 30µL of saline solution) was administered directly to the nerve following sciatic nerve crush injury. After administration, the wound was sutured and the site of incision was electroporated with five 25V pulses lasting 50ms each, delivered at 1Hz with an ECM830 Electro Square Porator ™ unit, to facilitate the transfection of siRNA into the cells. 20µL of the siRNA solution (3µL/0.06nmol of siRNA + 9µL of HiPerfect Transfection Reagent + 8µL of saline solution) was injected subcutaneously to the plantar surface of the right/ipsilateral (sciatic nerve crushed) hindpaw and electroporated as above. The injections were repeated at both side 3 times a week. A total of 12 injections spanning 28 days were administered to each mouse. The injections at the sciatic nerve crush site, except for the initial injection, which was administered directly to the nerve (following the procedure of sciatic nerve crush), were all done percutaneously above the incision site as the sutures were not reopened[58].

3.5 Cell culture

Adult mice were euthanized according to the procedure stated above in 3.2. The spinal cord was isolated and dorsal root ganglions (DRGs) (15 to 20, all levels of spinal cord) were harvested and placed into ice cold L-15 media (Thermo Fisher). DRGs were then rinsed twice, using fresh

L-15 media and placed into 1% collagenase D solution (Roche Applied Science, Budapest, HUN) dissolved in L-15 and incubated at 37°C for 45 minutes. Following collagenase D digestion, DRGs were resuspended through trituration to ensure that they reached a single cell suspension. This single cell suspension was centrifuged at 800RPM for 6 minutes at room temperature. The pellet of DRGs was then resuspended in fresh L-15 and poured through a 70μm mesh. The suspension was again centrifuged at 800RPM for 6 minutes and the pellet of DRGs was then resuspended in fresh L-15. This suspension mixture was then carefully pipetted and placed on top of 15% bovine serum albumin (BSA) dissolved in L-15. Centrifugation at 800RPM for 6 minutes at room temperature was again performed to passage the suspension mixture through 15% BSA gradient. Tissue debris and Schwann cells (supernatant) from this step were then removed and the pellet was resuspended in fresh media containing Dulbecco's Modified Eagle Medium (DMEM, Gibco), N-2 supplement (Gibco), NGF (Invitrogen), cytosine-β-arabinofuranoside (Sigma-Aldrich, St. Louis, MO), penicillin and streptomycin.

Equal amounts of the cell suspension (200μL) were distributed to each well of a 4-well chamber slide (Fisher, Walthan, MA) containing 800μL of prepared media. All 4 wells were pre-treated with 0.1% poly-L-lysine and 10μg/mL of laminin. All cell cultures in this project were incubated at 37°C for 24 hours.

3.6 *in vitro* Pcdh-γ knockdown experiment by AAV-Cre

DRGs (15-20) were harvested from C57BL/6 mice of both sexes (3 males, 3 females) with the genotype: Pcdh-$\gamma^{flox/flox}$. The Lefebvre laboratory from the University of Toronto had kindly donated 2 female adult Pcdh-γ double-floxed mice (Pcdh-$\gamma^{flox/flox}$) and a breeding colony was set up to maintain this line of mice. Cell cultures were prepared following the procedures stated above

in 3.5. Harvested DRGs were split evenly into two groups: i) Pcdh-γ knockdown group: those that received AAV-iCre-mCherry, ii) control group: those that received AAV-mCherry. AAV-iCre-mCherry or AAV-mCherry (Vector Biolab, PA, USA) was mixed with the cell culture media prior to seeding at a virus concentration of 500 plaque forming units (PFU) at the time of seeding[36]. Cell cultures were then incubated at 37°C for 24 hours to allow for transfection and after a day, were fixed according to the procedure stated below in 3.9.

3.7 In-cell western assay

To confirm the knockdown of Pcdh-γ, in-cell western assays were performed. DRG neurons from Pcdh-$\gamma^{flox/flox}$ mice (3 males, 3 females) were cultured and plated on a 96 well plate (refer to 3.5). Neurons from a single mouse were divided into two columns/groups: i) Pcdh-γ knockdown group: those that received AAV-iCre-mCherry, ii) control group: those that received AAV-mCherry. The plate was incubated at 37°C for 24 hours and following that, DRGs were fixed and permeabilized using methanol. After fixation, DRGs were rinsed twice with PBS, 2 minutes each. Next, the wells were incubated with Li-Cor Intercept blocking buffer (Li-Cor) for 1 hour at room temperature. Wells were then incubated with 1:100 mouse anti-Pcdh-γ antibody (Santa Cruz) diluted in Li-Cor blocking buffer overnight at 4°C. After primary antibody incubation, wells were rinsed with phosphate buffer saline with Tween® detergent (PBST) for three times, 5 minutes each. After rinsing, DRGs were stained with secondary antibody solution composed of 1:1000 goat anti-mouse Dylight 800 antibody (Invitrogen) diluted in Li-Cor blocking buffer for 1 hour at room temperature. Wells were once again rinsed with PBST and distilled water was added. Finally, the plate was analyzed using a Li-Cor Odyssey CLx infrared scanner[62]. For these experiments, the intensity of staining from each well within a column was averaged and used for statistical analyses.

3.8 *in vitro* Rac1 inhibition experiment

DRGs (15-20) were harvested from C57BL/6 Pcdh-$\gamma^{flox/flox}$ mice of both sexes (3 males, 3 females) and cell cultures were prepared following the procedures stated above in 3.5. Harvested DRGs were split evenly into four groups: i) Pcdh-γ knockdown group: those that received AAV-iCre-mCherry, ii) Pcdh-γ knockdown + Rac1 inhibitor group: those that received AAV-iCre-mCherry + Rac1 inhibitor, iii) control group: those that received AAV-mCherry and iv) control + Rac1 inhibitor group: those that received AAV-mCherry + Rac1 inhibitor. Similar to 3.6, AAV-iCre-mCherry or AAV-mCherry was mixed with the cell culture media prior to seeding at a virus concentration of 500 plaque forming units (PFU) at the time of seeding[36]. In addition to that, Rac1 inhibitor (Catalogue number: 10-2731, Focus Biomolecules, PA, USA) was added to the cell culture media for ii) Pcdh-γ knockdown + Rac1 inhibitor group and iv) control + Rac1 inhibitor group, at a concentration of 50mg/mL. Cell cultures were then incubated at 37°C for 24 hours and after a day, were fixed according to the procedure stated below in 3.9.

3.9 Cell culture immunocytochemistry

After 24 hours, cell cultures were fixed accordingly using 8% paraformaldehyde solution (PFA) in phosphate-buffered saline (PBS) and immunohistochemical staining was performed. To prevent osmotic shock, half of the culture media was removed from each well and replaced with 8% PFA in PBS to begin the fixation process. After 5 minutes, half of the solution from each well was again removed and replaced with 8% PFA in PBS and this was then left for fixation for 15 minutes. Fixative solution was then removed and the culture slide was rinsed three times with PBS, 5 minutes each. Cell culture slide was kept in PBS solution at 4°C until ready for immunohistostaining.

Prior to immunohistostaining, DRGs culture slide was blocked for 30 minutes using 30% normal goat serum (NGS) dissolved in PBS. Following blocking, DRGs were stained with primary antibody: monoclonal anti-β-tubulin III produced in mouse (Sigma Aldrich), for 75 minutes at a concentration ratio of 1:500. β-tubulin III is chosen because it is a microtubule element found almost exclusively in neurons. NF-200, which is widely used, has been shown to not expressed in unmyelinated C-fibers[63,64]. After primary antibody staining, the cell culture slide was rinsed 3 times with PBS, 5 minutes each to remove any unbound anti-β-tubulin III. The cell culture slide was then stained with secondary antibody: AlexaFluor488 goat anti-mouse, for 75 minutes at a concentration ratio of 1:500. After secondary antibody staining, the cell culture slide was again rinsed 3 times with PBS, 5 minutes each to remove any excess secondary antibody. For both the primary and secondary staining processes, the culture slide were incubated in a solution containing the respective antibody, 0.3% Triton-X 100, 0.1% NGS and PBS. After the last rinse, the cell culture slide was mounted with Vectashield DAPI-containing mountining media, coverslipped, sealed and kept at 4°C until ready for imaging.

3.10 DRG analyses and quantification

Following 3.9, DRG neurons were imaged under light microscope using AxioVision software. Only one DRG neuron was imaged at a time, except for the heteroneuronal/neighbouring neurite interaction study, where at least two nearby DRG neurons were required. Images taken were then analyzed using the WIS Neuromath software. Only those images which contained neurites that were stained bright enough to be detected by the Neuromath software were included. Neurite is defined as any processes arising from the cell body of a neuron, preceding the formation of axon or dendrite. In DRG, those sensory neurons do not possess dendrites and neurite outgrowth is an important proxy for axon growth. Neurite extension, average neurite projection length,

proportion of neurons sprouted, branches per neuron and branchpoints per neuron were quantified. Statistical tests were further performed to analyze these data using GraphPrism. MATLAB files containing tracing of neurite outgrowth for each DRG neuron generated by the Neuromath software were used for isoneuronal and heteroneuronal neurite crossing analyses. Isoneuronal neurite crossings are defined as axons which arise from the same DRG cell nucleus that touched/overlapped one another. Heteroneuronal neurite crossings are defined as those axons which arise from different DRG cell nuclei that touched/overlapped one another. MATLAB files containing the tracing of axons were overlaid with the original image taken under light microscope using Axio Vision and isoneuronal and heteroneuronal neurite crossings were then labelled manually.

3.11 Fluorescence intensity measurement

As an additional measure to confirm the knockdown of Pcdh-γ in DRGs that received AAV-iCre-mCherry, fluorescence intensity measurement was performed. Cell cultures were performed according to procedures stated in 3.5, where two wells received AAV-iCre-mCherry (Pcdh-γ knockdown group) and the other two received AAV-mCherry (control group). Following fixation and blocking protocol, primary antibody incubation was performed using anti-Pcdh-γ produced in mouse according to procedures stated in 3.9. However, only one of the two wells from both the Pcdh-γ knockdown group and control group received the primary antibody. Following primary antibody incubation, all wells were stained using AlexaFluor488 goat anti-mouse according to procedures stated in 3.9. Due to this different staining protocol, there are four different groups: i) Pcdh-γ knockdown group that received anti-Pcdh-γ antibody, ii) Pcdh-γ knockdown group that did not receive anti-Pcdh-γ antibody, iii) conrol group that received anti-Pcdh-γ antibody and iv) control group that did not receive anti-Pcdh-γ antibody.

DRG neurons were then imaged under light microscope using AxioVision software. At least three images from each group were taken and each cell in those images was then analyzed using Image J for its average raw integrated intensity and average integrated intensity. Average raw integrated intensity and average integrated intensity are similar measurements, except average raw integrated intensity takes cell's size into account (larger cells tend to have higher readings). Values from each group were compared and statistical test were performed to analyze these values using GraphPad Prism (refer below 3.15).

3.12 Footpad immunohistochemistry

Footpads were harvested from euthanized mice and placed into fixative solution immediately post-mortem containing paraformaldehyde (PFA), L-lysine and sodium m-periodate. Footpads were fixed in solutions for 24 hours for 12 to 24 hours at 4°C. Following fixation, footpads were rinsed twice with 0.1M Sorrenson's phosphate buffer and cryoprotected in 20% glycerol 0.1M Sorrenson's phosphate buffer solution. These footpad samples were kept at 4°C overnight and then dried off thoroughly with Kimwipes before getting embedded in optimal cutting temperature (OCT) blocks. OCT blocks were kept at -80°C until cryostat sectioning.

Footpad tissues were sectioned at a thickness of 25μm and mounted onto Super Frost Plus Slides (Thermo Fisher Scientific, Waltham, MA) and allowed to dry overnight. Footpad sections were then immersed in Tris-EDTA buffer and incubated at 60°C in a water bath for 75 minutes for antigen retrieval process. Following this, tissue sections were blocked in a solution containing 10% NGS, 1% BSA, 0.3% Triton-X 100 and PBS for 1 hour at room temperature. Tissue sections were then stained with primary antibody, rabbit anti PGP9.5 (EnCor, Biotech. Inc., Gainesville, FL) overnight at 4°C, in a concentration ratio of 1:500. PGP9.5 is chosen as it has been shown to be a

robust marker for visualizing epidermal sensory fibers and is the recommended standard by the European Federation of Neurological Societies (EFNS)[10]. Following primary incubation, tissue sections were rinsed 3 times with PBS, 5 minutes each. After rinsing, the tissue sections were stained with secondary antibody, AlexaFluor 546 goat anti rabbit for 1 hour at room temperature in a concentration ratio of 1:100. For both the primary and secondary antibody staining, the tissue sections were incubated in a solution containing 0.1% BSA, 0.04% EDTA, 0.3% Triton-X 100 and 1% NGS. After secondary antibody staining, the tissue sections were again rinsed 3 times with PBS, 5 minutes each then mounted with Vectashield DAPI-containing mounting media, coverslipped and sealed.

3.13 Confocal microscopy acquisition

Stained footpad sections were imaged using Leica SP5 confocal microscope with a 63x/1.2 objective lens. Z-stack images were obtained using a step size of 0.5µm. For each section, 5 consecutive frames were imaged and this were repeated over 3 randomly chosen sections on the slide. To minimize photobleaching, a protocol that allows for viewing and adjusting the specimens without initial exposure to the laser was developed and implemented. Typical confocal microscopy involves adjusting the field of vision using the focus knob while simultaneously viewing the specimen through the objective lens with laser light shining on the specimen. One downside of this technique is that the time taken inevitably exposed the specimen to the high intensity laser light coming from the phototube, thus risking the chances of photobleaching. By switching the confocal microscope into ‘live imaging mode’ and transferring the image from the microscope stage to the computer screen, the intensity of the laser light shone on the tissue sections were greatly reduced. This change in technique had significantly reduced photobleaching and enabled images with high clarity and superior contrast to be taken.

3.14 Quantification of footpad epidermal innervation

Using Image J software, confocal images taken were processed and epidermal innervation of footpads were analyzed in a blinded fashion for: i) number of axons per mm^2 (per epidermal area), ii) number of axons per mm (per epidermal length), iii) number of vertical axons per mm, iv) number of horizontal axons per mm, iv) number of branching from vertical axons, v) interfiber distances (10-30µm/ short; 30-50µm/ medium; >50µm/ long), vi) number of dermal axons, vii) number of vertical dermal axons, viii) number of horizontal dermal axons, ix) number of DAPI-stained nuclei per mm^2 (per epidermal area), x) number of DAPI-stained nuclei touching or in close contact (<10µm) with axons, xi) number of DAPI-stained nuclei in close contact per mm of axons and xii) DAPI-stained cell size.

Vertical axons were defined as those that showed 45° to 90° angle deviation from the subepidermal border (interface where nerve fibers penetrate the epidermal region). Horizontal axons were defined as those that showed 0° to 45° angle deviation from the subepidermal border. Similar horizontal and vertical nerve fibers classifications were also applied for dermal axon analyses. For dermal axon analyses, only those that exist within 50µm beneath the subepidermal border were counted. For number of DAPI-stained nuclei per area, a minimum of 50µm was traced across the upper epidermal border and all the DAPI-stained nuclei beneath the traced line was counted and divided by the thickness of traced epidermis area. For the number of DAPI-stained nuclei in close contact with axons, only those DAPI-stained cells that were within 10µm from the axons, based on an estimate of keratinocyte mean diameter, were counted to address interactions between axons and keratinocytes. For DAPI-stained cell size, 100 randomly selected DAPI-stained cells would be traced per footpad for determination of their areas and an average value were obtained.

3.15 Statistical analyses

Statistical analyses were performed using GraphPad Prism 9 software and Microsoft Excel. Paired Student's t-tests were used to compare differences between two groups and one-way ANOVA with Tukey post hoc analyses were used for experiments containing more than 2 groups. using one-way ANOVA with Tukey post hoc analysis will be performed for qRT-PCR (by Dr. Duraikannu). The null hypothesis was rejected if $p>0.05$. Values shown in figures and results are the mean±SEM.

Chapter 4: Results

4.1 Confirmation of Pcdh-γ knockdown in uninjured adult mouse DRG neuron through in-cell western assays and fluorescence intensity measurement.

To confirm the knockdown of Pcdh-γ in uninjured DRG mouse neurons, in-cell western assays were performed. Relative intensity measurement of Pcdh-γ staining was established using Odyssey® infrared imaging system by LICOR® and compared between DRGs that were transfected with AAV-iCre-mCherry (Pcdh-γ knockdown group) and DRGs that were transfected with AAV-mCherry (control group). Pcdh-γ knockdown group showed a significantly lower staining intensity of Pcdh-γ than control group, confirming the knockdown of Pcdh-γ (n=6 for each group; two-tailed paired t-test, p=0.048*) (Figure 6B). To further confirm the knockdown of Pcdh-γ in DRGs that were transfected with AAV-iCre-mCherry, we also performed fluorescence intensity measurement. A one-way ANOVA showed a significant difference in both the average integrated fluorescence intensity as well as the average raw integrated fluorescence intensity (n=4; one-way ANOVA, p=0.041*, 0.042* respectively) (Figure 7E, 7F). Average raw integrated intensity and average integrated intensity are similar measurements, except average raw integrated intensity takes cell's size into account (larger cells tend to have higher readings). Paired t-tests were also performed on both these measurements between Pcdh-γ knockdown group stained with anti-Pcdh-γ antibody and control group stained with anti-Pcdh-γ antibody. Consistent with the results from in-cell western assays, control group showed a significantly greater average integrated intensity and raw integrated intensity measurements than Pcdh-γ knockdown group (n=4 for each group; two-tailed paired t-test, p=0.042*, 0.043* respectively) (Figure 7E, 7F).

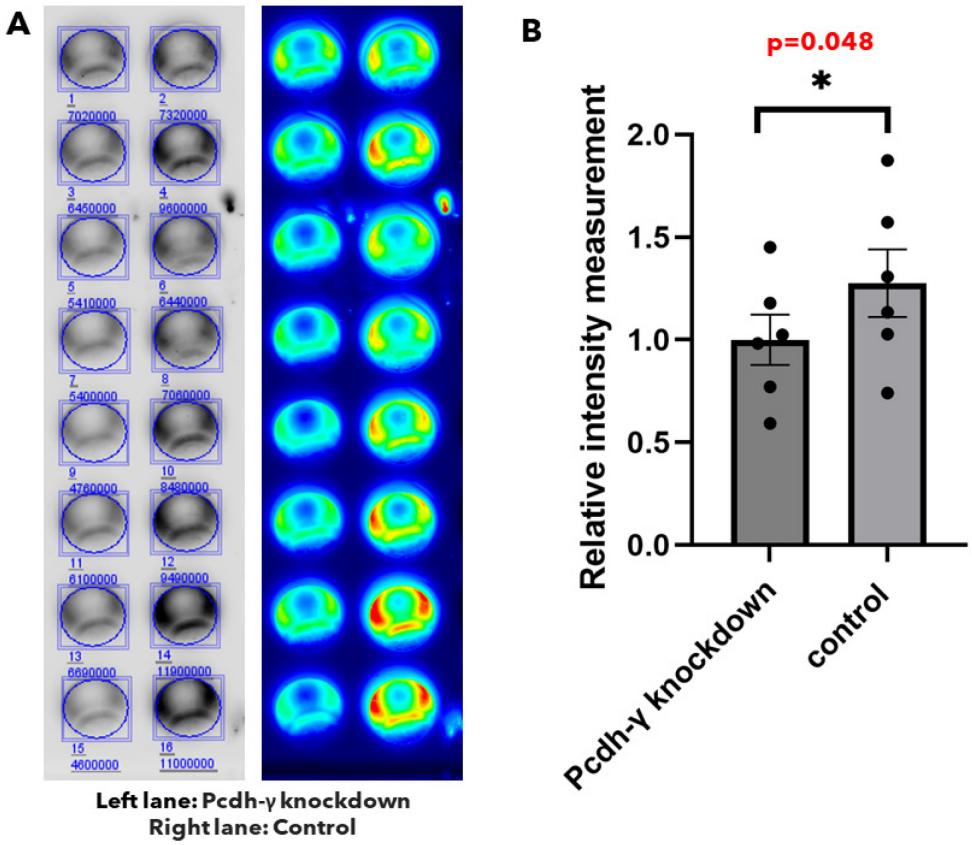

Figure 6: In-cell western assays showing the knockdown of Pcdh-γ in DRG neurons that were transfected with AAV-iCre-mCherry. **(A)** An example of in-cell western assay is shown, the left lane denotes the Pcdh-γ knockdown group while the right lane denotes the control group. The blue circles with the values showed the relative Pcdh-γ staining intensity measurement established by Odyssey® infrared imaging system. **(B)** Two-tailed paired t-test revealed that there is a significant difference in relative intensity measurement between Pcdh-γ knockdown group and control group (n=6 for each group; two-tailed paired t-test, p=0.048*). ***ns*** = not significant, *= ($p<0.05$), **= ($p<0.01$), ***= ($p<0.001$).

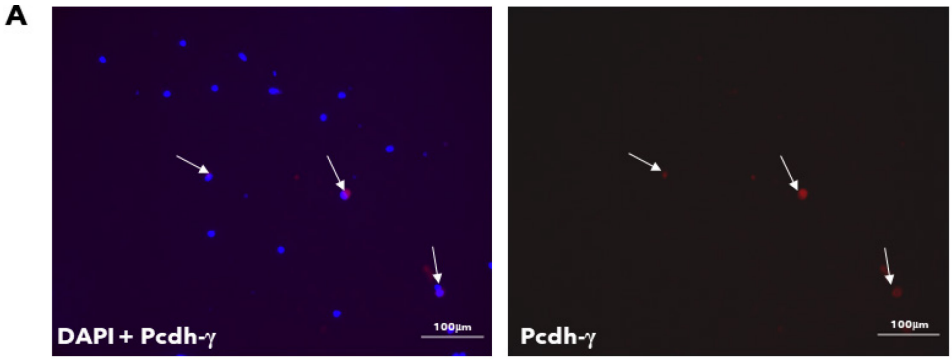

Pcdh-γ knockdown + anti-Pcdh-γ antibody

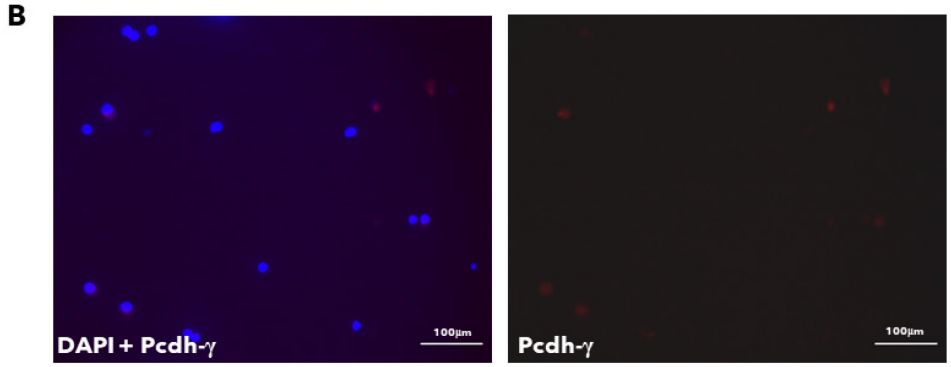

Pcdh-γ knockdown + no antibody

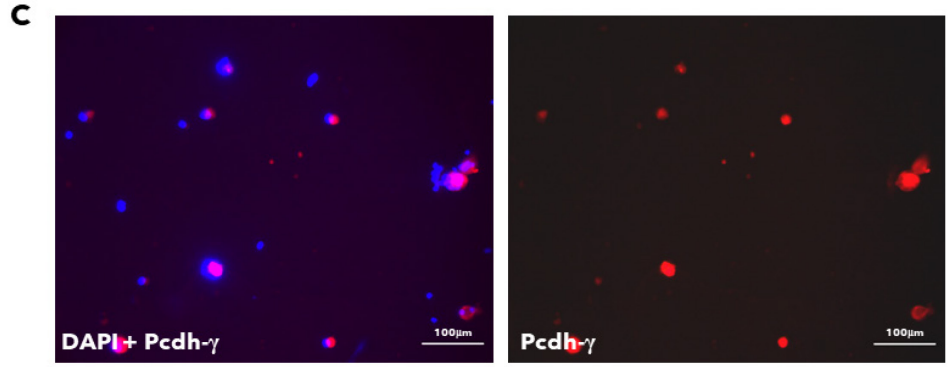

Control + anti-Pcdh-γ antibody

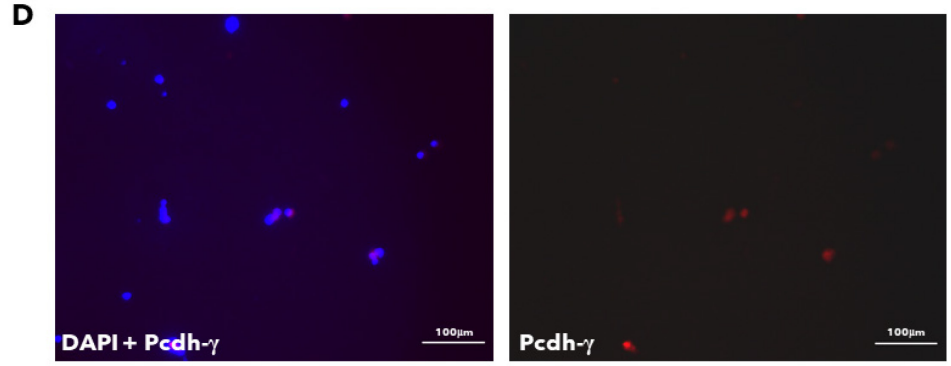

Control + no antibody

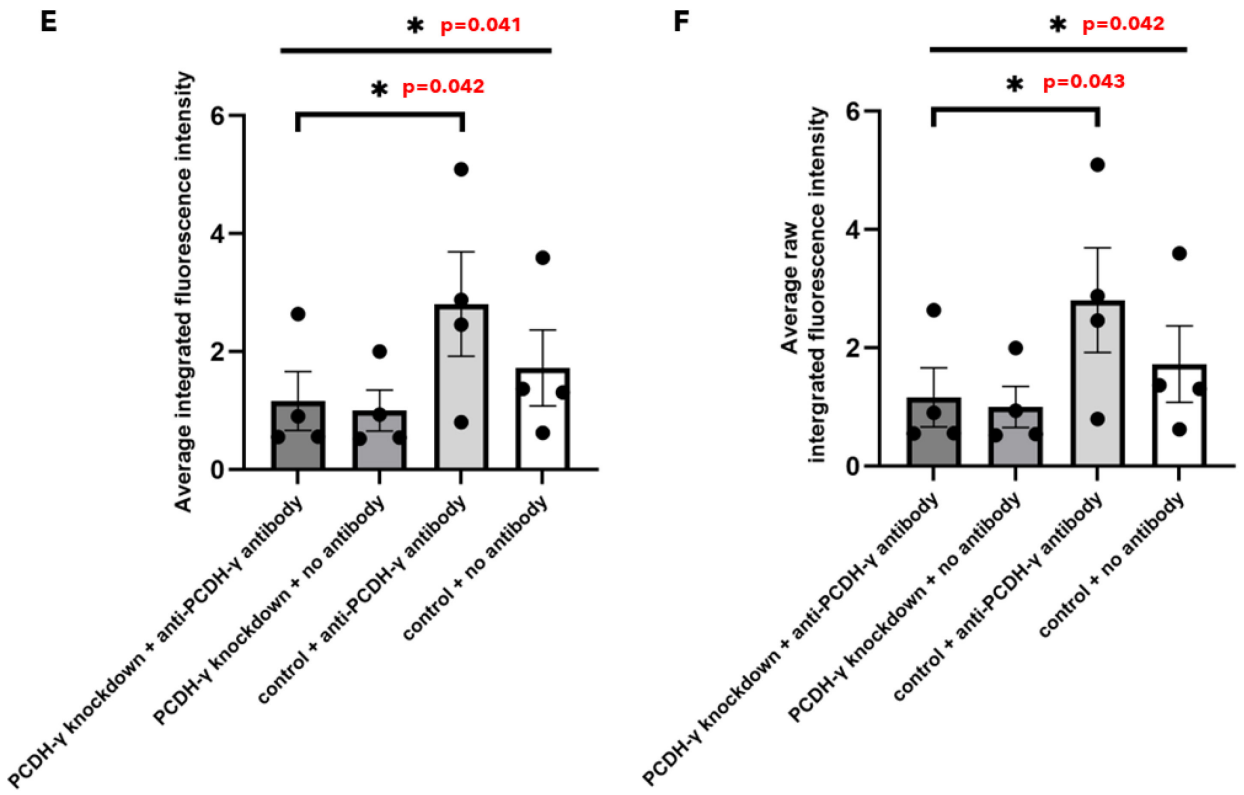

Figure 7: Fluorescence intensity measurement confirmed the knockdown of Pcdh-γ in uninjured mouse DRG neurons transfected with AAV-iCre-mCherry. (A-D) Light microscope images showing the fluorescence staining of DAPI + Pcdh-γ (left hand side) and Pcdh-γ only (right hand side) for i) Pcdh-γ knockdown group stained with anti-Pcdh-γ antibody, ii) Pcdh-γ knockdown group stained without anti-Pcdh-γ antibody, iii) control group stained with anti-Pcdh-γ antibody and iv) control group stained without anti-Pcdh-γ antibody. **(A)** White arrows denote DRG neurons that stained with anti-Pcdh-γ antibody in Pcdh-γ knockdown group. A total of 99 cells were analyzed across 15 randomly chosen images from 4 separate cell culture experiments for Pcdh-γ knockdown group stained with anti-Pcdh-γ antibody. **(B)** A total of 79 cells were analyzed across 15 randomly chosen images from 4 separate cell culture experiments for Pcdh-γ knockdown group stained without anti-Pcdh-γ antibody. **(C)** A total of 98 cells were analyzed across 14 randomly chosen images from 4 separate cell culture experiments for control group stained with anti-Pcdh-γ antibody. **(D)** A total of 89 cells were analyzed across 14 randomly chosen images from 4 separate cell culture experiments for control group stained without anti-Pcdh-γ antibody. **(E)** One-way ANOVA showed that there is a significant difference in the average integrated fluorescence intensity measurement across those four groups (p=0.041*). Two-tailed paired t-test revealed a significant difference between Pcdh-γ knockdown group stained with anti-Pcdh-γ antibody and control group stained with anti-Pcdh-γ antibody (p=0.042*). **(F)** One-way ANOVA showed that there is a significant difference in the average raw integrated fluorescence intensity measurement across those four groups (p=0.042*). Two-tailed paired t-test revealed a significant difference between Pcdh-γ knockdown group stained with anti-Pcdh-γ antibody and control group stained with anti-Pcdh-γ antibody (p=0.043*). ***ns*** = not significant, *= (p<0.05), **= (p<0.01), ***= (p<0.001).

4.2 Pcdh-γ knockdown in uninjured adult mouse DRG neuron led to greater total neurite extension and more branchpoints per neuron.

WIS Neuromath software was used to analyze the neurite outgrowth of DRG neurons. A total of 1385 DRG cells were analyzed across for 6 separate culture experiments for Pcdh-γ knockdown group and a total of 1424 DRG cells were analyzed across for 6 separate culture experiments for control group. Pcdh-γ knockdown group showed greater total neurite extension per neuron than control group, 4270.9±715.3μm versus 3106.1±462.4μm (n=6 for each group; two-tailed paired t-test, p=0.020*) (Figure 8E). Furthermore, the average projection length of a single neurite was also longer in Pcdh-γ knockdown group than control group, 456.0±48.4μm versus 343.8±38.5μm (n=6 for each group; two-tailed paired t-test, p=0.011*) (Figure 8I). On average, the proportion of DRG sprouted was also higher in Pcdh-γ knockdown group than control group, 0.81±0.03 versus 0.75±0.04 (n=6 for each group; two-tailed paired t-test, p=0.022*) (Figure 8F). The number of branches per neuron, meaning the number of projections from a single soma did not differ between Pcdh-γ knockdown group and control group (n=6; two-tailed paired t-test, p=0.058) (Figure 8G). However, the number of branchpoints per neuron were significantly higher in Pcdh-γ knockdown group than control group, 157.7±24.7 versus 107.1±16.8 (n=6 for each group; two-tailed paired t-test, p=0.024*) (Figure 8H). Branchpoints per neuron refer to the branching complexity of the dendritic trees, whether how many sub-branches each primary branch divided into[65]. Pcdh-γ knockdown group on average also showed more neurite self-crossings (isoneuronal interaction) than control group, 75.7±5.9 versus 57.6±6.0 (n=6 for each group; two-tailed paired t-test, p=0.0028**) (Figure 8J). Number of neighbouring neurite crossings (heteroneuronal interaction) was also higher in Pcdh-γ knockdown group than control group, 6.8±0.9 versus 2.1±0.6 (n=6 for each group; two-tailed paired t-test, p=0.00040***) (Figure 8K).

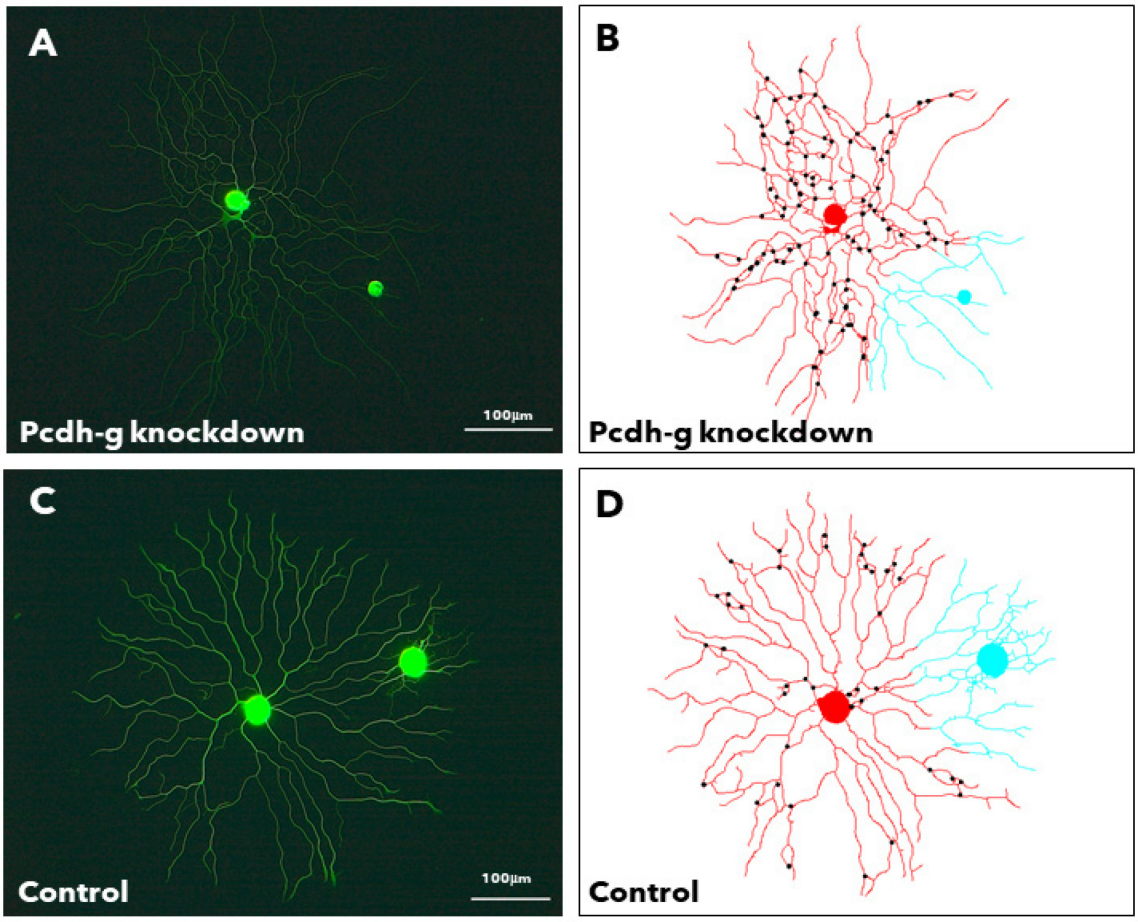
A
Pcdh-g knockdown
100μm
B
Pcdh-g knockdown
C
Control
100μm
D
Control

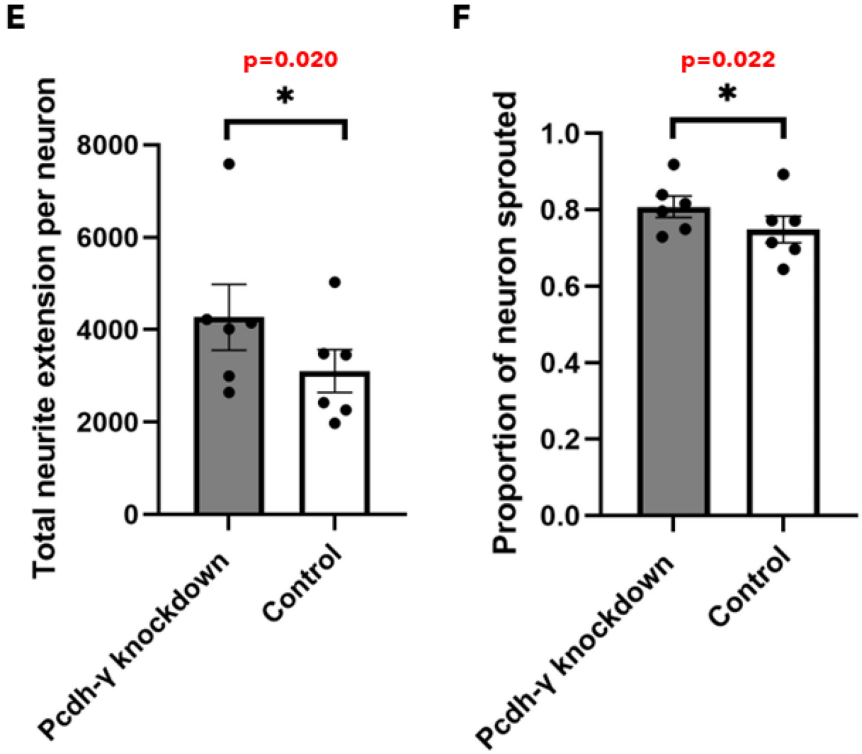
E
p=0.020
*
Total neurite extension per neuron
8000
6000
4000
2000
0
Pcdh-γ knockdown
Control
F
p=0.022
*
Proportion of neuron sprouted
1.0
0.8
0.6
0.4
0.2
0.0
Pcdh-γ knockdown
Control

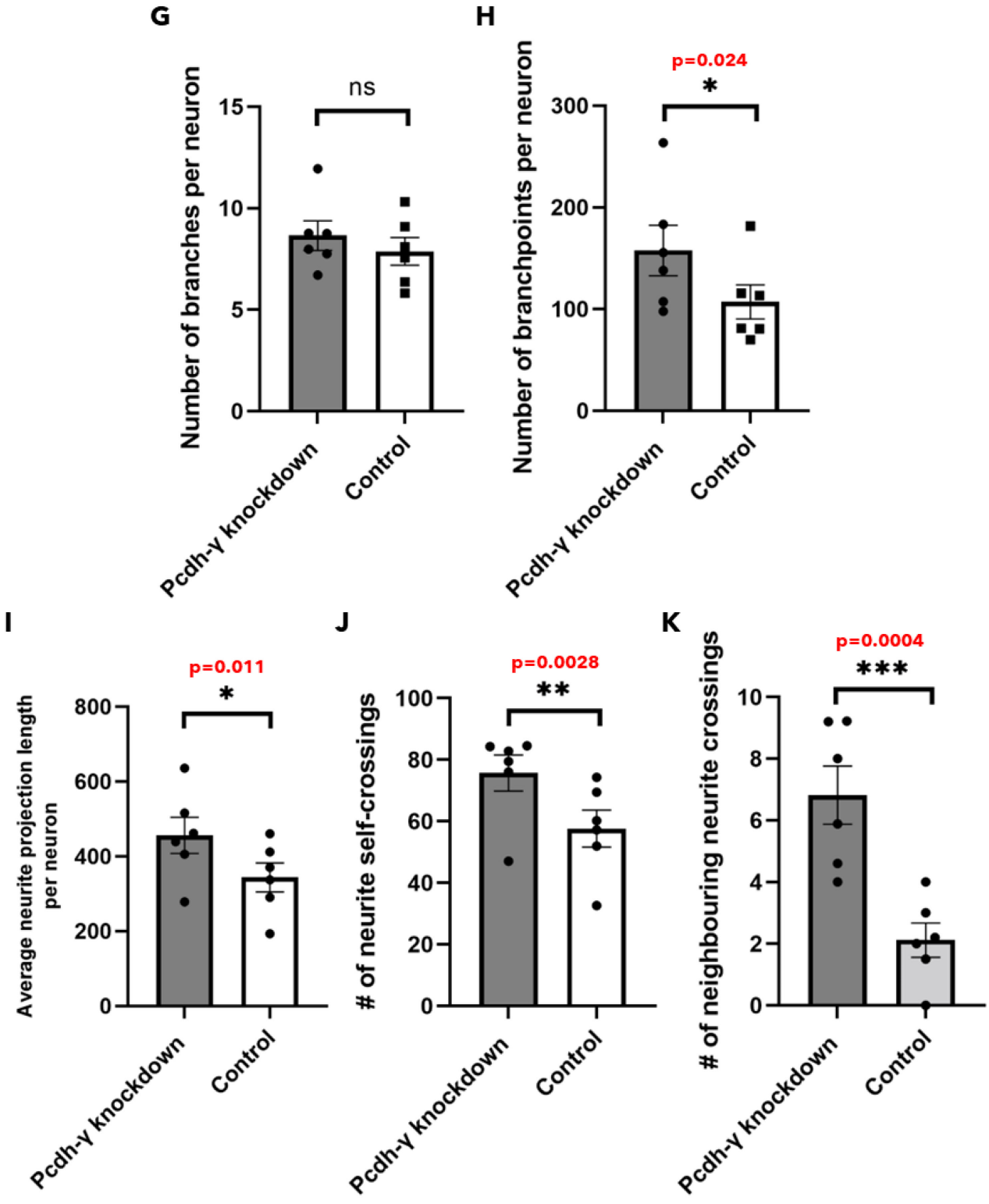
G
Number of branches per neuron
ns
15
10
5
0
Pcdh-γ knockdown
Control
H
Number of branchpoints per neuron
p=0.024
*
300
200
100
0
Pcdh-γ knockdown
Control
I
Average neurite projection length per neuron
p=0.011
*
800
600
400
200
0
Pcdh-γ knockdown
Control
J
# of neurite self-crossings
p=0.0028
**
100
80
60
40
20
0
Pcdh-γ knockdown
Control
K
# of neighbouring neurite crossings
p=0.0004
***
10
8
6
4
2
0
Pcdh-γ knockdown
Control

Figure 8: DRG neurons that received Pcdh-γ knockdown showed greater total neurite extension and more branchpoints per neuron. (A, C) Light microscope images showing representative DRG neurons from Pcdh-γ knockdown group and control group, respectively. **(A)** A total of 1385 DRG cells were analyzed across for 6 separate culture experiments for Pcdh-γ knockdown group. **(C)** A total of 1424 DRG cells were analyzed across for 6 separate culture experiments for control group. **(B, D)** Images showing the neurite tracing generated by WIS Neuromath software and the black dots denote the manual counting of neurite self-crossings. **(E)** Pcdh-γ knockdown group showed greater total neurite extension than control group, 4270.9±715.3μm versus 3106.1±462.4μm (n=6; two-tailed paired t-test, p=0.020*). **(F)** Pcdh-γ knockdown group showed greater proportion of neuron sprouted than control group, 0.81±0.03 versus 0.75±0.04 (n=6; two-tailed paired t-test, p=0.022*). **(G)** There is no significant difference in the number of branches per neuron between Pcdh-γ knockdown group and control group (n=6; two-tailed paired t-test, p=0.058). **(H)** Pcdh-γ knockdown group showed a greater number of branchpoints per neuron than control group, 157.7±24.7 versus 107.1±16.8 (n=6; two-tailed paired t-test, p=0.024*). **(I)** Pcdh-γ knockdown group showed longer projection length of a single neurite than control group, 456.0±48.4μm versus 343.8±38.5μm (n=6; two-tailed paired t-test, p=0.011*). **(J)** Pcdh-γ knockdown group showed more neurite self-crossings (isoneuronal interactions) than control group, 75.7±5.9 versus 57.6±6.0 (n=6; two-tailed paired t-test, p=0.0028**). **(K)** Pcdh-γ knockdown group showed more neighbouring neurite crossings (heteroneuronal interactions) than control group, 6.8±0.9 versus 2.1±0.6 (n=6; two-tailed paired t-test, p=0.00040***). ***ns*** = not significant, *= (p<0.05), **= (p<0.01), ***= (p<0.001).

4.3 Footpads of mice that received Pcdh-γ siRNA knockdown following sciatic nerve crush injury showed higher number of nerve fibers per epidermal length and area.

Anatomical observation and manual counting revealed that footpads of mice that received Pcdh-γ siRNA knockdown (PCDH siRNA ipsi group) displayed greater epidermal innervation than those that received scrambled siRNA (SCR siRNA ipsi group). On average, the PCDH siRNA ipsi group contained more axons per epidermal area (mm^2) and length (mm) than SCR siRNA ipsi group, 776.6±71.2 axons per mm^2 and 26.4±1.9 axons per mm versus 420.0±19.8 axons per mm^2 and 15.6±1.6 axons per mm (n=4 for each group, two-tailed unpaired t-test, p=0.0029**, 0.0047**) (Figure 9E, 9F). When we separated these intraepidermal nerve fibers (IENF) into either vertical epidermal axons (45˚ to 90˚ angle deviation from the subepidermal border) or horizontal epidermal axons (0˚ to 45˚ angle deviation from the subepidermal border), we found that PCDH siRNA ipsi group had significantly more vertical axons than SCR siRNA ipsi group, 22.5±2.9 vertical axons per mm versus 12.4±1.5 vertical axons per mm (n=4 for each group, two-tailed unpaired t-test, p=0.020*) (Figure 9G). However, there was no significant difference in the number of horizontal axons between PCDH siRNA ipsi and SCR siRNA ipsi groups (n=4 for each group, two-tailed unpaired t-test, p=0.63) (Figure 9H).

We also examined dermal innervation of these footpads. If Pcdh-γ does influence the morphology of peripheral neurons as we hypothesized, we explored whether changes might occur earlier before regenerating cutaneous sensory neurons penetrate the subepidermal border. We found no significant difference in the number of dermal axons between PCDH siRNA ipsi and SCR siRNA ipsi groups (n=4 for each group, two-tailed unpaired t-test, p=0.35) (Figure 10C). Separation of these dermal fibers into either vertical dermal axons (45˚ to 90˚ angle deviation from the subepidermal border) or horizontal dermal axons (0˚ to 45˚ angle deviation from the

subepidermal border) did not reveal any significant difference in both measurements between PCDH siRNA ipsi and SCR siRNA ipsi groups (n=4 for each group, two-tailed unpaired t-test, p=0.71, 0.077 respectively) (Figure 10D, 10E). The fact that we observed a significant difference between PCDH siRNA ipsi group and SCR siRNA ipsi group in the epidermal innervation but not dermal innervation might imply that the main interaction/impact from Pcdh-γ siRNA knockdown following sciatic nerve crush injury happened in the epidermis, where Pcdh-γ is expressed.

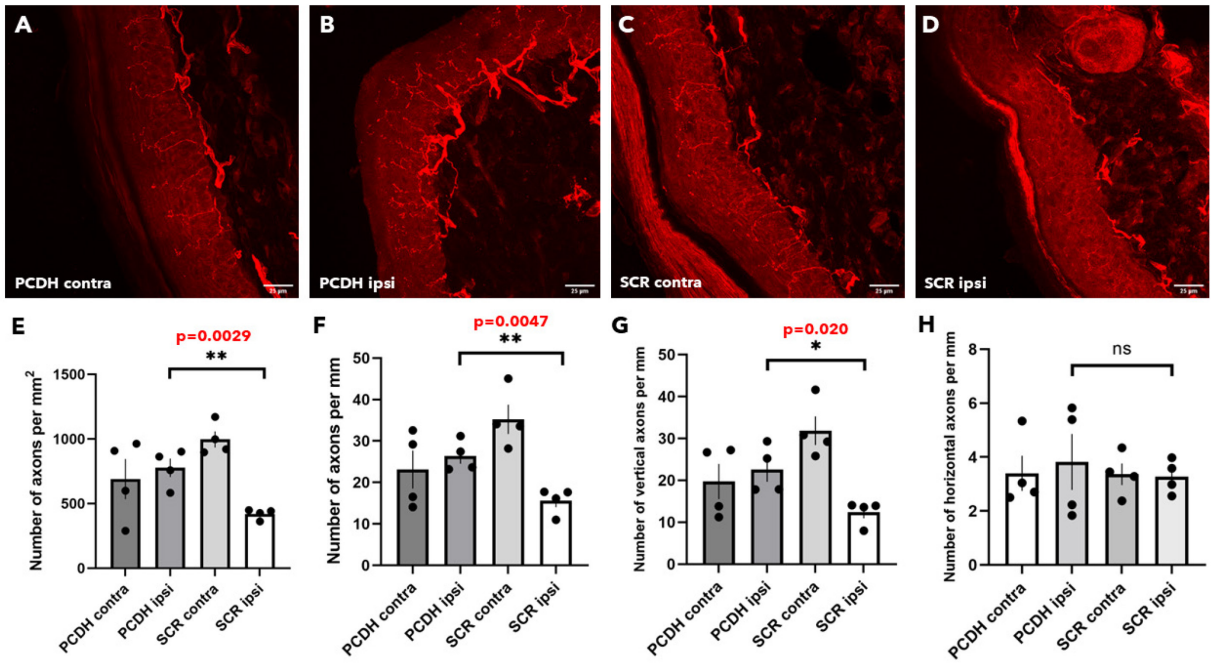

Figure 9: Epidermal reinnervation of the footpad of sciatic nerve crushed mice. Footpads that received Pcdh-γ siRNA knockdown following sciatic nerve crush injury shows increased epidermal reinnervation. **(A-D)** Z-stack images depicting epidermal innervation of footpads from PCDH siRNA contra **(A)**, PCDH siRNA ipsi **(B)**, SCR siRNA contra **(C)** and SCR siRNA ipsi **(D)** groups. Quantification of the total number of axons per mm2 of epidermis **(E)** and per mm of epidermis **(F)** is shown in addition to a breakdown of the number of vertical (45˚-90˚ from the subepidermal border; **G**) and horizontal (0˚-45˚ from the subepidermal border; **H**) axons per mm of the epidermis. Overall, mice treated with the Pcdh-γ siRNA (PCDH siRNA ipsi) possessed the greatest number of axons crossing from the dermis into the epidermis across all counting methods, except for horizontal axons per mm of epidermis. Analyses of the data using two-tailed unpaired t-tests between Pcdh-γ ipsi and Pcdh-γ gamma groups to determine the effects of Pcdh-γ knockdown on peripheral neuron regeneration following sciatic nerve crush injury revealed that the difference across all counting methods are significant, except for horizontal axons per mm (p=0.0029**; **E**) (p=0.0047**; **F**) (p=0.020*; **G**) (p=0.63; **H**). ***ns*** = not significant, *= (p<0.05), **= (p<0.01), ***= (p<0.001). n=4 for each group.

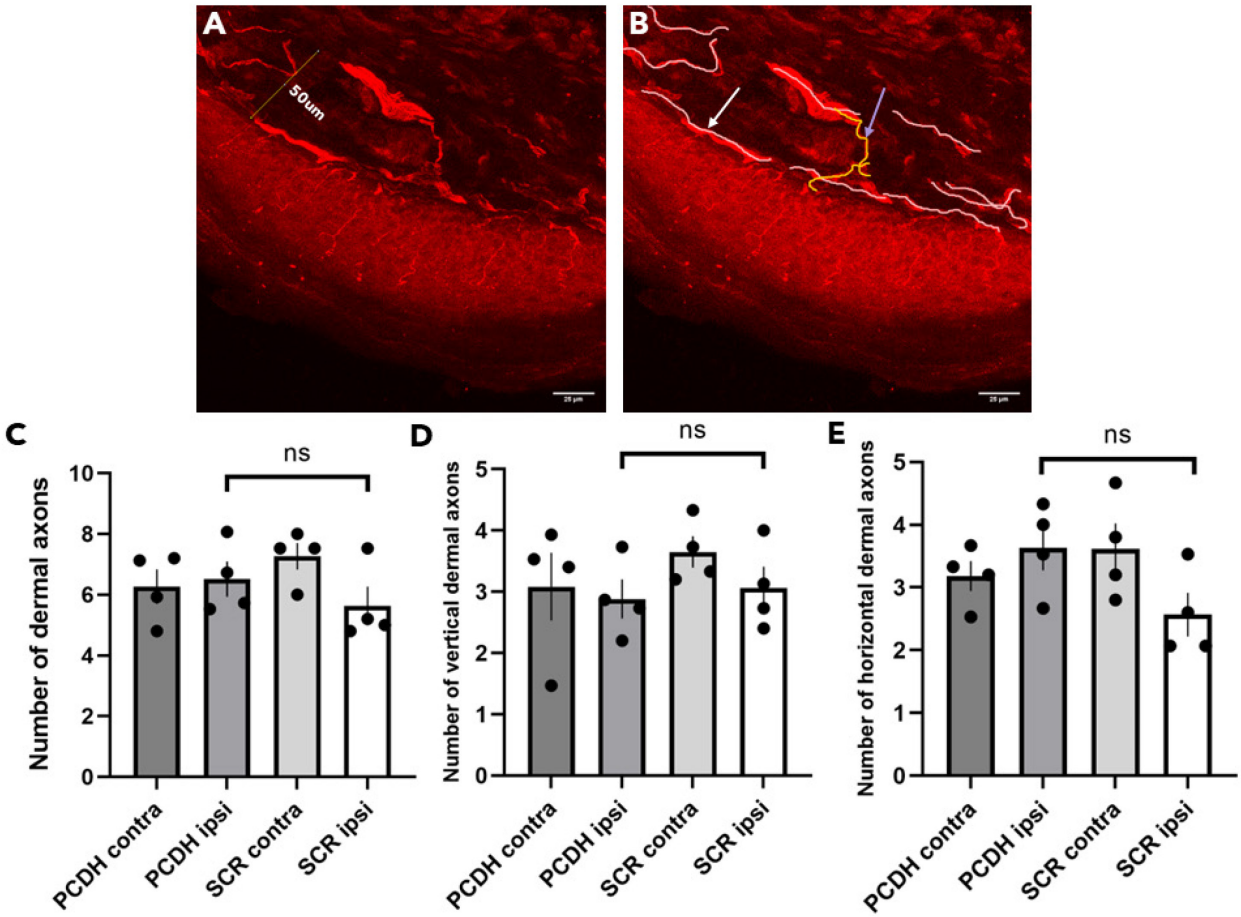

Figure 10: Dermal reinnervation of the footpad of sciatic nerve crushed mice following Pcdh-γ siRNA knockdown. Footpads that received Pcdh-γ siRNA knockdown following sciatic nerve crush injury did not show any significant difference from other groups in dermal reinnervation. **(A)** Z-stack image depicting analysis of footpad dermal innervation: 50µm beneath the subepidermal border. **(B)** Z-stack image showing an example of vertical dermal axon depicted by purple arrow and yellow tracing, and horizontal dermal axon depicted by white arrow and pink tracing. Quantification of the total number of dermal axons across groups are shown in **(C)** in addition to a breakdown of the number of vertical (45˚-90˚ from the subepidermal border; **D**) and horizontal (0˚-45˚ from the subepidermal border; **E**) dermal axons. Analyses of the data using two-tailed unpaired t-tests between PCDH siRNA ipsi and SCR siRNA ipsi groups to determine the effects of Pcdh-γ knockdown on dermal fiber count following sciatic nerve crush injury revealed that there is no significant difference across all dermal axon counting methods (p=0.35; **C**) (p=0.077; **D**) (p=0.71; **E**). ***ns*** = not significant, *= ($p<0.05$), **= ($p<0.01$), ***= ($p<0.001$). n=4 for each group.

4.4 Footpads of mice that received Pcdh-γ siRNA knockdown following sciatic nerve crush injury shows increased branching of vertical axons and shorter interfiber distances.

Since vertical axons are those that typically reached stratum corneum (the outermost layer of the epidermis) and pattern their innervation trees for detection of sensation, we decided to look at the number of branching from these vertical axons. PCDH siRNA ipsi group on average showed more vertical branching than SCR siRNA ipsi group, 0.05±0.017 number of vertical branches versus 0.0±0.00 (NO branching!) number of vertical branches (n=4 for each group, two-tailed unpaired t-test, p=0.024*) (Figure 11C). In other words, footpads of mice that received Pcdh-γ siRNA knockdown following sciatic nerve crush injury shows greater branching complexity in their epidermal innervation. The Lefebvre laboratory from University of Toronto showed that Pcdh-γ knockdown in the CNS led to fasciculation of dendrites in SACs and Purkinje neurons and we wonder if similar defect would be observed in the PNS[57]. Interestingly, we discovered that PCDH siRNA ipsi group tended to have their axons closer together when compared to SCR siRNA ipsi group. Since this is a measure not previously examined and taken into the consideration of the interfiber distances of SCR siRNA contra and PCDH siRNA contra groups (both control groups), we categorized interfiber distances into either 0-30μm (short), 30-50μm (medium) or >50μm (long). PCDH siRNA ipsi group had 68.66% of their interfiber distances in the short range, 26.21% in the medium range and 5.13% in the long range (Figure 12B). Meanwhile, SCR siRNA ipsi group had 53.30% of their interfiber distances in the short range, 25.00% in the medium range and 21.70% in the long range (Figure 12D).

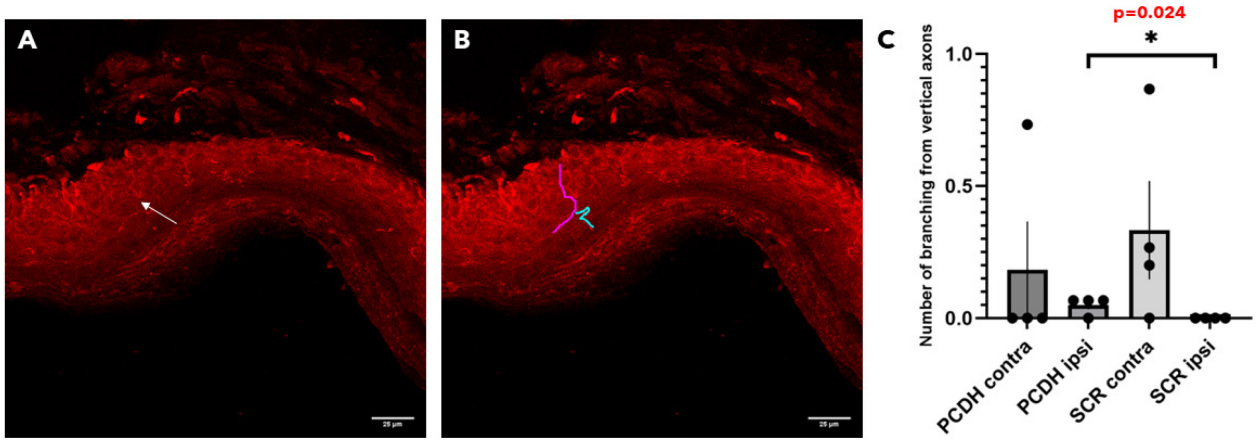

Figure 11: Vertical branching of footpad epidermal reinnervation in mice after sciatic nerve crush injury. (A) Z-stack image showing an example of vertical intraepidermal nerve fiber, depicted by white arrow. **(B)** Z-stack image showing the analysis of vertical branching. The vertical intraepidermal nerve fiber is shown in magenta tracing and its branch in cyan tracing. **(C)** There is a significant difference detected between PCDH siRNA ipsi and SCR siRNA ipsi groups in vertical branching, with PCDH siRNA ipsi group showing more vertical branches from axons (p=0.024*). ***ns*** = not significant, *= (p<0.05), **= (p<0.01), ***= (p<0.001). n=4 for each group.

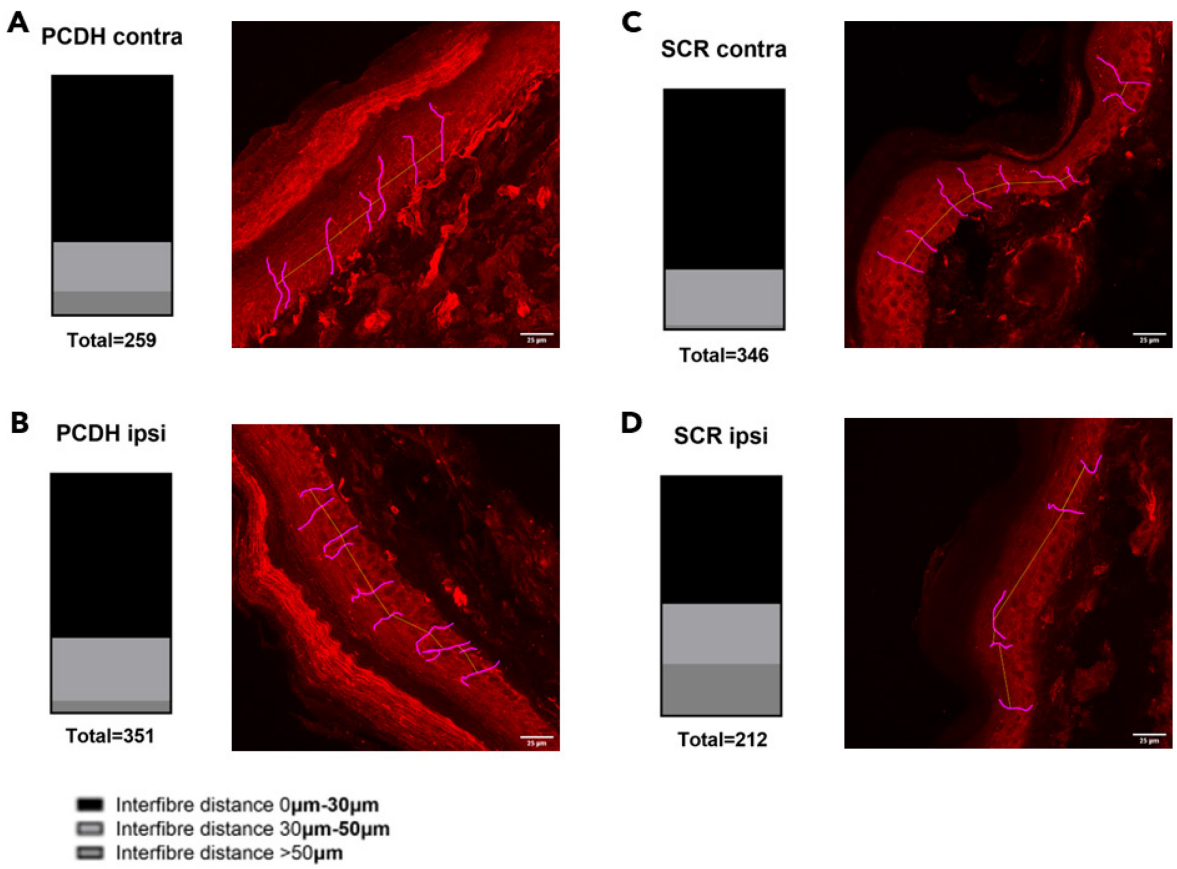

Figure 12: **Interfiber distance of the intraepidermal nerve fibers of the footpad of sciatic nerve crushed mice following Pcdh-γ siRNA knockdown.** Footpads of mice that received Pcdh-γ knockdown had shorter interfiber distances. **(A-D)** Vertical bars showing the distribution of the interfiber distance across PCDH siRNA contra, PCDH siRNA ipsi, SCR siRNA contra and SCR siRNA ipsi groups are shown. **(A-D)** Z-stack images showing analyses of interfiber distance across PCDH siRNA contra, PCDH siRNA ipsi, SCR siRNA contra and SCR siRNA ipsi groups. Interfiber distances are classified into 3 different categories, namely short (0-30µm), medium (30-50µm) and long (>50µm). Total of 259, 351, 346 and 212 interfiber distances are counted for PCDH siRNA contra, PCDH siRNA ipsi, SCR siRNA contra, SC ipsi groups respectively. n=4 for each group. **(A)** PCDH siRNA contra group had 69.50% of their interfiber distances in the 0-30µm range, 20.46% in the 30-50µm range and 10.04% in the >50µm range. **(B)** PCDH siRNA ipsi group had 68.7% of their interfiber distances in the 0-30µm range, 26.2% in the 30-50µm range and 5.1% in the >50µm range. **(C)** SCR siRNA contra group had 75.14% of their interfiber distances in the 0-30µm range, 23.12% in the 30-50µm range and 1.73% in the >50µm range. **(D)** SCR siRNA ipsi group had 53.3% of their interfiber distances in the 0-30µm range, 25.0% in the 30-50µm range and 21.7% in the >50µm range.

4.5 Footpads of mice that received Pcdh-γ knockdown contain more DAPI-stained nuclei per epidermal area and greater DAPI-stained cell size.

A recent study by Talagas and colleagues revealed that keratinocytes the most prominent cells within the epidermis, can communicate with sensory neurons and activate them through chemical synapses[66]. Therefore, we wonder if the greater epidermal innervation observed in PCDH siRNA ipsi group involves keratinocytes surrounding them and we stained for keratinocytes by analyzing the number of DAPI-stained nuclei per epidermal area. On average, PCDH siRNA ipsi group contained more DAPI-stained nuclei per mm^2 of epidermis than SCR siRNA ipsi group, 13073±327.7 DAPI-stained nuclei per mm^2 versus 11661±285.6 DAPI-stained nuclei per mm^2 (n=4 for each group, two-tailed unpaired t-test, p=0.018*) (Figure 13E). However, when we examined the number of DAPI-stained nuclei in close contact (<10μm) with or touching the IENF, we found no significant difference between those PCDH siRNA ipsi and SCR siRNA ipsi (n=4 for each group, two-tailed unpaired t-test, p=0.1466) (Figure 13G). To confirm this, we traced and recorded the length of IENF and analyzed the number of DAPI-stained nuclei in close contact per mm of IENF. Again, there is no significant difference between those two groups (n=4 for each group, two-tailed unpaired t-test, p=0.82) (Figure 13H). Finally, we examined the size of DAPI-stained nuclei to see if there was a significant difference between PCDH siRNA ipsi and SCR siRNA ipsi groups. We found no significant difference in the DAPI-stained cell size between PCDH siRNA ipsi group and SCR siRNA ipsi group (n=4 for each group, two-tailed unpaired t-test, p=0.21) (Figure 13F). However, a significant difference was detected in DAPI-stained cell size between PCDH siRNA ipsi group and PCDH siRNA contra group, with the former showing a larger DAPI-stained cell size, 58.0±2.29$μm^2$ versus 51.57±0.85um^2 (n=4 for each group, two-tailed unpaired t-test, p=0.039*) (Figure 13F). Seeing this unexpected finding, we decided to

compare the DAPI-stained cell size of PCDH siRNA contra group with SCR siRNA contra group, both of which received no injury and acted as negative controls. There is, however, no significant difference in terms of DAPI-stained cell size between PCDH siRNA contra and SCR siRNA contra groups (n=4 for each group, two-tailed unpaired t-test, p=0.45) (Figure 13F).

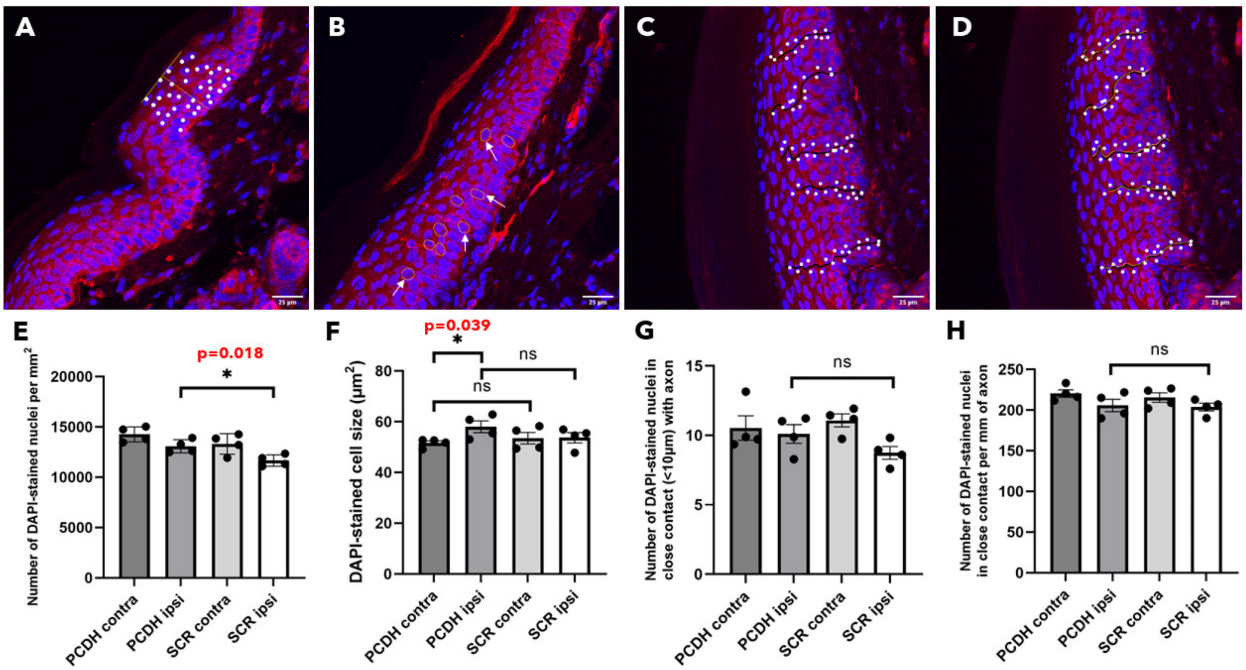

Figure 13: Number of DAPI-stained nuclei per mm^2 of epidermis, DAPI-stained cellular size and number of DAPI-stained nuclei in close contact with axon of the footpad of sciatic nerve crushed mice following Pcdh-γ siRNA knockdown. Footpads of mice that received Pcdh-γ knockdown contain more DAPI-stained nuclei per epidermal area. Z-stack images depicting the analyses for number of DAPI-stained nuclei per mm2 of epidermis **(A)**, DAPI-stained cellular size **(B)**, number DAPI-stained nuclei in close contact (<10µm) with axon **(C)** and number DAPI-stained nuclei in close contact per mm of axon **(D)** are shown. Examples of traced cell for the analysis of DAPI-stained cellular size are shown using white arrows in **B**. There was no significant difference between PCDH siRNA ipsi and SCR siRNA ipsi groups across all analyses except for the number DAPI-stained nuclei per mm^2 of epidermis (p=0.018*; **E**) (p=0.21; **F**) (p=0.15; **G**) (p=0.82; **H**). A significant difference in DAPI-stained cellular size between PCDH siRNA ipsi and PCDH siRNA contra groups was detected (p=0.039*; **F**). However, there was no significant difference detected in DAPI-stained cellular size between PCDH siRNA contra group and its respective counterpart, SCR siRNA contra group (p=0.45; **F**). ***ns*** = not significant, *= (p<0.05), **= (p<0.01), ***= (p<0.001). n=4 for each group.

4.6 Rac1 inhibition reverts the increased branchpoints observed in Pcdh-γ knockdown DRG neurons.

Suo et al. showed that knockdown of Pcdh-α and -γ in hippocampal neurons led to dendritic branching simplification defects. Rac1V12, a constitutively active form of Rac1, was able to rescue the dendritic branching simplification defects and Rac1 inhibition alone in the hippocampal neurons was sufficient to recapitulate those defects. Rac1V12, however, failed to rescue the spine loss in Pcdh clusters knockdown hippocampal neurons[51]. Based on this CNS finding, we proposed that Rac1 might be a downstream signaling molecule of Pcdh-γ knockdown. WIS Neuromath software was used to analyze the neurite outgrowth of DRG neurons, similar to previous experiments. A total of 674 DRG cells were analyzed across for 6 separate culture experiments for Pcdh-γ knockdown group. A total of 736 DRG cells were analyzed across for 6 separate culture experiments for Pcdh-γ knockdown + Rac 1 inhibitor group. A total of 761 DRG cells were analyzed across for 6 separate culture experiments for control group. A total of 857 DRG cells were analyzed across for 6 separate culture experiments for control + Rac 1 inhibitor group. Consistent with our previous experiments (refer to 4.2, Figure 8), Pcdh-γ knockdown group showed greater total neurite extension per neuron, proportion of neuron sprouted, number of branchpoints per neuron than control group (n=6; two-tailed paired t-test, p=0.028*, 0.033*, 0.028*, respectively) (Figure 14). There was also no significant difference in the number of branches per neuron between these two groups, similar to what we observed in previous experiments (n=6; two-tailed paired t-test, p=0.23). However, the significant difference in the average neurite projection length per neuron that we previously observed in 4.2 was not replicated (n=6; two-tailed paired t-test, p=0.23).

When we compared Pcdh-γ knockdown group with Pcdh-γ knockdown + Rac1 inhibitor group, the former displayed greater total neurite extension per neuron, proportion of neuron sprouted, number of branches and branchpoints per neuron (n=6; two-tailed paired t-test, p=0.013*, 0.026*, 0.0028**, 0.0045**, respectively). Pcdh-γ knockdown group showed greater total neurite extension than Pcdh-γ knockdown + Rac1 inhibitor group, 3560.2±314.1μm versus 2485.4± 322.4μm (n=6; two-tailed paired t-test, p=0.013*) (Figure 14E). Pcdh-γ knockdown group also showed greater proportion of neuron sprouted than Pcdh-γ knockdown + Rac1 inhibitor group, 0.76±0.02 versus 0.69±0.03 (n=6; two-tailed paired t-test, p=0.026*) (Figure 14F). Furthermore, Pcdh-γ knockdown group showed a greater number of branches per neuron than Pcdh-γ knockdown + Rac1 inhibitor group, 7.8±0.5 versus 6.5±0.5 (n=6; two-tailed paired t-test, p=0.0028**) (Figure 14G). Finally, Pcdh-γ knockdown group showed a greater number of branchpoints per neuron than Pcdh-γ knockdown + Rac1 inhibitor group, 117.4±12.7 versus 64.8±9.9 (n=6; two-tailed paired t-test, p=0.0045**) (Figure 14H). However, there was no significant difference in the average neurite projection length per neuron between Pcdh-γ knockdown group and Pcdh-γ knockdown group with Pcdh-γ knockdown + Rac1 inhibitor group (n=6; two-tailed paired t-test, p=0.24) (Figure 14I).

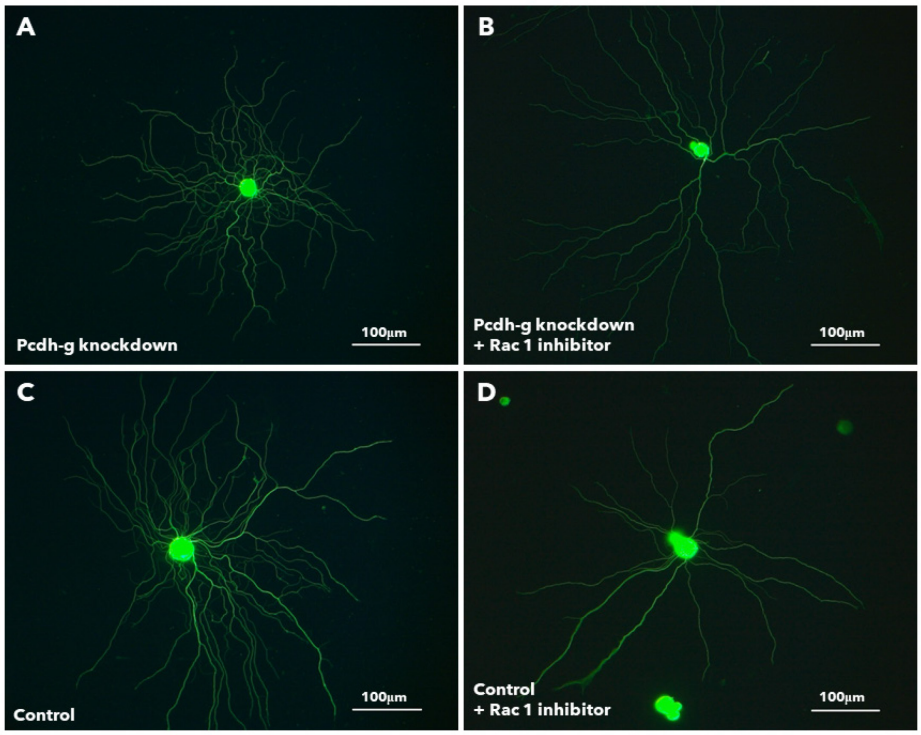
A
Pcdh-g knockdown
100µm
B
Pcdh-g knockdown
+ Rac 1 inhibitor
100µm
C
Control
100µm
D
Control
+ Rac 1 inhibitor
100µm

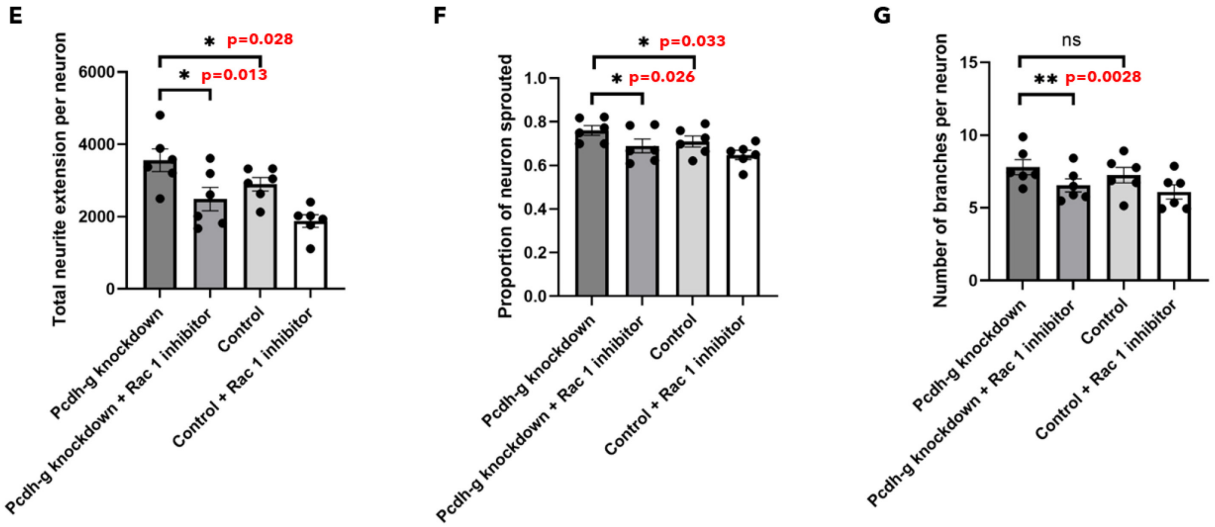
E
Total neurite extension per neuron
6000
4000
2000
0
* p=0.028
* p=0.013
Pcdh-g knockdown
Pcdh-g knockdown + Rac 1 inhibitor
Control
Control + Rac 1 inhibitor
F
Proportion of neuron sprouted
1.0
0.8
0.6
0.4
0.2
0.0
* p=0.033
* p=0.026
Pcdh-g knockdown
Pcdh-g knockdown + Rac 1 inhibitor
Control
Control + Rac 1 inhibitor
G
Number of branches per neuron
15
10
5
0
ns
** p=0.0028
Pcdh-g knockdown
Pcdh-g knockdown + Rac 1 inhibitor
Control
Control + Rac 1 inhibitor

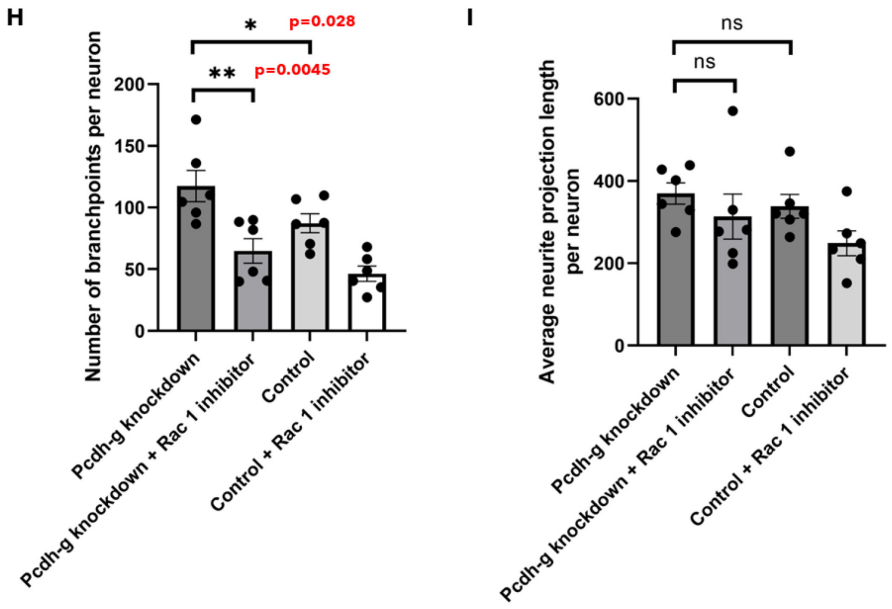

Figure 14: Rac1 inhibition reverts the increased branchpoints observed in Pcdh-γ knockdown DRG neurons. (A, B, C, D) Light microscope images showing representative DRG neurons from Pcdh-γ knockdown group, Pcdh-γ knockdown + Rac1 inhibitor group, control group and control + Rac 1 inhibitor group, respectively. **(A)** A total of 674 DRG cells were analyzed across all 6 separate culture experiments for Pcdh-γ knockdown group. **(B)** A total of 736 DRG cells were analyzed across all 6 separate culture experiments for Pcdh-γ knockdown + Rac1 inhibitor group. **(C)** A total of 761 DRG cells were analyzed across all 6 separate culture experiments for control group. **(D)** A total of 857 DRG cells were analyzed across all 6 separate culture experiments for control + Rac 1 inhibitor group. **(E)** Pcdh-γ knockdown group showed greater total neurite extension than Pcdh-γ knockdown + Rac1 inhibitor group, 3560.2±314.1µm versus 2485.4±322.4µm (n=6; two-tailed paired t-test, p=0.013*). **(F)** Pcdh-γ knockdown group showed greater proportion of neuron sprouted than Pcdh-γ knockdown + Rac1 inhibitor group, 0.76±0.02 versus 0.69±0.03 (n=6; two-tailed paired t-test, p=0.026*). **(G)** Pcdh-γ knockdown group showed a greater number of branches per neuron than Pcdh-γ knockdown + Rac1 inhibitor group, 7.8±0.5 versus 6.5±0.5 (n=6; two-tailed paired t-test, p=0.0028**). **(H)** Pcdh-γ knockdown group showed a greater number of branchpoints per neuron than Pcdh-γ knockdown + Rac1 inhibitor group, 117.4±12.7 versus 64.8±9.9 (n=6; two-tailed paired t-test, p=0.0045**). **(I)** There was no significant difference between Pcdh-γ knockdown group and Pcdh-γ knockdown + Rac1 inhibitor group in average neurite projection length per neuron (n=6; two-tailed paired t-test, p=0.24). **(E, F, G, H, I)** Consistent with our previous experiment (section 4.2, Figure 8), Pcdh-γ knockdown group showed greater total neurite extension per neuron, proportion of neuron sprouted, number of branchpoints per neuron than control group, and no significant difference in number of branches per neuron (n=6; two-tailed paired t-test, p=0.028*, 0.033*, 0.028*, 0.23, respectively). However, there was no significant difference between Pcdh-γ knockdown group and control group in average neurite projection length per neuron (n=6; two-tailed paired t-test, p=0.24). ***ns*** = not significant, *= ($p<0.05$), **= ($p<0.01$), ***= ($p<0.001$).

Chapter 5: Discussion

5.1 Knockdown of Pcdh-γ through AAV-Cre recombinase system and siRNA

A common method to decipher the function of a protein is to silence the protein and examine how a cell or its environment changes in response[58]. Previously, our lab has shown that knockdown of Rb1, a tumor suppressor protein, through administration of Rb1 siRNA or by using adenovirus-Cre recombinase system was associated with improved axon regeneration in mice following a sciatic nerve transection injury[36]. Using similar ideology, our lab has also shown that pharmacological inhibition or siRNA knockdown of other tumor suppressor proteins, such as PTEN and APC, was associated with enhanced neuronal plasticity and improved intrinsic regeneration capacity following PNI[34,35]. In my project, instead of looking at tumor suppressor protein, I explored the role of Pcdh-γ, a cell-adhesion molecule that has been proposed by researchers to be a strong candidate to serve as cell identity marker in the mammalian nervous system. By knocking down Pcdh-γ using AAV-Cre recombinase system *in vitro* and through administration of Pcdh-γ siRNA *in vivo*, I studied the roles of Pcdh-γ in skin epidermal reinnervation process. The main advantages of using AAV-Cre recombinase system for knockdown *in vitro* are its low immunogenicity and stable expression of transgene[67,68]. Meanwhile, the main advantages of using siRNA for knockdown in vivo include low chances of off-target effects and high transduction efficiency[69,70]. For the *in vitro* DRG culture experiment, Pcdh-γ knockdown were verified through in-cell western assay and fluorescence intensity measurement (refer to 4.1). For the *in vivo* sciatic nerve crush experiment, Pcdh-γ knockdown in footpads of mice were verified through real-time quantitative reverse transcription polymerase chain reaction (qRT-PCR) by Dr. Long in her PhD work[58].

5.2 Impacts of Pcdh-γ knockdown on axon growth

Knockdown of Pcdh-γ *in vitro* in uninjured adult DRG neurons led to increased total neurite extension per neuron and greater proportion of neuron sprouted, both of which are signs of enhanced neuronal plasticity (refer to 4.2). The greater average neurite projection length per neuron that we observed in Pcdh-γ knockdown group when compared to the control group in section 4.2 (Experiment 1: AAV-Cre) was not replicated in section 4.6 (Experiment 3: AAV-Cre + Rac1 inhibitor). Despite this discrepancy, the increased total neurite extension per neuron that we observed in Pcdh-γ knockdown group when compared to control group was consistent across these two experiments. One thing worth noting is that the measure of average neurite projection length looks at one single projection per neuron while total neurite extension includes all the projections and processes emanating from a single neuron. Therefore, total neurite extension is a more convincing measurement to assess a neuron outgrowth. In our *in vivo* experiment, footpads of mice that receive Pcdh-γ siRNA knockdown following sciatic nerve crush injury showed greater signs of epidermal reinnervation, consistent with the results from our *in vitro* experiment. Specifically, footpads that received Pcdh-γ siRNA knockdown exhibited greater IENFD (higher counts of axon fibers per epidermal length and area) (refer to 4.3). To see if the greater IENFD that we observed from PCDH siRNA ipsi group translates into behavioural context, Dr. Long performed nerve conduction analyses and behavioural assays to compare these mice to the controls that received scrambled siRNA. Surprisingly, the compound motor action potential (CMAP) and sensory nerve action potential (SNAP) were comparable between PCDH siRNA ipsi and SCR siRNA ipsi groups[58]. This discrepancy between the histological and electrophysiological findings could be explained by the types of neurons that we are measuring in the footpad epidermal innervation and the types of neurons being activated in those nerve conduction studies. Muscle

fibers that contribute to the CMAP and SNAP typically have diameters between 30 to 70μm, which corresponds to type Aα fibers[71]. These fibers do not penetrate the epidermis, unlike the IENF that we are counting in the footpad epidermal innervation, which are type Aδ and C fibers. It is possible that the larger diameter fibers, which do not penetrate the subepidermal border, hence having shorter reinnervation distances have already regenerated to the same degree in both the PCDH siRNA ipsi and SCR siRNA ipsi groups by the time of testing while the smaller diameter fibers that need to penetrate the subepidermal border and innervate the epidermis have yet to do so.

However, this does not explain why we did not see a significant difference between PCDH siRNA ipsi and SCR siRNA ipsi groups in the behavioural assays: Von Frey test and Hargreaves test[58], both of which should activate type Aδ and C fibers. With the PCDH siRNA ipsi group showing higher IENFD, we would expect the mice to show heightened pain sensation: reduced mechanical threshold in the von Frey test (mechanical allodynia) and reduced withdrawal latency in the Hargreaves test (thermal hyperalgesia). One possible explanation for this is that there might be changes occurring on the CNS end of these cutaneous sensory axons (in the spinal cord/cortices) that were not captured in our experiments. Perhaps the greater innervation of branches we observed in the epidermis are all from a single DRG neuron (from the same parent neuron). In this scenario, while more axons are observed in the epidermis, they are from branches of the smaller pool of reinnervating parent axons, and therefore are unable to transmit greater sensory information than the scrambled siRNA treated group. Another possible explanation would be that those IENFs are of the Aδ or C fiber subtype that express transient receptor potential member 8 (TRPM8), the principal detector of cold[72,73]. We did not perform any cold sensitivity test such as menthol test or cold plate test and these will be a valuable assay in the future to elucidate the identity and function of those IENF. Furthermore, it is to be reminded that the mice that underwent sciatic nerve crush

injury received buprenorphine for three days post-surgery and this might have left a lasting impact on the sensory and pain behaviours of these mice when we later performed those behavioural assays. However, this is unlikely as behavioral assays performed on these mice 14 days and 28 days post-surgery still showed no significant difference between the PCDH siRNA ipsi and SCR siRNA ipsi groups. To this end, a more direct measure of the changes in the number of IENFs would be to record the firing activities of these axon trunks to mechanical and heat stimuli. This will remove the confounds arising from the upstream CNS pathways that are being activated during those withdrawal responses.

5.3 Impacts of Pcdh-γ knockdown on branching complexity

Pcdh-γ knockdown DRG neurons did not show any significant difference in the number of branches per neuron when compared to controls, but they exhibited a significantly higher number of branchpoints per neuron. In other words, Pcdh-γ knockdown does not affect the number of processes arising from the soma but the complexity of branching for each process was significantly greater in the Pcdh-γ knockdown group. A recent study by Molumby and colleagues showed that pyramidal neuron expressing only one of the 22 Pcdh-γ variable exons can exhibit either exuberant or minimal dendrite complexity depending on the Pcdh-γ isoforms expressed in its surrounding. If the Pcdh-γ isoforms expressed in the surroundings were congruent with those expressed on the neuron, then homophilic binding between the isoforms were promoted and thus leading to increased dendritic complexity. On the contrary, mismatching of Pcdh-γ isoforms led to reduced homophilic interactions and thus lower dendritic complexity[74]. Therefore, one plausible explanation for the observed greater total neurite extension and branchpoints per neuron is that the knockdown of Pcdh-γ led to a reduction in the diversity of Pcdh-γ isoforms expressed. This

indirectly promotes homophilic binding between the matching Pcdh-γ isoforms, thus resulting in the increased DRG neurite outgrowth.

In the CNS, wild type expression of Pcdh-γ isoforms is required to establish neurite self-avoidance, enabling the neurons to properly spread their branches into the receptive field while allowing neurites from other subtypes to coexist. Lefebvre and colleagues showed that conditional knockout of Pcdh-γ in Purkinje neurons and SACs disrupted neurite self-avoidance, leading to fasciculation of sister neurites[57]. This CNS finding is in line with our observation that DRG neurons which had their Pcdh-γ knocked down showed increased sister and neighbouring neurite crossings. Based on these findings, it could be argued that Pcdh-γ besides mediating branching complexity of a neuron, also plays a role in neurite self/non-self recognition. Through knocking down Pcdh-γ, the diversity of Pcdh-γ isoforms being expressed was reduced and homophilic binding of the remaining isoforms was promoted, causing the neurons to misrecognize a non-self neurite as self. It is worth noting that homophilic binding of DSCAM, a molecule that has been proposed by researchers to act as cell identity marker in Drosophila melanogaster, results in repulsive signal which leads to neurite self-avoidance. However, for Pcdh-γ, at least in the PNS (DRG neurons), the opposite seems to be true. Homophilic binding of Pcdh-γ seems to result in attractive signal that promotes axon growth and branching[57,74].

We also noticed that footpads of PCDH siRNA ipsi group that received Pcdh-γ siRNA knockdown following sciatic nerve crush injury displayed shorter interfiber distances when compared to SCR siRNA ipsi group. In the same paper by Molumby and colleagues, the researchers demonstrated that pyramidal neurons which were surrounded by astrocytes which had their Pcdh-γ knocked out displayed significantly less dendritic arborization (reduced branchpoints per neuron and shorter total neurite extension)[74]. Staining of Pcdh-γ in the footpads by Dr. Long

revealed that it is expressed not only in the peripheral neurons but also in keratinocytes[58]. Therefore, it could be argued that the increased epidermal reinnervation and shorter interfiber distance that we observed in PCDH siRNA ipsi group footpads are a result of increased homophilic interactions between the Pcdh-γ isoforms expressed on the IENF and keratinocytes. However, whether the shorter interfiber distance that we observed in PCDH siRNA ipsi group is a direct consequence of having greater epidermal reinnervation following Pcdh-γ siRNA knockdown or a result of increased homophilic interactions between congruent Pcdh-γ isoforms remains to be investigated.

One caveat of having a greater number of branchpoints in axons is that there is a potential failure in the conduction of action potentials in the sensory axons due to the current leakage at/around the branchpoints. Sodium channels are expressed throughout the axon shaft and are especially concentrated near the branchpoints where the surface area is great. With more sodium channels present, there is a greater amount of current leakage out of those axons and hence action potential could fail to propagate, especially if entering into a larger diameter branch[75]. Therefore, there may be opposing actions of Pcdh-γ knockdown as an increase in sprouting would promote sensory transmission but an increase in branchpoints could potentially decrease sensory transmission.

5.4 Impacts of Pcdh-γ knockdown on keratinocytes

Recent studies have shown that the most prominent cell type in the epidermis, keratinocyte can function as a nociceptor to communicate or even directly activate sensory neurons through synaptic-like contacts[66,76,77]. Surprisingly, we found that there were more DAPI-stained keratinocytes per epidermal area in PCDH siRNA ipsi group than SCR siRNA ipsi group. We wonder if this has a part to play in the greater epidermal reinnervation that we observed in PCDH

siRNA ipsi group. Therefore, we addressed this question in greater detail and analyzed the DAPI-stained keratinocyte size and the number of keratinocytes in close contact (<10μm) with IENF. We did not detect any significant difference in the DAPI-stained keratinocyte size or the number of keratinocytes in close contact with IENF between PCDH siRNA ipsi and SCR siRNA ipsi groups. However, PCDH siRNA ipsi group showed a significantly greater DAPI-stained keratinocyte size than PCDH siRNA contra group. Whether Pcdh-γ siRNA treatment led to an increase in keratinocyte size remains to be investigated, but this interesting finding suggested that there might be a Pcdh-γ mediated interaction between the sensory axons and the keratinocytes which altered the morphological characteristics of the latter.

5.5 Rac1 as a possible downstream signaling molecule of Pcdh-γ

In the CNS, knockdown of Pcdh clusters (Pcdh-α and Pcdh-γ) led to a loss of dendritic spines and branching simplification in the hippocampal neurons, both of which could be recapitulated with Rac1 inhibition alone. Suo et al. showed that through transfecting the cells with Rac1V12 (a constitutively active form of Rac1), the dendritic branching simplification defect could be rescued, indicating that Pcdh clusters might regulate dendritic morphogenesis through Rac1 activation. However, it is to be noted that Rac1V12 failed to reverse the spine loss defect (loss of typical mushroom/stub-shaped dendritic spines) observed in those hippocampal neurons[51]. Given this CNS finding, we wonder if the greater total neurite extension and branchpoints per neuron that we observed from Pcdh-γ knockdown group rely on Rac1 activities. Our in vitro experiment revealed that Rac1 inhibition attenuated the increased branchpoints per neuron that we observed from Pcdh-γ knockdown. Moreover, Rac1 inhibition also nullified the greater total neurite extension per neuron and the higher proportion of neuron sprouted that we observed in Pcdh-γ knockdown group. Interestingly, we also noticed that there is a significant difference in the

number of branches per neuron between Pcdh-γ knockdown group and Pcdh-γ knockdown + Rac1 inhibitor group, with the later showing a significantly reduced number of branches per neuron (refer to 4.6, Figure 14).

This finding is contradictory to the CNS finding by Suo and colleagues. Specifically, in the CNS, Rac1 activation is required to restore normal dendrite morphology in hippocampal neurons (to rescue branching simplification defects resulted from Pcdh clusters knockdown). In our case, Rac1 inhibition attenuated the increased total neurite extension and branchpoints per neuron resulted from Pcdh-γ knockdown. In other words, Rac1 activation reverts neurite outgrowth defects to control level in the CNS while Rac1 inhibition reverts neurite outgrowth changes to control level in the PNS. This discrepancy in Rac1 findings can be attributed to the different effects Pcdh-γ knockdown has on neurite outgrowth in the CNS and PNS. In the CNS, Pcdh-γ knockdown seems to reduce neuronal plasticity, leading to a decrease in neurite outgrowth; while in the PNS, Pcdh-γ knockdown seems to augment neuronal plasticity, leading to an increase in neurite outgrowth. This implicates to us that Pcdh-γ might regulate neurite outgrowth and morphogenesis differently depending on the system and cell types. In support of this explanation, it is worth noting that knocking down Pcdh-γ in different neuronal subtypes leads to different kinds of branching defects. For instance, in the SACs and Purkinje neurons, knockdown of Pcdh-γ was associated with dendrites fasciculation and extensive overlapping of sister dendrites. In the cerebral cortex or hippoccampus, knockdown of Pcdh-γ in the pyramidal neurons was associated with dendritic simplification defects. In our study, knockdown of Pcdh-γ in the DRG neuron was associated with increased neurite extension, higher number of branchpoints per neuron and increased sister and neighbouring neurite crossings, a result more similar to those observed in SACs and Purkinje neurons. Notably, SACs and Purkinje neurons are both considered plantar neurons, where their

neurites arborize in a single orientation. The cutaneous sensory neurons that we are interested in, show similar morphology to planar neurons in the sense that their axon terminates as axon branches in the epidermis and innervate a specific region of the skin. In short, despite the discrepancy of Rac1 actions in the CNS and PNS, our findings support the role of Rac1 as a downstream signaling of Pcdh-γ, particularly in the growth and morphology of sensory neurons.

5.6 Limitations

One major limitation of this project is the lack of data regarding the skin epidermal innervation of conditional Pcdh-γ knockout mice (global Pcdh-γ knockout has been associated with neonatal lethality)[54,78]. Comparison of the footpad epidermal innervation between conditional Pcdh-γ knockout mice and wild type C57/BL6 mice would be important for us to understand the role played by Pcdh-γ in the PNS during developmental stages. Due to time constraints, at the time of writing, our lab is still in the process of breeding for mice with conditional Pcdh-γ genotype: Pcdh-γ $^{flox/flox}$;Advilin-Cre/wt. Current progress on this breeding process or experiment is shown in Figure 15. With help from the Health Science Laboratory Animal Services (HSLAS) at University of Alberta, we have managed to obtain mice with a single Pcdh-γ floxed allele. It is interesting to note that in the process of breeding for Pcdh-γ conditional knockout mice, we often received mice with dermatitis. Due to ethical concerns, these mice were euthanized by the HSLAS veterinarian before we had the chance to sample their tissues for genotype. After looking at our *in vivo* experiment result where footpads of mice that received Pcdh-γ siRNA following sciatic nerve crush injury showed increased skin epidermal reinnervation, it appears to us that dermatitis might be a phenotype for those conditional Pcdh-γ knockout mice. We have informed the HSLAS staffs to not euthanize these mice if the dermatitis is not detrimental (to treat the dermatitis instead) and

if it is detrimental, to harvest tissue samples from these mice after euthanasia. However, whether dermatitis observed in those mice is a consequence of conditional Pcdh-γ knockout remains to be investigated.

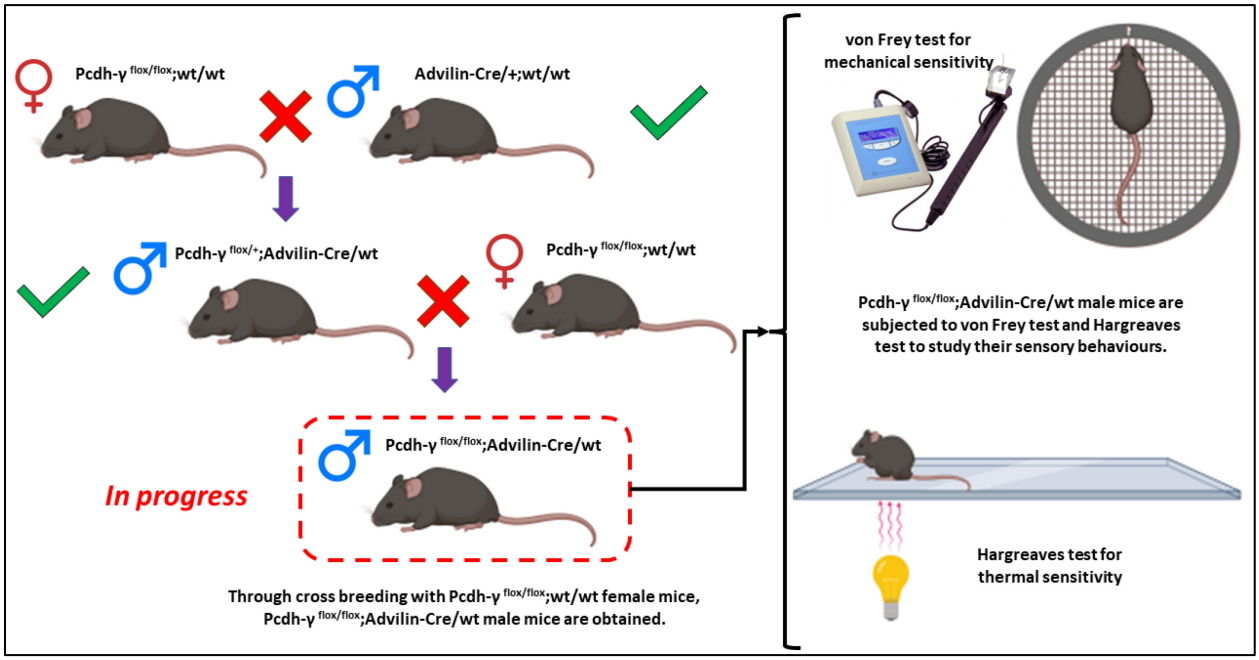

Figure 15: Current progress on breeding for Pcdh-γ conditional knockout mice and behavioural tests that are waiting to be conducted on these mice.

There has also been concern of possible Pcdh-γ expression in non-neuronal cells such as satellite cells, Schwann cells (SCs) and keratinocytes, which may be driving some of the results that we are seeing instead of them being intrinsic to the neurons[58]. In the CNS, Pcdh-γ is known to be expressed on the astrocytes and interactions between the Pcdh-γ isoforms on the astrocytes and neurons have been shown to mediate dendritic branching[54,74]. Results from our *in vivo* experiments supported the idea that there is expression of Pcdh-γ on keratinocytes and we did not identify the molecule in PNS glial cells nor Schwann cells[58]. Specifically, footpads that received Pcdh-γ siRNA knockdown showed more DAPI-stained keratinocytes per epidermal area when

compared to controls, indicating that there might a Pcdh-γ mediated interaction between the sensory axons and keratinocytes. Nevertheless, this does not diminish the significance of our study to explore the role of Pcdh-γ in the PNS.

5.7 Future directions

In the CNS, expression of Pcdh-γ varies among isoforms, with certain isoforms being preferentially expressed in particular laminae or cell types. However, at a regional level, the expression of Pcdh-γ is one of overlapping rather than mutually exclusive (meaning that neurons that reside at a certain location, for example: in the skin, shows a list of common isoforms that they all expressed, instead of each expressing a unique/different list of isoforms)[38,79]. Given the stochastic expression of Pcdh-γ isoforms and the combinatorial formation of Pcdh-γ multimers, it would be important for us to first delineate the identities of Pcdh-γ isoforms being expressed on the cells/regions of interest. For our project, singe-cell RNA sequencing of DRG neurons would be ideal to help us understand which Pcdh-γ isoforms are preferentially expressed in the sensory nervous system and to establish the causal relationship between the effects of Pcdh-γ knockdown with its respective Pcdh-γ isoforms. Furthermore, given the possibility of Pcdh-γ expression on non-neuronal cells such as keratinocytes, single-cell RNA sequencing of keratinocytes would also be crucial to help us understand the Pcdh-γ interactions between these two cell types.

RNA sequencing of mouse DRG and footpad before and after sciatic nerve crush injury for both Pcdh-γ knockdown group and control group is also important to help us understand the role played by Pcdh-γ in peripheral nerve regeneration. This piece of data would allow us to understand the temporal profile of Pcdh-γ expression following PNI and provide us with insights of the downstream signaling pathways of Pcdh-γ. Specifically, by comparing the RNA sequencing data

between Pcdh-γ knockdown group and control group following PNI, we will be able to decipher the genes/group of genes which are responsible for the greater epidermal reinnervation observed in the PCDH siRNA ipsi group (refer to 4.3). This data will also allow us to determine whether it is a group of gene that regulates the function of Rac1 as we hypothesized or is there any other downstream signaling molecules that are driving the results that we are seeing.

Several studies have shown that mice that experienced sciatic nerve crush injury were often able to exhibit full functional recovery without any intervention. Sciatic nerve transection injury, however, rarely achieved full functional recovery[80–83]. In the case of a nerve crush, the gross structure of the nerve is maintained and axons are able to regrow through their original paths and reinnervate their respective targets. On the contrary, a nerve transection completely destroys the nerve trunk, leaving a gap at the site of injury. Newly regrowing axons are now required to traverse the gap to reinnervate their original targets. This process of re-establishing neuronal network requires not only the axons to regenerate quickly enough to avoid the distal nerve stump from becoming chronically denervated and lost all regenerative potential, but also demands proper targeting and patterning of axonal territories. By employing a sciatic nerve transection model, we might better decipher the role played by Pcdh-γ in the axon pathfinding and target reinnervation processes.

Chapter 6: Conclusion

Peripheral nerve regeneration and repair remain among the greatest challenges in the field of regenerative medicine[84]. Despite the ability of peripheral nerve to regenerate, suboptimal functional recovery is often seen in PNI and PND patients. Sensory, motor and autonomic disabilities due to incomplete regeneration can be very incapacitating for the patients, severely impacting their quality of life. Limitations such as slow axonal growth rate and inability to sustain RAGs upregulation, need to be overcome if breakthrough in the treatments for PNI and PND is to be made. Besides providing extrinsic support for the regenerating nerve through microsurgical techniques and nerve guidance conduits, enhancing the intrinsic regenerative capacity of the nerve is of similar importance. Several tumor suppressor proteins studied by the Zochodne laboratory, including Rb, APC, PTEN, have shown promising experimental results as a potential modulator for improving axon regeneration through their knockdown following PNI[34–36]. However, a successful peripheral axon regeneration is not entirely related to the speed of regrowth in axons. The proper patterning of axon branches and reaching the correct reinnervation targets are also crucial in determining the functional outcomes of a peripheral nerve regeneration. Aberrant axon projection and improper patterning of axon branches are often associated with neuropathic pain following PNI or PND[7,15,73].

In this project, we explore the roles of Pcdh-γ, a molecule that has recently come under research spotlight as a strong candidate to serve as cell identity marker in the mammalian nervous system, in the context of peripheral axon regeneration. Our *in vitro* and *in vivo* experiments revealed that Pcdh-γ might have a role to play in axon growth and patterning. In uninjured cultured DRG neurons, knockdown of Pcdh-γ was associated with greater total neurite extension and more branchpoints per neuron. In footpads of mice that experienced sciatic nerve crush injury,

knockdown of Pcdh-γ was associated with greater epidermal reinnervation, shorter interfiber distance and more keratinocytes per epidermal area. These interesting results warrant further studies as it might provide insight for developing novel molecular approach for treating PNI and PND. Given that sensation forms a major part of our interaction with the world, it is of utmost importance for us to understand the molecular mechanisms underlying peripheral axon regeneration so that we can better preserve this ability, especially in the context of experiencing PNI or PND.

References

1. Glatte P, Buchmann SJ, Hijazi MM, Illigens BMW, Siepmann T. Architecture of the Cutaneous Autonomic Nervous System. *Front Neurol*. 2019;10. doi:10.3389/fneur.2019.00970

2. Crawford LTK, Caterina MJ. Functional Anatomy of the Sensory Nervous System: Updates From the Neuroscience Bench. *Toxicol Pathol*. 2020;48(1):174-189. doi:10.1177/0192623319869011

3. Li NY, Onor GI, Lemme NJ, Gil JA. Epidemiology of Peripheral Nerve Injuries in Sports, Exercise, and Recreation in the United States, 2009 - 2018. *Phys Sportsmed*. 2021;49(3):355-362. doi:10.1080/00913847.2020.1850151

4. Peripheral neuropathy - Symptoms and causes - Mayo Clinic. Accessed June 18, 2022. https://www.mayoclinic.org/diseases-conditions/peripheral-neuropathy/symptoms-causes/syc-20352061

5. Zochodne DW. The challenges of diabetic polyneuropathy: A brief update. *Curr Opin Neurol*. 2019;32(5):666-675. doi:10.1097/WCO.0000000000000723

6. Sulaiman W, Gordon T. *Neurobiology of Peripheral Nerve Injury, Regeneration, and Functional Recovery: From Bench Top Research to Bedside Application*.

7. Zochodne DW. *The Challenges and Beauty of Peripheral Nerve Regrowth*. Vol 17.; 2012.

8. Abraira VE, Ginty DD. The sensory neurons of touch. *Neuron*. 2013;79(4):618-639. doi:10.1016/j.neuron.2013.07.051

9. Wang F, Julien DP, Sagasti A. Journey to the skin: Somatosensory peripheral axon guidance and morphogenesis. *Cell Adh Migr*. 2013;7(4):388-394. doi:10.4161/cam.25000

10. Lauria G, Cornblath DR, Johansson O, et al. *EFNS Guidelines on the Use of Skin Biopsy in the Diagnosis of Peripheral Neuropathy*. http://rsb.info.nih.gov/

11. Hogan QH. Labat lecture: The primary sensory neuron: Where it is, what it does, and why it matters. *Reg Anesth Pain Med*. 2010;35(3):306-311. doi:10.1097/AAP.0b013e3181d2375e

12. Grueber WB, Sagasti A. Self-avoidance and tiling: Mechanisms of dendrite and axon spacing. *Cold Spring Harb Perspect Biol*. 2010;2(9). doi:10.1101/cshperspect.a001750

13. Taniguchi M, Yuasa S, Fujisawa H, et al. *Disruption of Semaphorin III/D Gene Causes Severe Abnormality in Peripheral Nerve Projection*. Vol 19.; 1997.

14. Kitsukawa T, Shimizu M, Sanbo M, et al. *Neuropilin-Semaphorin III/D-Mediated Chemorepulsive Signals Play a Crucial Role in Peripheral Nerve Projection in Mice*. Vol 19.; 1997.

15. Höke A. Mechanisms of Disease: What factors limit the success of peripheral nerve regeneration in humans? *Nat Clin Pract Neurol*. 2006;2(8):448-454. doi:10.1038/ncpneuro0262

16. Gaudet AD, Popovich PG, Ramer MS. Wallerian degeneration: Gaining perspective on inflammatory events after peripheral nerve injury. *J Neuroinflammation*. 2011;8. doi:10.1186/1742-2094-8-110

17. Grafstein B. *The Nerve Cell Body Response to Axotomy*. Vol 48.; 1975.

18. Harty BL, Monk KR. Unwrapping the unappreciated: recent progress in Remak Schwann cell biology. *Curr Opin Neurobiol*. 2017;47:131-137. doi:10.1016/j.conb.2017.10.003

19. Abdo H, Calvo-Enrique L, Martinez Lopez J, et al. *Specialized Cutaneous Schwann Cells Initiate Pain Sensation Downloaded From*. Vol 365.; 2019. http://science.sciencemag.org/

20. Erge1 VMK v, Ra Tto KAG, Rch A, Sk I1 EW, Richardson2 PM. *Neurotrophins and Nerve Injury in the Adult*.; 1996. https://royalsocietypublishing.org/

21. Ma TC, Willis DE. What makes a RAG regeneration associated? *Front Mol Neurosci*. 2015;8(AUGUST). doi:10.3389/fnmol.2015.00043

22. Lowery LA, Vactor D van. The trip of the tip: Understanding the growth cone machinery. *Nat Rev Mol Cell Biol*. 2009;10(5):332-343. doi:10.1038/nrm2679

23. Denny JB. *Molecular Mechanisms, Biological Actions, and Neuropharmacology of the Growth-Associated Protein GAP-43*. Vol 4.; 2006.

24. Seijffers R, Mills CD, Woolf CJ. ATF3 increases the intrinsic growth state of DRG neurons to enhance peripheral nerve regeneration. *Journal of Neuroscience*. 2007;27(30):7911-7920. doi:10.1523/JNEUROSCI.5313-06.2007

25. Toth CC, Willis D, Twiss JL, et al. *Locally Synthesized Calcitonin GeneYRelated Peptide Has a Critical Role in Peripheral Nerve Regeneration*. https://academic.oup.com/jnen/article/68/3/326/2917178

26. Tetzlaff W, Zwiers ' H, Lederiq2 ' K, Cassar L, Bisby' MA. *Axonal Transport and Localization of B-50/GAP=43=like Lmmunoreactivity in Regenerating Sciatic and Facial Nerves of the Rat*.; 1989.

27. Inbal R, Rousso M, Ashur H, Devor M, Wall ' PD. *Clinical Section Collateral Sprouting in Skin and Sensory Recovery after Nerve Injury In*.

28. Healy C, Lequesne PM, Lynn B. *Collateral Sprouting of Cutaneous Nerves in Man*. Vol 119.; 1996. https://academic.oup.com/brain/article/119/6/2063/466631

29. Collyer E, Catenaccio A, Lemaitre D, et al. Sprouting of axonal collaterals after spinal cord injury is prevented by delayed axonal degeneration. *Exp Neurol*. 2014;261:451-461. doi:10.1016/j.expneurol.2014.07.014

30. Navarro X, Vivó M, Valero-Cabré A. Neural plasticity after peripheral nerve injury and regeneration. *Prog Neurobiol*. 2007;82(4):163-201. doi:10.1016/j.pneurobio.2007.06.005

31. David S, Aguayo AJ. Axonal elongation into peripheral nervous system "bridges" after central nervous system injury in adult rats. *Science (1979)*. 1981;214(4523):931-933. doi:10.1126/science.6171034

32. Bruce HM, Bronson FH, Massey A, et al. *Extensive Elongation of Axons from Rat Brain into Peripheral Nerve Grafts*. Vol 184. Rockefeller University Press; 1959.

33. Sulaiman OAR, Gordon T. *Effects of Short-and Long-Term Schwann Cell Denervation on Peripheral Nerve Regeneration, Myelination, and Size*.; 2000.

34. Christie KJ, Webber CA, Martinez JA, Singh B, Zochodne DW. PTEN inhibition to facilitate intrinsic regenerative outgrowth of adult peripheral axons. *Journal of Neuroscience*. 2010;30(27):9306-9315. doi:10.1523/JNEUROSCI.6271-09.2010

35. Duraikannu A, Martinez JA, Chandrasekhar A, Zochodne DW. Expression and Manipulation of the APC-β-Catenin Pathway During Peripheral Neuron Regeneration. *Sci Rep*. 2018;8(1). doi:10.1038/s41598-018-31167-1

36. Christie KJ, Krishnan A, Martinez JA, et al. Enhancing adult nerve regeneration through the knockdown of retinoblastoma protein. *Nat Commun*. 2014;5. doi:10.1038/ncomms4670

37. Langley JN. *NOTE ON REGENERATION OF PRE:-GANGLIONIC FIBRES OF THE SYMPATHETIC*.

38. Zipursky SL, Sanes JR. Chemoaffinity revisited: Dscams, protocadherins, and neural circuit assembly. *Cell*. 2010;143(3):343-353. doi:10.1016/j.cell.2010.10.009

39. Sperry RW. *VISUOMOTOR COORDINATION IN T H E NEWT (TRITURUS VTRIDESCENS) AFTER REGENERATION O F THE OPTIC NERVE1*.

40. Sperry RW. *CHEMOAFFINITY IN THE ORDERLY GROWTH OF NERVE FIBER PATTERNS AND CONNECTIONS**.; 1963.

41. Sperry RW. *OPTIC NERVE REGENERATION WITH RETURN OF VISION IN ANURANS*.

42. Meyerr RL[. *Roger Sperry and His Chemoaf_nity Hypothesis*. Vol 25.

43. Grueber WB, Sagasti A. Self-avoidance and tiling: Mechanisms of dendrite and axon spacing. *Cold Spring Harb Perspect Biol*. 2010;2(9). doi:10.1101/cshperspect.a001750

44. Zhu H, Hummel T, Clemens JC, Berdnik D, Zipursky SL, Luo L. Dendritic patterning by Dscam and synaptic partner matching in the Drosophila antennal lobe. Published online 2006. doi:10.1038/nn1652

45. Zhan XL, Clemens JC, Neves G, et al. *Analysis of Dscam Diversity in RegulatingAxon Guidance InDrosophilaMushroom Bodies*. Vol 43. Flanagan and Vanderhaeghen; 2004.

46. Wang J, Zugates CT, Liang IH, Lee CHJ, Lee T. *Drosophila Dscam Is Required for Divergent Segregation of Sister Branches and Suppresses Ectopic Bifurcation of Axons et al So If Axon Bifurcation Leads to Formation of "Twin" Growth Cones, How Can These Growth Cones with the Same Cell Fate Faithfully In the MB Neuropil, Most Axons*. Vol 33. de Belle and Heisenberg; 2002.

47. Phillips GR, Tanaka H, Frank M, et al. *Protocadherins Are Targeted to Subsets of Synapses and Intracellular Organelles in Neurons*.; 2003.

48. Junghans D, Heidenreich M, Hack I, Taylor V, Frotscher M, Kemler R. Postsynaptic and differential localization to neuronal subtypes of protocadherin β16 in the mammalian central nervous system. *European Journal of Neuroscience*. 2008;27(3):559-571. doi:10.1111/j.1460-9568.2008.06052.x

49. Schreiner D, Weiner JA. Combinatorial homophilic interaction between γ-protocadherin multimers greatly expands the molecular diversity of cell adhesion. *Proc Natl Acad Sci U S A*. 2010;107(33):14893-14898. doi:10.1073/pnas.1004526107

50. Hurata Y, Hamada S, Morishita H, Mutoh T, Yagi T. Interaction with protocadherin-γ regulates the cell surface expression of protocadherin-α. *Journal of Biological Chemistry*. 2004;279(47):49508-49516. doi:10.1074/jbc.M408771200

51. Suo L, Lu H, Ying G, Capecchi MR, Wu Q. Protocadherin clusters and cell adhesion kinase regulate dendrite complexity through Rho GTPase. *J Mol Cell Biol*. 2012;4(6):362-376. doi:10.1093/jmcb/mjs034

52. Hummel T, Vasconcelos ML, Clemens JC, Fishilevich Y, Vosshall LB, Lawrence Zipursky S. *Axonal Targeting of Olfactory Receptor in Drosophila Is Controlled by Dscam*. Vol 37.; 2003.

53. Hasegawa S, Hamada S, Kumode Y, et al. The protocadherin-α family is involved in axonal coalescence of olfactory sensory neurons into glomeruli of the olfactory bulb in mouse. *Molecular and Cellular Neuroscience*. 2008;38(1):66-79. doi:10.1016/j.mcn.2008.01.016

54. Wang X, Weiner JA, Levi S, et al. *Gamma Protocadherins Are Required for Survival of Spinal Interneurons Formation, and Synaptic Remodeling (Tomaselli et Al*. Vol 36.; 2002. www.celera.com

55. Garrett AM, Schreiner D, Lobas MA, Weiner JA. γ-Protocadherins Control Cortical Dendrite Arborization by Regulating the Activity of a FAK/PKC/MARCKS Signaling Pathway. *Neuron*. 2012;74(2):269-276. doi:10.1016/j.neuron.2012.01.028

56. Ledderose J, Dieter S, Schwarz MK. Maturation of postnatally generated olfactory bulb granule cells depends on functional γ-protocadherin expression. *Sci Rep*. 2013;3. doi:10.1038/srep01514

57. Lefebvre JL, Kostadinov D, Chen W v., Maniatis T, Sanes JR. Protocadherins mediate dendritic self-avoidance in the mammalian nervous system. *Nature*. 2012;488(7412):517-521. doi:10.1038/nature11305

58. Long R. *Patterning Principles in Vertebrate Sensory Systems*.; 2020.

59. Hua ZL, Emiliani FE, Nathans J. Rac1 plays an essential role in axon growth and guidance and in neuronal survival in the central and peripheral nervous systems. *Neural Dev*. 2015;10(1). doi:10.1186/s13064-015-0049-3

60. Hall A. Rho family GTPases. In: *Biochemical Society Transactions*. Vol 40. ; 2012:1378-1382. doi:10.1042/BST20120103

61. Kim H, Takegahara N, Choi Y. Protocadherin-7 regulates osteoclast differentiation through intracellular SET-binding domain-mediated rhoa and rac1 activation. *Int J Mol Sci*. 2021;22(23). doi:10.3390/ijms222313117

62. *In Cell Western (ICW) Protocol*.; 2018. Accessed June 29, 2022. https://www.rockland.com/resources/in-cell-western-protocol/#:~:text=In%2Dcell%20Western%20assays%20(ICW,imaging%20system%20by%20LICOR%C2%AE.

63. Bae JY, Mun CJ, Kim YS, Ahn DK, Bae YC. Quantitative ultrastructural analysis of fibers expressing parvalbumin, calretinin, calbindin D-28k, stage specific embryonic antigen-4, and phosphorylated neurofilament 200 in the peripheral sensory root of the rat trigeminal ganglion. *Journal of Comparative Neurology*. 2018;526(14):2204-2214. doi:10.1002/cne.24476

64. Ruscheweyh R, Forsthuber L, Schoffnegger D, Sandkühler J. Modification of classical neurochemical markers in identified primary afferent neurons with Aβ-, Aδ-, and C-fibers after chronic constriction injury in mice. *Journal of Comparative Neurology*. 2007;502(2):325-336. doi:10.1002/cne.21311

65. Golani O, Galun M, Rishal I. *WIS-NeuroMath-User Guide WIS-NeuroMath Neuronal Morphology Analysis Tool User Guide*.; 2006.

66. Talagas M, Lebonvallet N, Leschiera R, et al. Keratinocytes Communicate with Sensory Neurons via Synaptic-like Contacts. *Ann Neurol*. 2020;88(6):1205-1219. doi:10.1002/ana.25912

67. Ahmed BY, Chakravarthy S, Eggers R, et al. *Efficient Delivery of Cre-Recombinase to Neurons in Vivo and Stable Transduction of Neurons Using Adeno-Associated and Lentiviral Vectors*.; 2004. http://www.biomedcentral.com/1471-2202/5/4

68. Advantages and drawbacks of AAV vector-mediated gene transfer | GeneMedi. Accessed July 9, 2022. https://www.genemedi.net/i/advantage-drawbacks-aav-vector

69. Dana H, Mahmoodi Chalbatani G, Mahmoodzadeh H, et al. *Molecular Mechanisms and Biological Functions of SiRNA*. Vol 13.; 2017. www.ijbs.org

70. Campeau E, Gobeil S. RNA interference in mammals: Behind the screen. *Brief Funct Genomics*. 2011;10(4):215-226. doi:10.1093/bfgp/elr018

71. Bromberg MB. An Electrodiagnostic Approach to the Evaluation of Peripheral Neuropathies. *Phys Med Rehabil Clin N Am*. 2013;24(1):153-168. doi:10.1016/j.pmr.2012.08.020

72. Bautista DM, Siemens J, Glazer JM, et al. The menthol receptor TRPM8 is the principal detector of environmental cold. *Nature*. 2007;448(7150):204-208. doi:10.1038/nature05910

73. Crawford LTK, Caterina MJ. Functional Anatomy of the Sensory Nervous System: Updates From the Neuroscience Bench. *Toxicol Pathol*. 2020;48(1):174-189. doi:10.1177/0192623319869011

74. Molumby MJ, Keeler AB, Weiner JA. Homophilic Protocadherin Cell-Cell Interactions Promote Dendrite Complexity. *Cell Rep*. 2016;15(5):1037-1050. doi:10.1016/j.celrep.2016.03.093

75. Hari K, Lucas-Osma AM, Metz K, et al. *GABA Facilitates Spike Propagation through Branch Points of Sensory Axons in the Spinal Cord*.

76. Ritter-Jones M, Najjar S, Albers KM. Keratinocytes as modulators of sensory afferent firing. *Pain*. 2016;157(4):786-787. doi:10.1097/j.pain.0000000000000490

77. Baumbauer KM, DeBerry JJ, Adelman PC, et al. Keratinocytes can modulate and directly initiate nociceptive responses. doi:10.7554/eLife.09674.001

78. Weiner JA, Wang X, Carlos Tapia J, Sanes JR. *Gamma Protocadherins Are Required for Synaptic Development in the Spinal Cord*.; 2004. www.pnas.orgcgidoi10.1073pnas.0407931101

79. Zou C, Huang W, Ying G, Wu Q. Sequence analysis and expression mapping of the rat clustered protocadherin gene repertoires. *Neuroscience*. 2007;144(2):579-603. doi:10.1016/j.neuroscience.2006.10.011

80. Dun XP, Parkinson DB. Transection and crush models of nerve injury to measure repair and remyelination in peripheral nerve. In: *Methods in Molecular Biology*. Vol 1791. Humana Press Inc.; 2018:251-262. doi:10.1007/978-1-4939-7862-5_20

81. Lee J il, Gurjar AA, Talukder MAH, et al. A novel nerve transection and repair method in mice: histomorphometric analysis of nerves, blood vessels, and muscles with functional recovery. *Sci Rep*. 2020;10(1). doi:10.1038/s41598-020-78481-1

82. Bauder AR, Ferguson TA. Reproducible mouse sciatic nerve crush and subsequent assessment of regeneration by whole mount muscle analysis. *Journal of Visualized Experiments*. 2012;(60). doi:10.3791/3606

83. Vogelaar CF, Vrinten DH, Hoekman MFM, Brakkee JH, Burbach JPH, Hamers FPT. Sciatic nerve regeneration in mice and rats: Recovery of sensory innervation is followed by a slowly retreating neuropathic pain-like syndrome. *Brain Res*. 2004;1027(1-2):67-72. doi:10.1016/j.brainres.2004.08.036

84. Carvalho CR, Oliveira JM, Reis RL. Modern Trends for Peripheral Nerve Repair and Regeneration: Beyond the Hollow Nerve Guidance Conduit. *Front Bioeng Biotechnol*. 2019;7. doi:10.3389/fbioe.2019.00337

Appendix

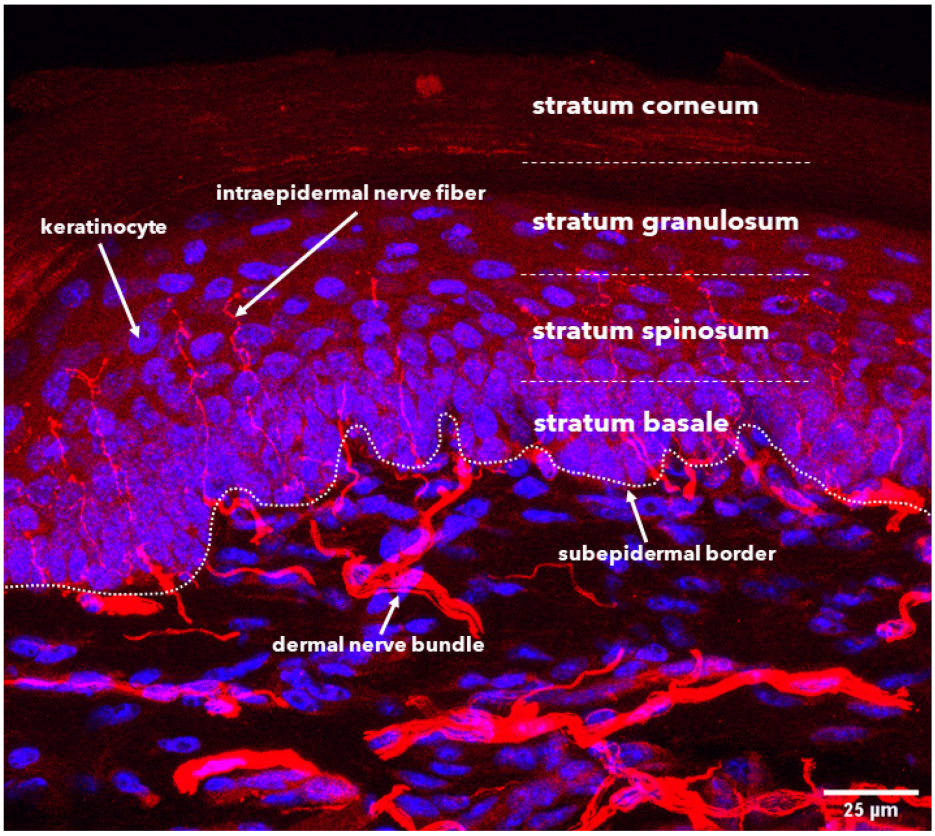

Figure 1: Structure of footpad epidermal innervation. A representative confocal image taken from mouse footpad epidermis section. Intrapidermal nerve fibers (IENF) penetrate the subepidermal border and consist of mainly Aδ and C fibers.

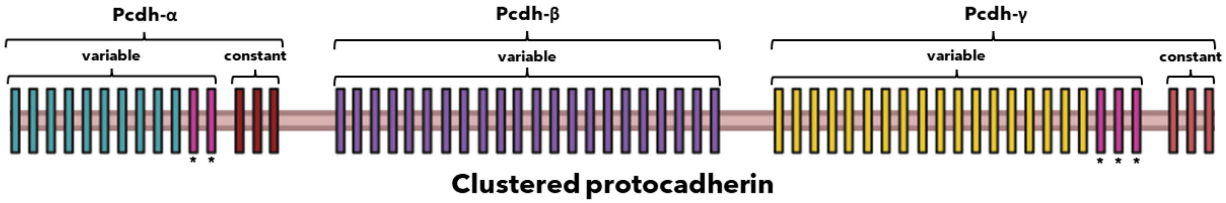

Figure 2: Organization of the mammalian clustered protocadherin (Pcdh) gene. The gene is organized into three subclusters: Pcdh-α (cyan), Pcdh-β (purple) and Pcdh-γ (yellow). Pcdh-α and Pcdh-γ contain variable exons and constant exons while Pcdh-β contains only variable exons. Variable exons marked with * are more closely related to each other than with those within their subclusters. During splicing, a unique promoter is chosen stochastically to encode a single variable exon and then spliced onto the 3 constant exons downstream which encode for the intracellular domain. Pcdh-β does not contain constant exons and each of its 22 variable exons encode the entire transmembrane protein with unique intracellular domain.

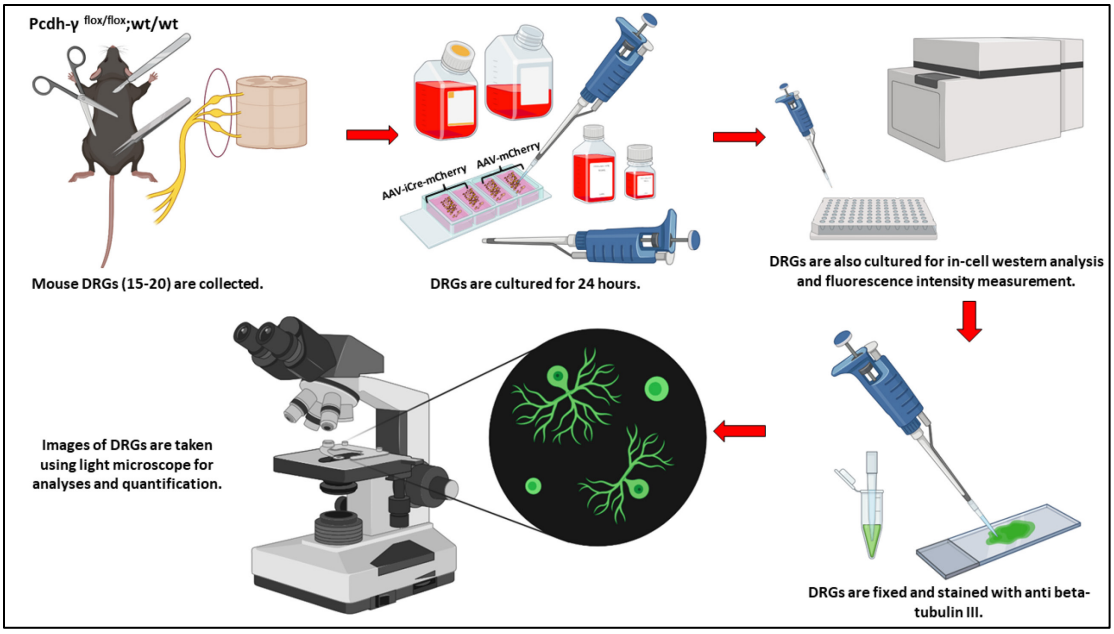

Figure 3: A summarized version of the experimental plan for Experiment 1. Objective: To re-evaluate the in vitro impact of Pcdh-γ knockdown on neurite outgrowth, using adeno-associated virus (AAV) expressing Cre recombinase on mouse DRG neurons with floxed Pcdh-γ gene ($Pcdh^{flox/flox}$).

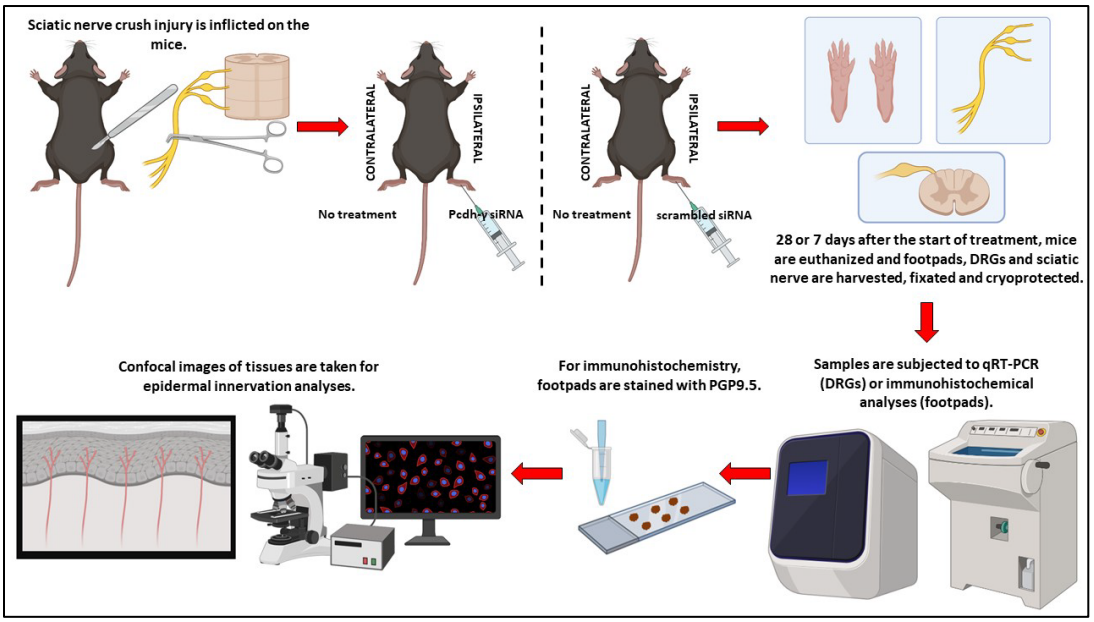

Figure 4: A summarized version of the experimental plan for Experiment 2. Objective: To determine the in vivo effect of Pcdh-γ knockdown on peripheral axon regeneration following an injury using mouse model.

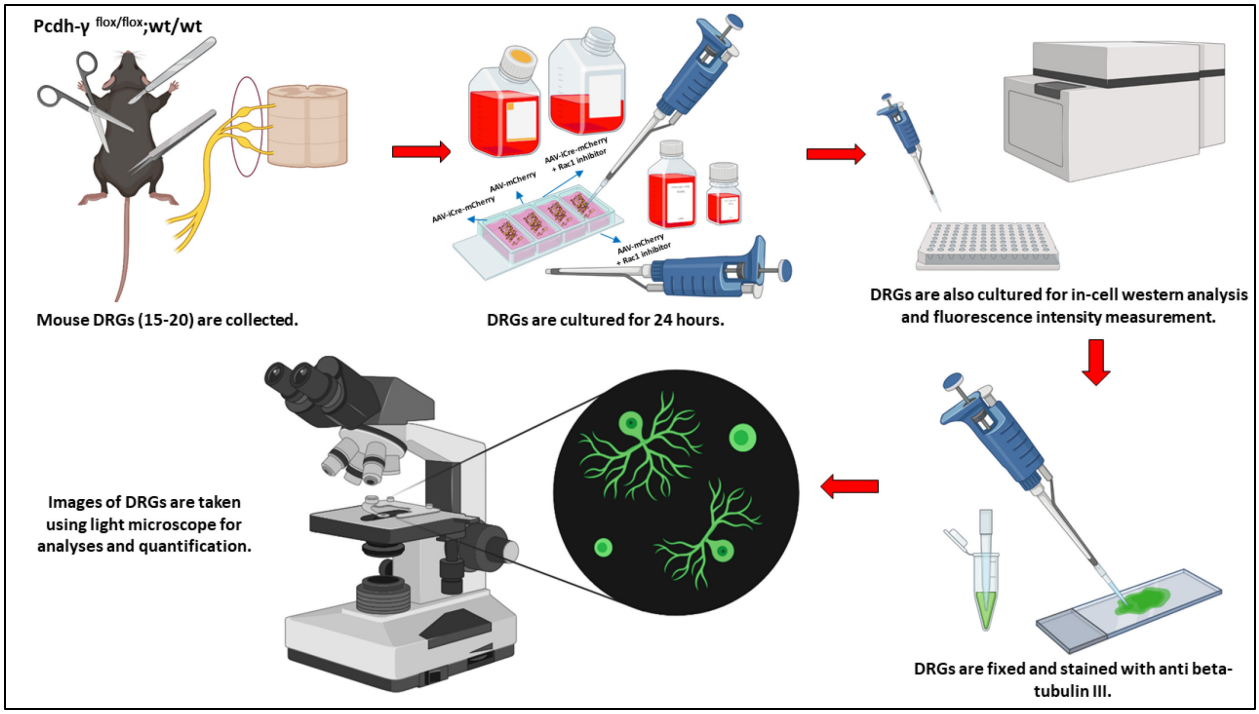

Figure 5: A summarized version of the experimental plan for Experiment 3. Objective: To determine the impact of Rac1 inhibition on DRG neurite outgrowth as one of the possible downstream signaling cascade for Pcdh-γ knockdown.

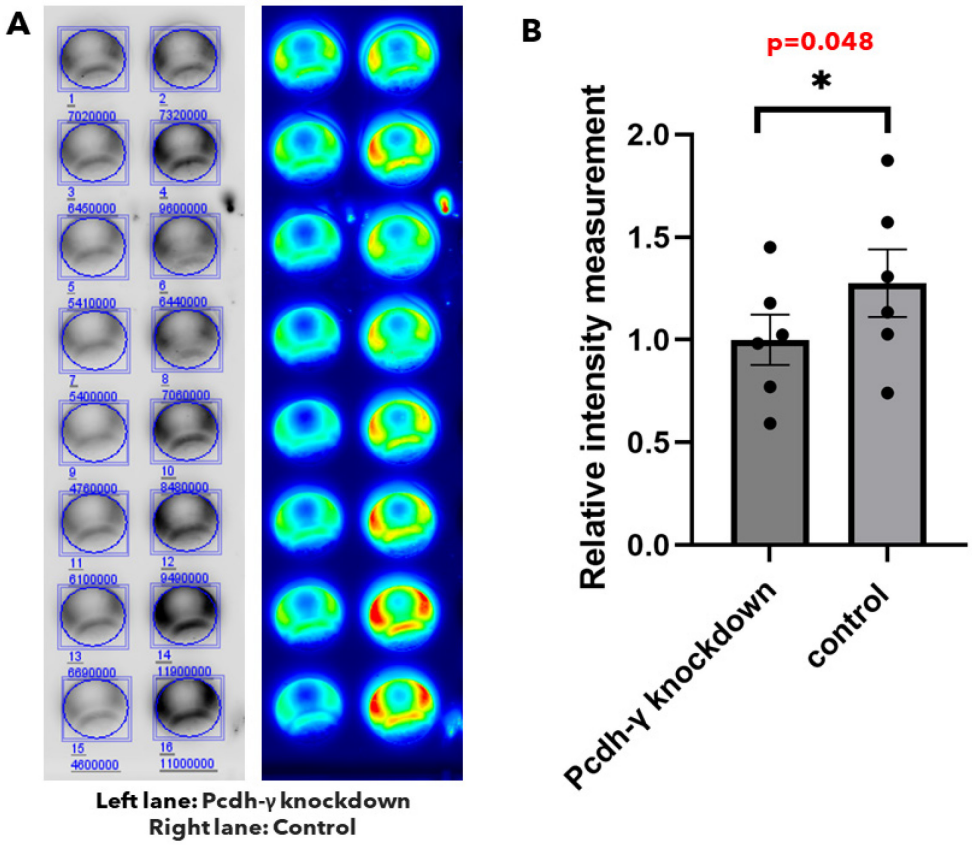

Figure 6: In-cell western assays showing the knockdown of Pcdh-γ in DRG neurons that were transfected with AAV-iCre-mCherry. (A) An example of in-cell western assay is shown, the left lane denotes the Pcdh-γ knockdown group while the right lane denotes the control group. The blue circles with the values showed the relative Pcdh-γ staining intensity measurement established by Odyssey® infrared imaging system. **(B)** Two-tailed paired t-test revealed that there is a significant difference in relative intensity measurement between Pcdh-γ knockdown group and control group (n=6 for each group; two-tailed paired t-test, p=0.048*). ***ns*** = not significant, *= ($p<0.05$), **= ($p<0.01$), ***= ($p<0.001$).

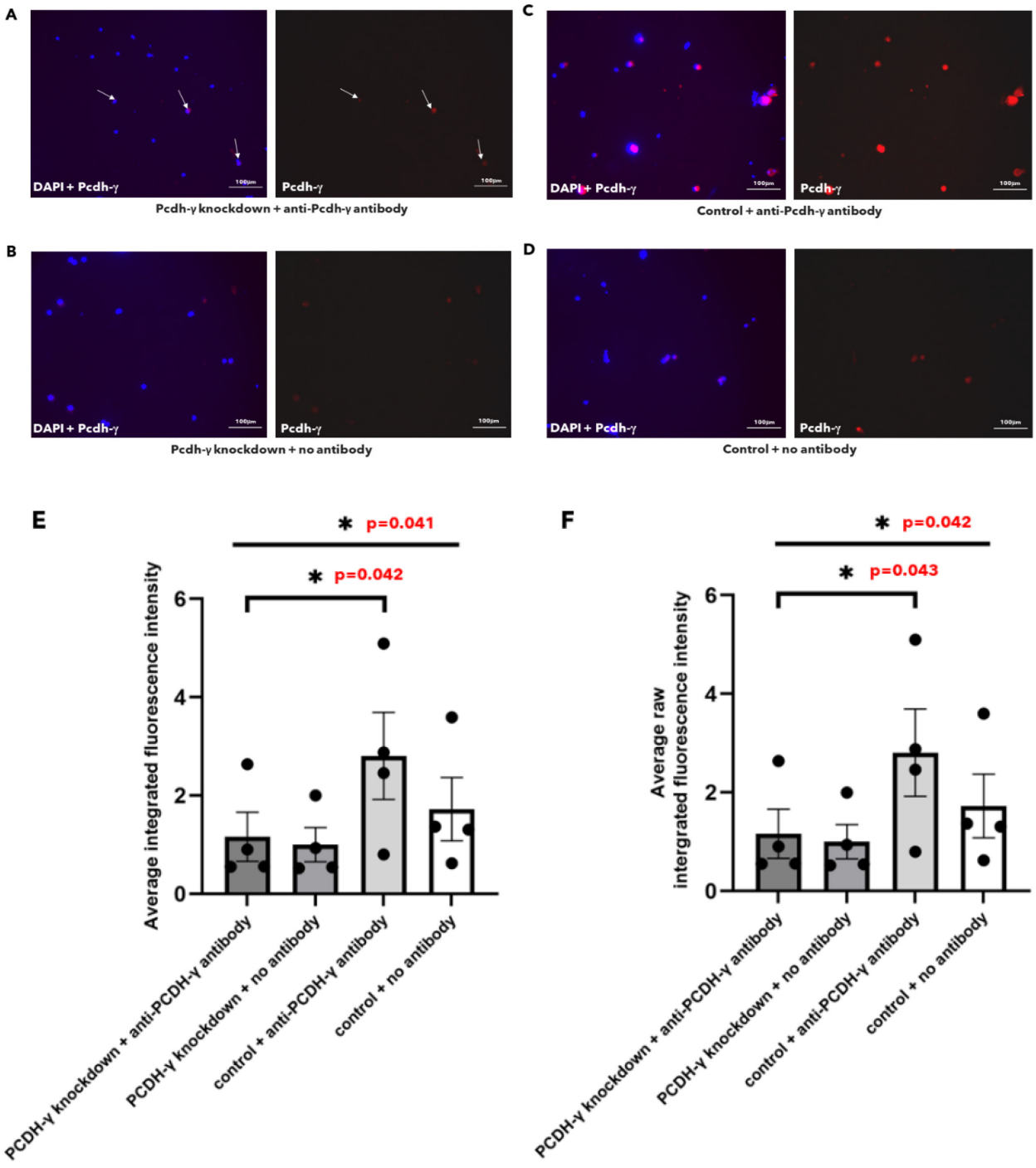

Figure 7: Fluorescence intensity measurement confirmed the knockdown of Pcdh-γ in uninjured mouse DRG neurons transfected with AAV-iCre-mCherry. (A-D) Light microscope images showing the fluorescence staining of DAPI + Pcdh-γ (left hand side) and Pcdh-γ only (right hand side) for i) Pcdh-γ knockdown group stained with anti-Pcdh-γ antibody, ii) Pcdh-γ knockdown group stained without anti-Pcdh-γ antibody, iii) control group stained with anti-Pcdh-γ antibody and iv) control group stained without anti-Pcdh-γ antibody. **(A)** White arrows denote DRG neurons that stained with anti-Pcdh-γ antibody in Pcdh-γ knockdown group. A total

of 99 cells were analyzed across 15 randomly chosen images from 4 separate cell culture experiments for Pcdh-γ knockdown group stained with anti-Pcdh-γ antibody. **(B)** A total of 79 cells were analyzed across 15 randomly chosen images from 4 separate cell culture experiments for Pcdh-γ knockdown group stained without anti-Pcdh-γ antibody. **(C)** A total of 98 cells were analyzed across 14 randomly chosen images from 4 separate cell culture experiments for control group stained with anti-Pcdh-γ antibody. **(D)** A total of 89 cells were analyzed across 14 randomly chosen images from 4 separate cell culture experiments for control group stained without anti-Pcdh-γ antibody. **(E)** One-way ANOVA showed that there is a significant difference in the average integrated fluorescence intensity measurement across those four groups (p=0.041*). Two-tailed paired t-test revealed a significant difference between Pcdh-γ knockdown group stained with anti-Pcdh-γ antibody and control group stained with anti-Pcdh-γ antibody (p=0.042*). **(F)** One-way ANOVA showed that there is a significant difference in the average raw integrated fluorescence intensity measurement across those four groups (p=0.042*). Two-tailed paired t-test revealed a significant difference between Pcdh-γ knockdown group stained with anti-Pcdh-γ antibody and control group stained with anti-Pcdh-γ antibody (p=0.043*). ***ns*** = not significant, *= ($p<0.05$), **= ($p<0.01$), ***= ($p<0.001$).

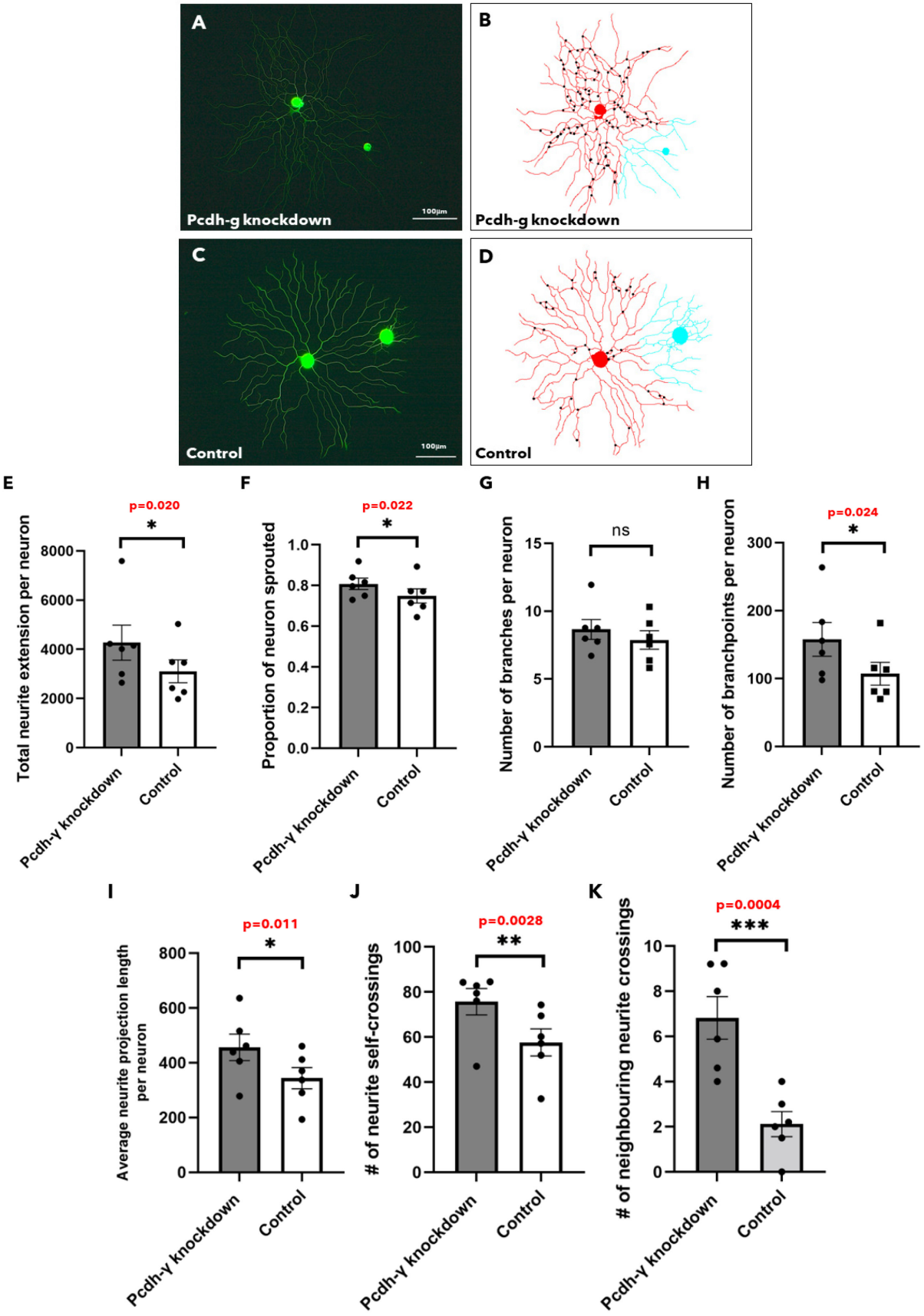
A
Pcdh-g knockdown
100µm
B
Pcdh-g knockdown
C
Control
100µm
D
Control
E
p=0.020
*
Total neurite extension per neuron
8000
6000
4000
2000
0
Pcdh-γ knockdown
Control
F
p=0.022
*
Proportion of neuron sprouted
1.0
0.8
0.6
0.4
0.2
0.0
Pcdh-γ knockdown
Control
G
ns
Number of branches per neuron
15
10
5
0
Pcdh-γ knockdown
Control
H
p=0.024
*
Number of branchpoints per neuron
300
200
100
0
Pcdh-γ knockdown
Control
I
p=0.011
*
Average neurite projection length per neuron
800
600
400
200
0
Pcdh-γ knockdown
Control
J
p=0.0028
**
# of neurite self-crossings
100
80
60
40
20
0
Pcdh-γ knockdown
Control
K
p=0.0004
***
# of neighbouring neurite crossings
10
8
6
4
2
0
Pcdh-γ knockdown
Control

Figure 8: DRG neurons that received Pcdh-γ knockdown showed greater total neurite extension and more branchpoints per neuron. (A, C) Light microscope images showing representative DRG neurons from Pcdh-γ knockdown group and control group, respectively. **(A)** A total of 1385 DRG cells were analyzed across for 6 separate culture experiments for Pcdh-γ knockdown group. **(C)** A total of 1424 DRG cells were analyzed across for 6 separate culture experiments for control group. **(B, D)** Images showing the neurite tracing generated by WIS Neuromath software and the black dots denote the manual counting of neurite self-crossings. **(E)** Pcdh-γ knockdown group showed greater total neurite extension than control group, 4270.9±715.3μm versus 3106.1±462.4μm (n=6; two-tailed paired t-test, p=0.020*). **(F)** Pcdh-γ knockdown group showed greater proportion of neuron sprouted than control group, 0.81±0.03 versus 0.75±0.04 (n=6; two-tailed paired t-test, p=0.022*). **(G)** There is no significant difference in the number of branches per neuron between Pcdh-γ knockdown group and control group (n=6; two-tailed paired t-test, p=0.058). **(H)** Pcdh-γ knockdown group showed a greater number of branchpoints per neuron than control group, 157.7±24.7 versus 107.1±16.8 (n=6; two-tailed paired t-test, p=0.024*). **(I)** Pcdh-γ knockdown group showed longer projection length of a single neurite than control group, 456.0±48.4μm versus 343.8±38.5μm (n=6; two-tailed paired t-test, p=0.011*). **(J)** Pcdh-γ knockdown group showed more neurite self-crossings (isoneuronal interactions) than control group, 75.7±5.9 versus 57.6±6.0 (n=6; two-tailed paired t-test, p=0.0028**). **(K)** Pcdh-γ knockdown group showed more neighbouring neurite crossings (heteroneuronal interactions) than control group, 6.8±0.9 versus 2.1±0.6 (n=6; two-tailed paired t-test, p=0.00040***). ***ns*** = not significant, *= (p<0.05), **= (p<0.01), ***= (p<0.001).

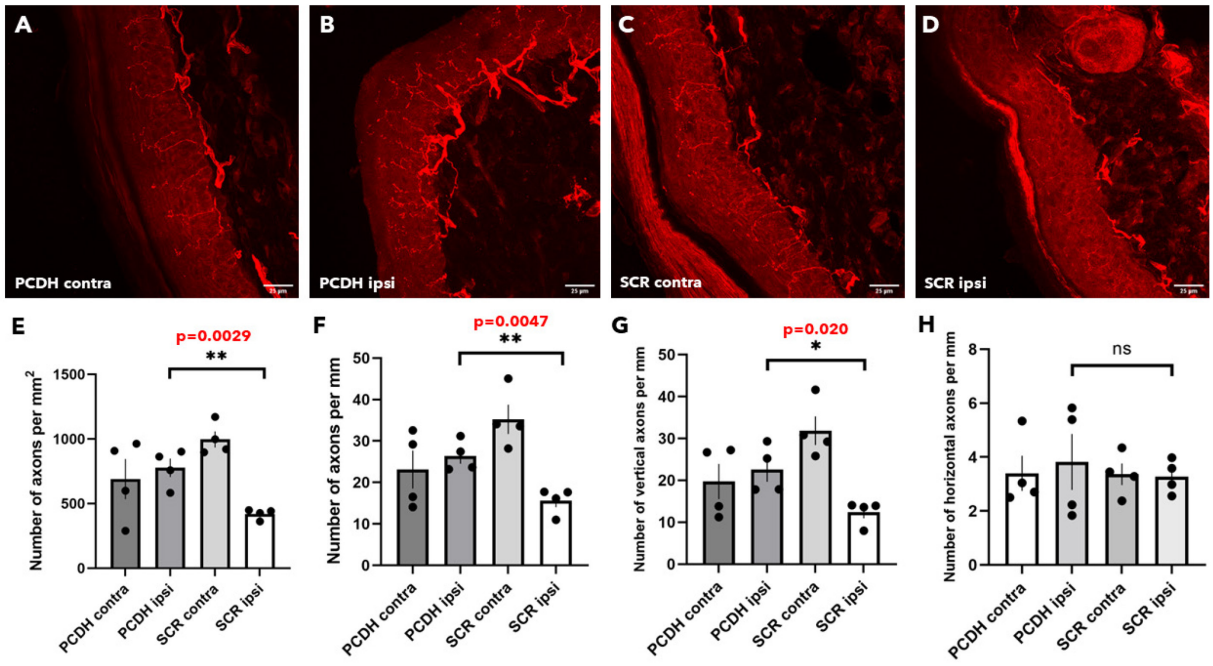

Figure 9: Epidermal reinnervation of the footpad of sciatic nerve crushed mice. Footpads that received Pcdh-γ siRNA knockdown following sciatic nerve crush injury shows increased epidermal reinnervation. **(A-D)** Z-stack images depicting epidermal innervation of footpads from PCDH siRNA contra **(A)**, PCDH siRNA ipsi **(B)**, SCR siRNA contra **(C)** and SCR siRNA ipsi **(D)** groups. Quantification of the total number of axons per mm2 of epidermis **(E)** and per mm of epidermis **(F)** is shown in addition to a breakdown of the number of vertical (45˚-90˚ from the subepidermal border; **G**) and horizontal (0˚-45˚ from the subepidermal border; **H**) axons per mm of the epidermis. Overall, mice treated with the Pcdh-γ siRNA (PCDH siRNA ipsi) possessed the greatest number of axons crossing from the dermis into the epidermis across all counting methods, except for horizontal axons per mm of epidermis. Analyses of the data using two-tailed unpaired t-tests between Pcdh-γ ipsi and Pcdh-γ gamma groups to determine the effects of Pcdh-γ knockdown on peripheral neuron regeneration following sciatic nerve crush injury revealed that the difference across all counting methods are significant, except for horizontal axons per mm (p=0.0029**; **E**) (p=0.0047**; **F**) (p=0.020*; **G**) (p=0.63; **H**). ***ns*** = not significant, *= (p<0.05), **= (p<0.01), ***= (p<0.001). n=4 for each group.

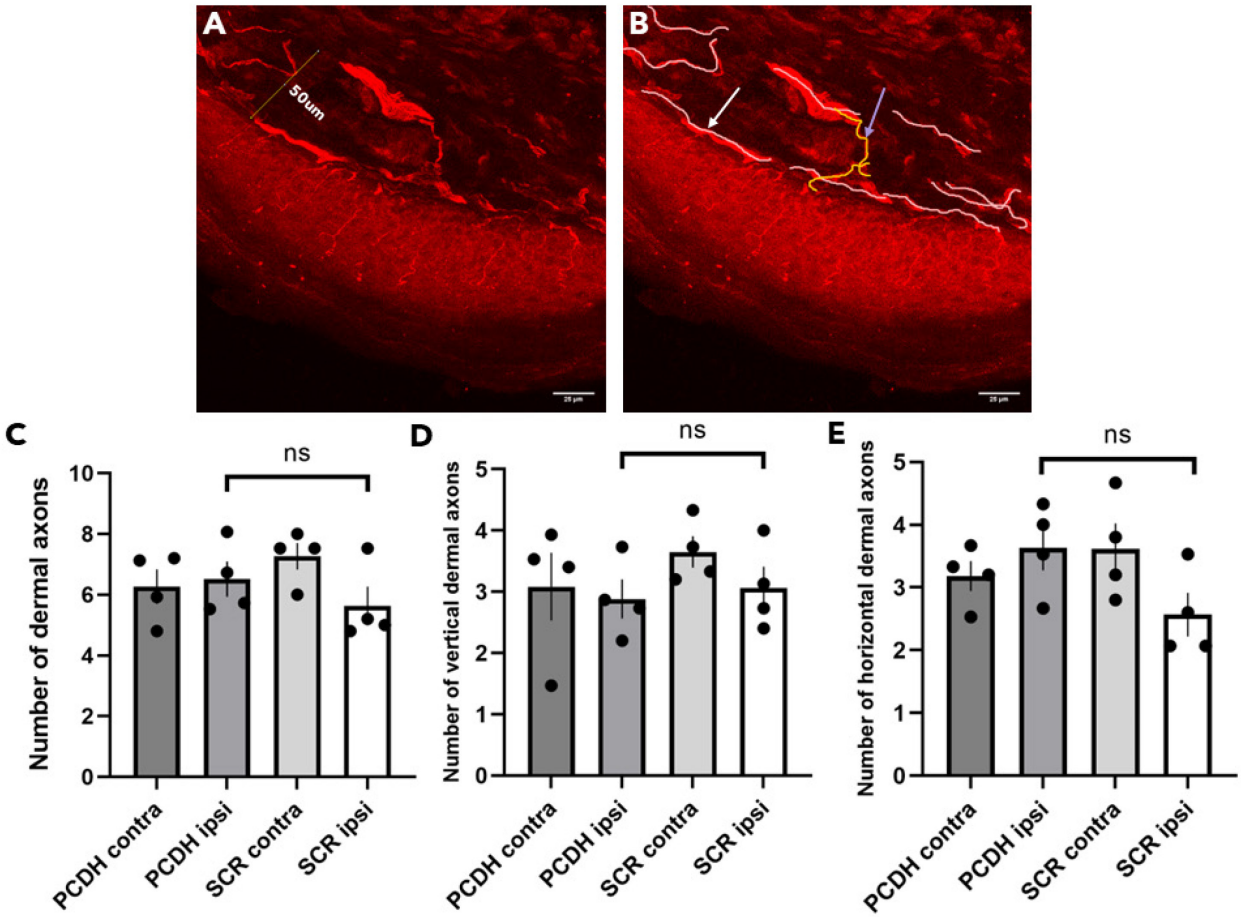

Figure 10: Dermal reinnervation of the footpad of sciatic nerve crushed mice following Pcdh-γ siRNA knockdown. Footpads that received Pcdh-γ siRNA knockdown following sciatic nerve crush injury did not show any significant difference from other groups in dermal reinnervation. **(A)** Z-stack image depicting analysis of footpad dermal innervation: 50µm beneath the subepidermal border. **(B)** Z-stack image showing an example of vertical dermal axon depicted by purple arrow and yellow tracing, and horizontal dermal axon depicted by white arrow and pink tracing. Quantification of the total number of dermal axons across groups are shown in **(C)** in addition to a breakdown of the number of vertical (45˚-90˚ from the subepidermal border; **D**) and horizontal (0˚-45˚ from the subepidermal border; **E**) dermal axons. Analyses of the data using two-tailed unpaired t-tests between PCDH siRNA ipsi and SCR siRNA ipsi groups to determine the effects of Pcdh-γ knockdown on dermal fiber count following sciatic nerve crush injury revealed that there is no significant difference across all dermal axon counting methods (p=0.35; **C**) (p=0.077; **D**) (p=0.71; **E**). ***ns*** = not significant, *= ($p<0.05$), **= ($p<0.01$), ***= ($p<0.001$). n=4 for each group.

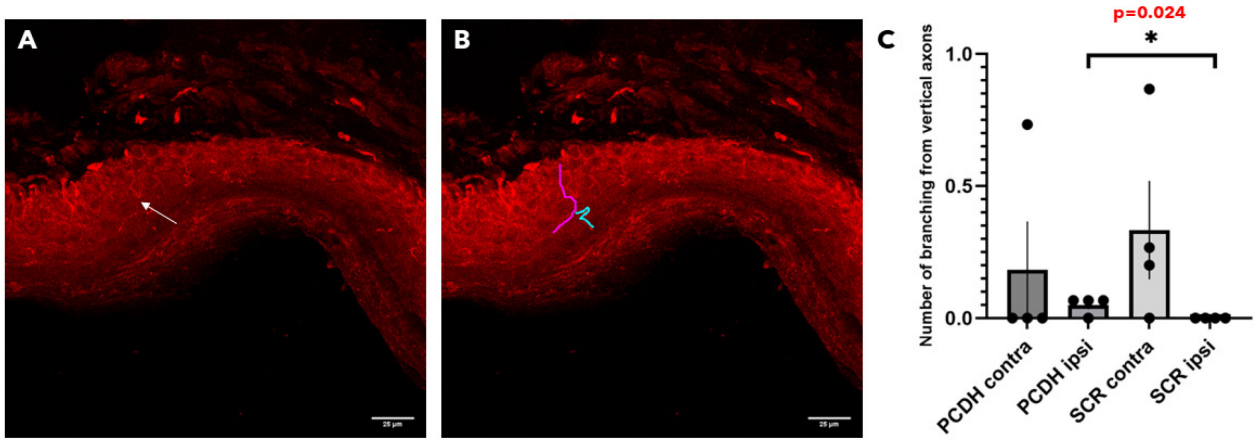

Figure 11: Vertical branching of footpad epidermal reinnervation in mice after sciatic nerve crush injury. (A) Z-stack image showing an example of vertical intraepidermal nerve fiber, depicted by white arrow. **(B)** Z-stack image showing the analysis of vertical branching. The vertical intraepidermal nerve fiber is shown in magenta tracing and its branch in cyan tracing. **(C)** There is a significant difference detected between PCDH siRNA ipsi and SCR siRNA ipsi groups in vertical branching, with PCDH siRNA ipsi group showing more vertical branches from axons (p=0.024*). ***ns*** = not significant, *= (p<0.05), **= (p<0.01), ***= (p<0.001). n=4 for each group.

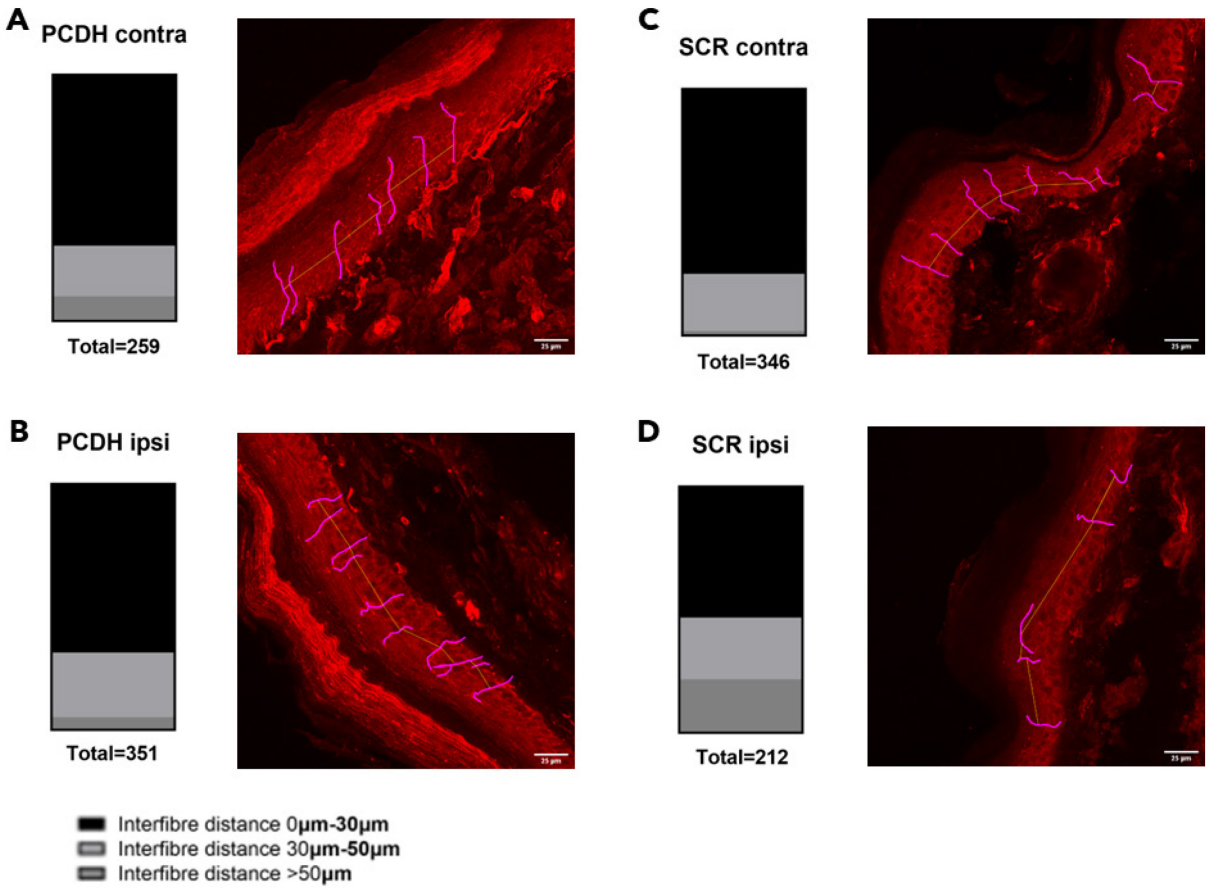

Figure 12: Interfiber distance of the intraepidermal nerve fibers of the footpad of sciatic nerve crushed mice following Pcdh-γ siRNA knockdown. Footpads of mice that received Pcdh-γ knockdown had shorter interfiber distances. **(A-D)** Vertical bars showing the distribution of the interfiber distance across PCDH siRNA contra, PCDH siRNA ipsi, SCR siRNA contra and SCR siRNA ipsi groups are shown. **(A-D)** Z-stack images showing analyses of interfiber distance across PCDH siRNA contra, PCDH siRNA ipsi, SCR siRNA contra and SCR siRNA ipsi groups. Interfiber distances are classified into 3 different categories, namely short (0-30µm), medium (30-50µm) and long (>50µm). Total of 259, 351, 346 and 212 interfiber distances are counted for PCDH siRNA contra, PCDH siRNA ipsi, SCR siRNA contra, SC ipsi groups respectively. n=4 for each group. **(A)** PCDH siRNA contra group had 69.50% of their interfiber distances in the 0-30µm range, 20.46% in the 30-50µm range and 10.04% in the >50µm range. **(B)** PCDH siRNA ipsi group had 68.7% of their interfiber distances in the 0-30µm range, 26.2% in the 30-50µm range and 5.1% in the >50µm range. **(C)** SCR siRNA contra group had 75.14% of their interfiber distances in the 0-30µm range, 23.12% in the 30-50µm range and 1.73% in the >50µm range. **(D)** SCR siRNA ipsi group had 53.3% of their interfiber distances in the 0-30µm range, 25.0% in the 30-50µm range and 21.7% in the >50µm range.

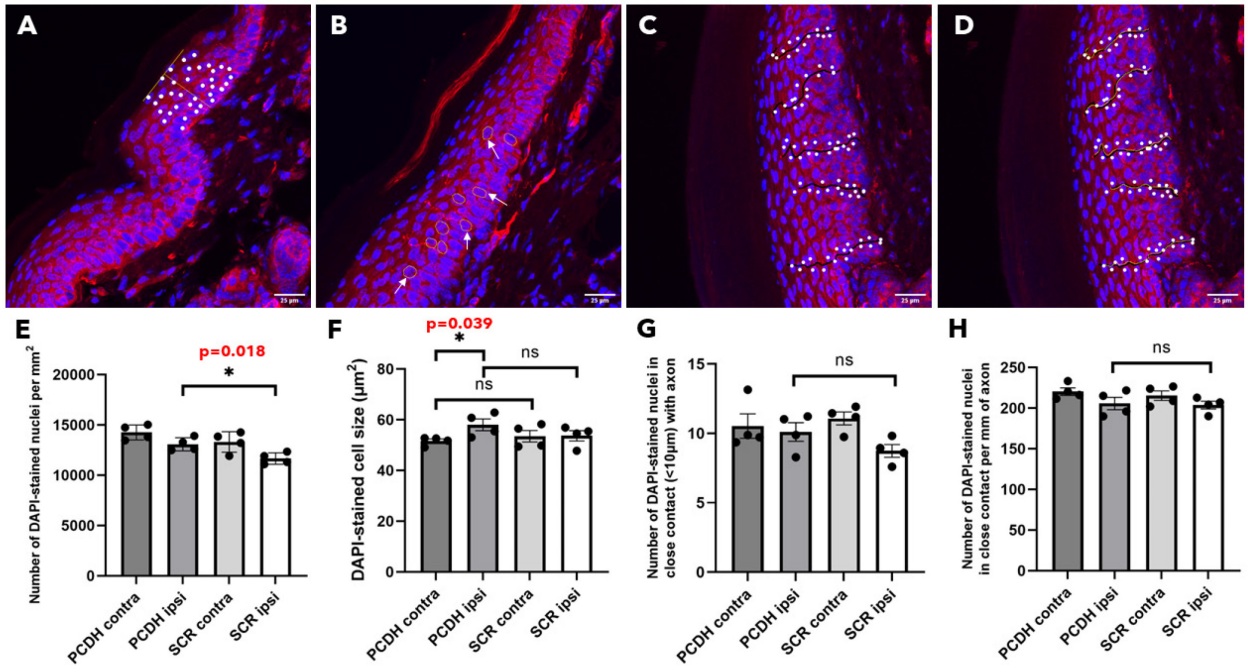

Figure 13: Number of DAPI-stained nuclei per mm2 of epidermis, DAPI-stained cellular size and number of DAPI-stained nuclei in close contact with axon of the footpad of sciatic nerve crushed mice following Pcdh-γ siRNA knockdown. Footpads of mice that received Pcdh-γ knockdown contain more DAPI-stained nuclei per epidermal area. Z-stack images depicting the analyses for number of DAPI-stained nuclei per mm2 of epidermis **(A)**, DAPI-stained cellular size **(B)**, number DAPI-stained nuclei in close contact (<10μm) with axon **(C)** and number DAPI-stained nuclei in close contact per mm of axon **(D)** are shown. Examples of traced cell for the analysis of DAPI-stained cellular size are shown using white arrows in **B**. There was no significant difference between PCDH siRNA ipsi and SCR siRNA ipsi groups across all analyses except for the number DAPI-stained nuclei per mm^2 of epidermis (p=0.018*; **E**) (p=0.21; **F**) (p=0.15; **G**) (p=0.82; **H**). A significant difference in DAPI-stained cellular size between PCDH siRNA ipsi and PCDH siRNA contra groups was detected (p=0.039*; **F**). However, there was no significant difference detected in DAPI-stained cellular size between PCDH siRNA contra group and its respective counterpart, SCR siRNA contra group (p=0.45; **F**). **ns** = not significant, *= (p<0.05), **= (p<0.01), ***= (p<0.001). n=4 for each group.

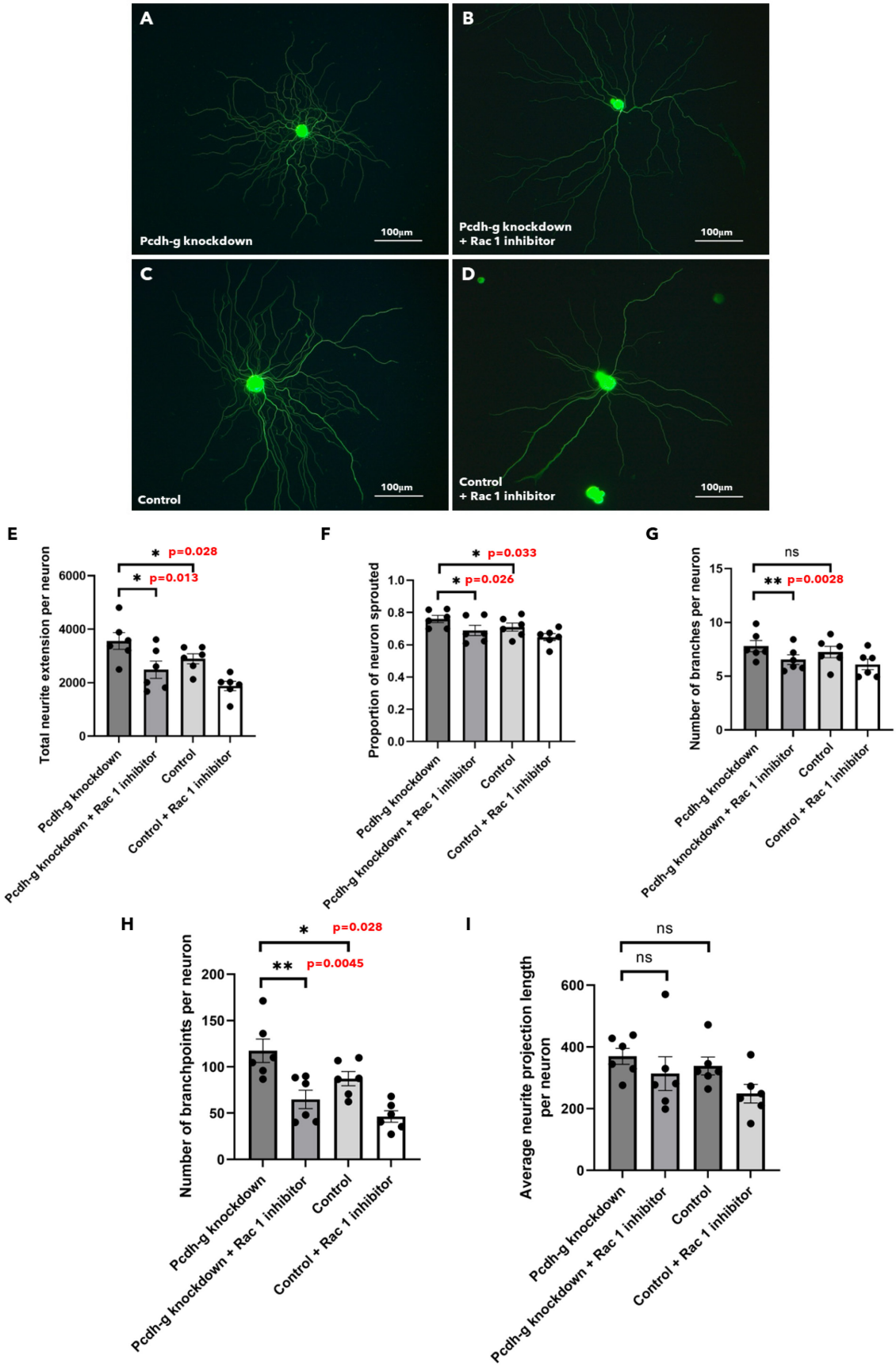
A
Pcdh-g knockdown
100µm
B
Pcdh-g knockdown
+ Rac 1 inhibitor
100µm
C
Control
100µm
D
Control
+ Rac 1 inhibitor
100µm
E
Total neurite extension per neuron
* p=0.028
* p=0.013
Pcdh-g knockdown
Pcdh-g knockdown + Rac 1 inhibitor
Control
Control + Rac 1 inhibitor
F
Proportion of neuron sprouted
* p=0.033
* p=0.026
G
Number of branches per neuron
ns
** p=0.0028
H
Number of branchpoints per neuron
* p=0.028
** p=0.0045
I
Average neurite projection length per neuron
ns
ns

Figure 14: Rac1 inhibition reverts the increased branchpoints observed in Pcdh-γ knockdown DRG neurons. (A, B, C, D) Light microscope images showing representative DRG neurons from Pcdh-γ knockdown group, Pcdh-γ knockdown + Rac1 inhibitor group, control group and control + Rac 1 inhibitor group, respectively. **(A)** A total of 674 DRG cells were analyzed across all 6 separate culture experiments for Pcdh-γ knockdown group. **(B)** A total of 736 DRG cells were analyzed across all 6 separate culture experiments for Pcdh-γ knockdown + Rac1 inhibitor group. **(C)** A total of 761 DRG cells were analyzed across all 6 separate culture experiments for control group. **(D)** A total of 857 DRG cells were analyzed across all 6 separate culture experiments for control + Rac 1 inhibitor group. **(E)** Pcdh-γ knockdown group showed greater total neurite extension than Pcdh-γ knockdown + Rac1 inhibitor group, 3560.2±314.1µm versus 2485.4±322.4µm (n=6; two-tailed paired t-test, p=0.013*). **(F)** Pcdh-γ knockdown group showed greater proportion of neuron sprouted than Pcdh-γ knockdown + Rac1 inhibitor group, 0.76±0.02 versus 0.69±0.03 (n=6; two-tailed paired t-test, p=0.026*). **(G)** Pcdh-γ knockdown group showed a greater number of branches per neuron than Pcdh-γ knockdown + Rac1 inhibitor group, 7.8±0.5 versus 6.5±0.5 (n=6; two-tailed paired t-test, p=0.0028**). **(H)** Pcdh-γ knockdown group showed a greater number of branchpoints per neuron than Pcdh-γ knockdown + Rac1 inhibitor group, 117.4±12.7 versus 64.8±9.9 (n=6; two-tailed paired t-test, p=0.0045**). **(I)** There was no significant difference between Pcdh-γ knockdown group and Pcdh-γ knockdown + Rac1 inhibitor group in average neurite projection length per neuron (n=6; two-tailed paired t-test, p=0.24). **(E, F, G, H, I)** Consistent with our previous experiment (section 4.2, Figure 8), Pcdh-γ knockdown group showed greater total neurite extension per neuron, proportion of neuron sprouted, number of branchpoints per neuron than control group, and no significant difference in number of branches per neuron (n=6; two-tailed paired t-test, p=0.028*, 0.033*, 0.028*, 0.23, respectively). However, there was no significant difference between Pcdh-γ knockdown group and control group in average neurite projection length per neuron (n=6; two-tailed paired t-test, p=0.24). **ns** = not significant, *= ($p<0.05$), **= ($p<0.01$), ***= ($p<0.001$).

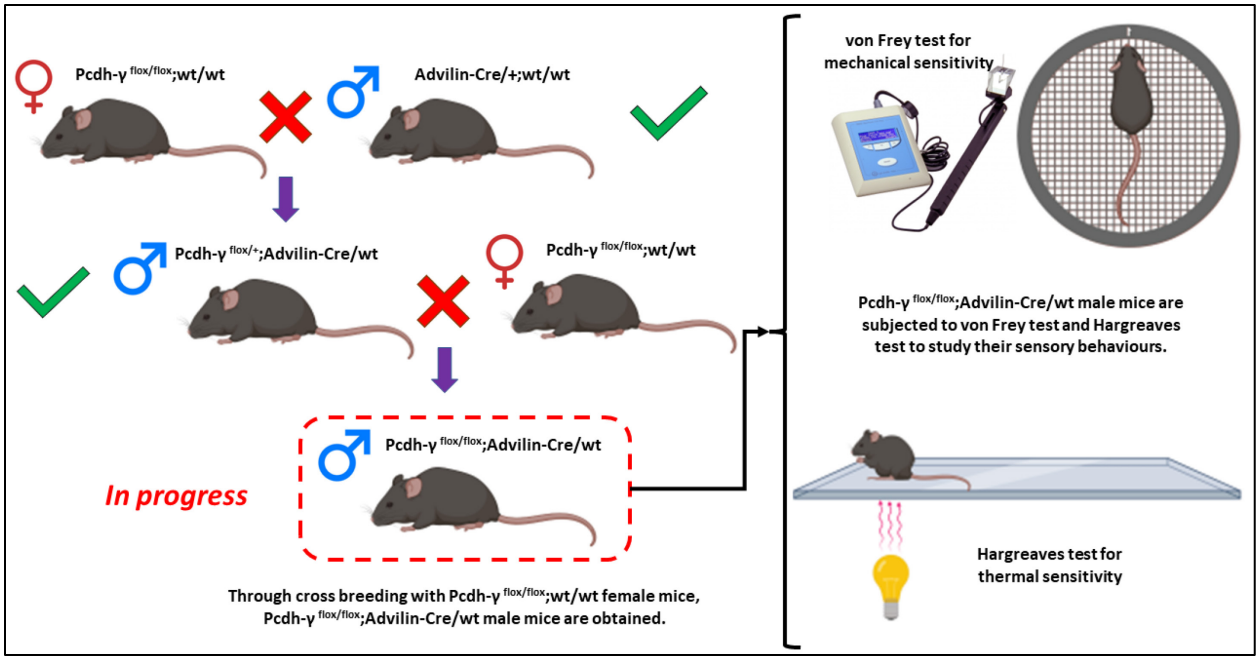

Figure 15: Current progress on breeding for Pcdh-γ conditional knockout mice and behavioural tests that are waiting to be conducted on these mice.